UNIVERSITY OF OKLAHOMA

GRADUATE COLLEGE

BOSON JOSEPHSON JUNCTIONS BASED ON EXCITON-POLARITON CONDENSATES

A DISSERTATION

SUBMITTED TO THE GRADUATE FACULTY

in partial fulfillment of the requirements for the

Degree of

DOCTOR OF PHILOSOPHY

By HUA WANG

Norman, Oklahoma

2025

BOSON JOSEPHSON JUNCTIONS BASED ON
EXCITON-POLARITON CONDENSATES

A DISSERTATION APPROVED FOR THE
HOMER L. DODGE DEPARTMENT OF PHYSICS AND ASTRONOMY

BY THE COMMITTEE CONSISTING OF

Dr. Kieran Mullen, Chair

Dr. Bruno Uchoa

Dr. Joseph Tischler

Dr. Doerte Blume

Dr. Binbin Weng

Acknowledgements

Throughout my exceptionally long journey of doctoral study, I have drawn courage and inspiration from the wonderful people around me. For this, I am forever grateful.

First and foremost, I thank my dissertation advisor, Prof. Kieran Mullen. When I started graduate school, I had many fears and tried to stay in a safe zone shaped by my limited experiences. I lacked confidence in understanding solid-state physics, let alone pursuing condensed matter theory. Prof. Mullen recognized the potential in me and helped me see beyond those fears. His clear and insightful teaching style enabled me to overcome my initial knowledge barrier, and he encouraged me to follow my intellectual curiosity rather than assigning me a predefined project. By working with him, I started to enjoy exploring broader areas of physics and stayed passionate about it.

I am also deeply grateful to Dr. Hong-Yi Xie, a remarkably talented research fellow. When I encountered technical challenges, Dr. Xie offered detailed and thoughtful guidance that helped me overcome the second knowledge barrier, from solid-state physics to modern condensed matter theory. To me, he exemplifies the qualities of a self-motivated and creative scientist.

Next, I thank my friends among fellow students, especially Yang Li, Geo Jose, Saesun Kim, Shan Zhong, Alex Kerr, Dylan Frizzell, Delaram Nematollahi, and Colin Riggert, for the encouragement and inspiration they gave me, and the joy we shared during this journey.

To my girlfriend, Yingyue—thank you for your unwavering support. The Ph.D. study takes a toll on both body and mind. You encouraged me to adopt a healthier lifestyle and stood by me through the emotional highs and lows. Now it's my turn to support you.

Last but not least, I thank my parents for their unconditional love and support. My time studying abroad has been far longer than they ever expected, yet they never doubted my decisions to take on new challenges. Their belief in me has been a constant source of strength.

Abstract

This dissertation is a theoretical treatise on the Josephson effect in dilute quantum gases of excitons and exciton-polaritons. An exciton is a kind of elementary excitation in semiconductors, which, through strong coupling with photons, can form a light-matter hybrid particle called an exciton-polariton. Similar to superconducting systems, excitons and exciton-polaritons show superfluidity and phase coherence in their Bose-Einstein condensates, which allows us to explore macroscopic quantum phenomena such as the Josephson effect.

This dissertation surveys the existing experiments of polariton Josephson junctions, focusing on optical control, and proposes an alternative method focusing on electrical control. A theoretical model unifying the two approaches is developed based on the microscopic mechanisms of exciton-polaritons. The unique dynamics of the proposed device, including the switching between oscillation modes, the externally driven and intrinsic chaotic behaviors, are discussed in detail.

Contents

Chapter 1

Introduction

Quantum coherence in many-body systems has long been a focus of fundamental physics, because it explains how quantum phenomena can spontaneously arise in macroscopic objects governed by classical physics. Many closely related phenomena have been found over a broad range of materials and temperatures, from Bose-Einstein condensates of alkali metal vapors at nanokelvins [1, 2] to exotic states in cuprates [3] that persist up to $\sim 130\,\mathrm{K}$ [4]. Studies of these systems have enriched our understanding of quantum information [5], and stimulated the development of quantum computation [6], quantum communication [7], quantum sensing [8], and quantum simulation [9]. At the heart of various quantum technologies is the Josephson junction, a device harnessing supercurrents induced by phase differences in macroscopic coherent states of quantum particles.

A conventional Josephson junction consists of two superconductors separated by a thin insulating layer, where the correlated tunneling of the Cooper pairs gives rise to the coupling current between the two superconductors known as the Josephson effect [10]. However, the essential idea of breaking phase continuity in the macroscopic wavefunction can apply to a broader range of systems. For example, Bose-Einstein condensates of dilute boson gases can be described by their macroscopically occupied mean field wavefunction, and therefore also have the potential to demonstrate the Josephson effect.

Inspired by the dipole trap technique in cold atom experiments, the bosonic Josephson junction was first proposed based on a double harmonic trap, where two finite-size

Bose-Einstein condensates are weakly coupled due to overlapping of wavefunctions in the barrier [11, 12]. Rich phenomena due to enhanced particle interactions, such as quantum self-trapping effect, have been predicted and observed in the bosonic Josephson junction [13, 14]. Remarkable progress in manipulating these ultracold-atom systems has been achieved based on dynamical light shaping techniques [15, 16, 17].

Excitons, a type of elementary excitation in semiconductors, can be described as electron-hole pairs bound by their Coulomb attraction, and behave like bosons at dilute densities of common experiments. Furthermore, their close relation to optical excitation, allows us to explore the mixed states of excitons and photons, which leads to interesting macroscopic phenomena at different physical limits, such as lasing, superradience, and bosonic condensation [18].

Advances in nanofabrication technology have enabled the study of excitons and photons confined in low-dimensional geometries. In particular, microcavities formed by dielectric Bragg reflectors and active semiconducting layers can host a type of hybrid boson called "exciton-polariton", that is a coherent superposition of one photon and one exciton [19, 20]. The two-dimensional gases of microcavity polaritons exhibit condensation and superfluidity even near room temperature [21, 22, 23, 24, 25, 26] because they have extremely low effective masses. This and their insensitivity to crystal disorder [27, 28, 29] make them promising systems to explore the Josephson effect.

Given that microcavities are based on nanostructures in solid state materials, and exciton-polaritons are light-matter hybrid particles, it is possible to use a wide range of experimental techniques including electrical and optical control.

The pioneering experimental studies on the polariton Josephson effect operate in a non-equilibrium limit and focus on optical control. Although many signature dynamics of boson junctions have been observed in these experiments, the short-lived coherence and limited selections of initial state pose challenges for polariton junctions to fulfill their full potential as active quantum devices.

This dissertation aims to resolve some of these challenges by proposing a new design of exciton-polariton junction operating in thermal equilibrium and focusing on electrical

control. The main body is organized as follows: Chapter 2 discusses the microscopic theory of excitons and exciton-polaritons, Chapter 3 discusses the relaxation mechanisms and coherence properties of exciton-polariton condensates, Chapter 4 discusses the Josephson effect in general and examples in dilute boson gases, and Chapter 5 discusses the proposed polariton junction and its unique dynamics.

Before delving deep into the details, I would like to make a few remarks on the history of the Josephson effect and exciton-polariton condensates.

1.1 A Brief History of Superconductivity and Josephson Effect

Superconductivity was first discovered in 1911 by Kamerlingh Onnes, when he found that the resistance of a solid mercury sample suddenly vanished at the temperature of 4.2 Kelvin. In 1933, Walther Meissner and Robert Ochsenfeld discovered the expelling of magnetic fields from superconductors, known as the Meissner effect. The latter implies that superconductivity is not simply the perfect conducting limit of classical physics, hence the first significant macroscopic quantum phenomenon.

The first successful phenomenological theory was developed by Fritz London and Heinz London(1935)[30]. The London equations describe the responses to external electrical and magnetic fields based on a superconducting fluid density.

In 1950, Ginzburg and Landau modified the London theory by introducing a pseudo wavefunction related to the superconducting density, which is also the order parameter used in formulating the Ginzburg-Landau free energy. As the order parameter takes a non-zero value to minimize free energy density, the supercurrent occurs, signaling a phase transition where the symmetry in the ground state spontaneously breaks.

In 1953, Brian Pippard, motivated by penetration experiments of magnetic fields, proposed a new scale parameter called the coherence length to address the stiffness in the macroscopic wavefunction. John Bardeen argued in the 1955 paper "Theory of the Meissner Effect in Superconductors" [31] that this property can arise from a microscopic theory

with an energy gap. This energy gap was found in Leon Cooper's 1956 paper "Bound Electron Pairs in a Degenerate Fermi Gas" [32], where he calculated the bound states of electrons subject to an attractive force. Bardeen, Cooper, and John Robert Schrieffer assembled these ideas in their paper "Theory of superconductivity" [33]. The BCS theory named after them is the first successful microscopic theory of superconductivity.

Inspired by the idea of spontaneous broken symmetry and the BCS microscopic theory, Brian Josephson worked out the correlated tunneling of Cooper pairs, presented in his 1962 paper "Possible new effects in superconductive tunneling" [34]. Philip Anderson and John Rowell claimed the first experimental observation of the Josephson effect in the paper "Probable Observation of the Josephson Superconducting Tunneling Effect" [35] in 1963.

It is noteworthy that in 1959 Lev Gor'kov proved the Ginzburg-Landau theory can be rigorously derived as a physical limit of the BCS theory [36]. Therefore, the Josephson effect is also widely accepted in the form of the Ginzburg-Landau theory, which can be related to different detailed microscopic mechanisms.

1.2 A Brief History of Exciton-Polariton and Bose-Einstein Condensation

The term "exciton" was first introduced by Yakov Frenkel, in his attempt to interpret narrow photoemission lines observed in organic molecular crystals [37][38], where the crystal potential is treated as a perturbation to the Coulomb interaction between the bare electron-hole pair. A Frenkel exciton has a typical spatial extension of the size of a unit cell, and its binding energy is on the order of $100 - 300$ meV.

In the late 1930s, Gregory Wannier and Nevill Mott established the concept of excitons in semiconductor crystals [39][40]. In this case, the Coulomb interaction between the electron-hole is weakened by the dielectric background; therefore, the periodic crystal field dominates the energy spectrum. A natural approach is to treat the electron and hole as quasi-particles based on semiconductor band states. The typical spatial extension

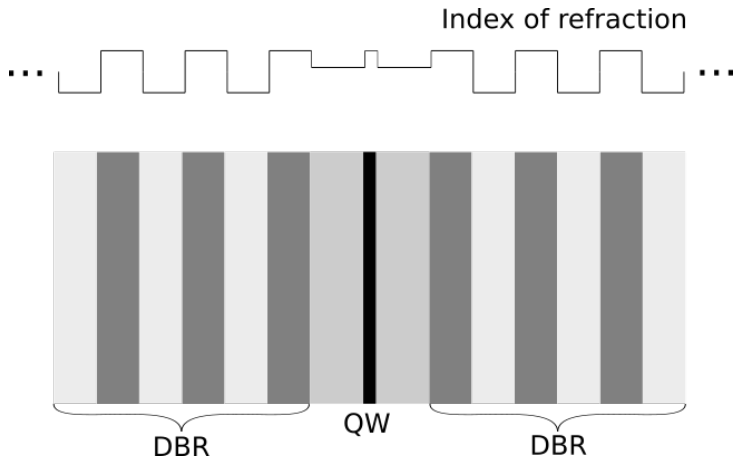

Figure 1.1: A sketch of microcavity. QW stands for the quantum well, DBR stands for distributed Bragg reflector.

of a Wannier-Mott exciton is about 10 times the size of the lattice constant, and the binding energy is a few meV. The charge transfer exciton is an intermediate case between a Frenkel and a Wannier-Mott exciton, which usually extends to adjacent unit cells and has a static electric dipole moment.

In the mid-1950s, there was a common understanding among theorists that the physical properties of an exciton are strongly influenced by its coupling to external radiation fields. In a paper published in 1958, Solomon Pekar predicted *additional light waves* in the emission spectrum mediated by exciton states [41]. The term "polariton" later appeared independently in the works of John Hopfield [42] and Vladimir Agranovich [43]. A few years later, the existence of the exciton-polariton was verified in bulk semiconductor GaAs by nonlinear optical spectroscopy[44]. But up to that point, the excitons were formed in bulk samples, and the photons are distributed in continuous free space; therefore, the exciton-polaritons only left an elusive trace in optical properties of the bulk samples.

The development of nanostructure fabrication enabled the much-desired confinement of excitons and photons. In 1992, Claude Weisbuch claimed the first successful exciton-photon normal mode coupling[45]. The device known as microcavity was originally invented for vertical-cavity surface emission lasers (VCSELs), where the active region is sandwiched by two distributed Bragg reflectors (DBRs). Each reflector is formed from periodically stacked thin layers of dielectric materials or wide-gap semiconductors (see

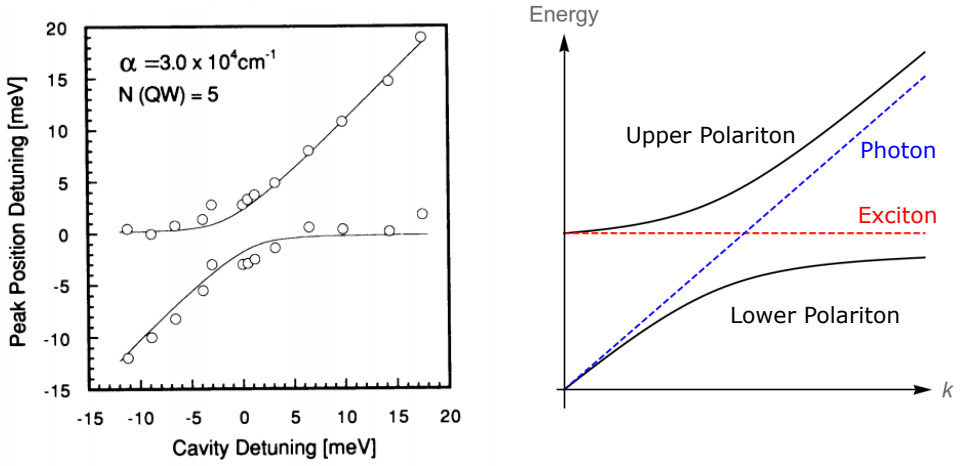

Figure 1.2: Weisbuch's experiment results compared to the theoretical prediction of linear coupling model. The calculation that generates these dispersion curves will be presented in section 2.5

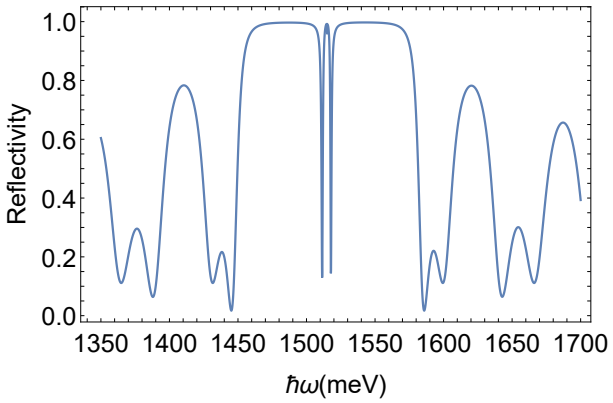

Figure 1.3: Reflection spectrum of a microcavity calculated based on typical parameters of GaAs, the double-dip in the center showing Rabi splitting is the experimental evidence sought after for strong coupling.

Figure 1.1). In a specially designed microcavity, only a specific longitudinal mode is resonant with the direct gap transition of the semiconductor; an efficient one-to-one normal mode coupling is thus made possible, resulting in a uniquely defined polariton as a free particle in 2D space.

Given the two-dimensional nature of cavity polariton, one could only explore a finite-size condensate at a length scale smaller than its Berezinskii–Kosterlitz–Thouless(BKT) transition [46], either by increasing polariton density locally by optical pumping [27], or by confining the polariton gas with a potential trap [47]. The following chapters will show how each condensing scheme can lead to a scenario of the Josephson effect, despite the different microscopic mechanisms.

Chapter 2

Microscopic Theory of Exciton-Polariton

The early theories of exciton-polaritons [42] [41] were developed assuming an effective continuous medium, where the macroscopic electric polarization **P** is treated as a part of the electromagnetic wave. This approach suffices for phenomena induced by the linear responses of semiconductors to external light waves, such as the additional frequency components in the reflection/absorption spectrum.

The main ideas of this dissertation involve the detailed engineering of the single-polariton state and nonlinear interaction effects, where the microscopic theories are crucial. Therefore, this chapter introduces the exciton, photon, and strong coupling mechanisms in first and second quantized formalisms. It is loosely based on [19] [20] with emphasis on polariton trapping and controlling methods, including a detailed discussion of electrical control via the exciton Stark effect incorporated in my original research work.

2.1 Exciton as Many-Body Excitation in Electron Gas

In real space, one can write down a Hamiltonian for an interacting electron gas in d dimensions. For convenience, define the background dielectric constant $\varepsilon_B = 4\pi\varepsilon_0\varepsilon_r$,

$$H_e = \int \hat{\Psi}^\dagger(\mathbf{r})\Big(-\frac{\hbar^2}{2m}\nabla^2 + V(\mathbf{r})\Big)\hat{\Psi}(\mathbf{r})d^d\mathbf{r} + \frac{1}{2}\iint \hat{\Psi}^\dagger(\mathbf{r})\hat{\Psi}^\dagger(\mathbf{r}')\frac{e^2}{\varepsilon_B|\mathbf{r}-\mathbf{r}'|}\hat{\Psi}(\mathbf{r}')\hat{\Psi}(\mathbf{r})d^d\mathbf{r}d^d\mathbf{r}'. \tag{2.1}$$

The field operator for electrons is defined as

$$\hat{\Psi}(\mathbf{r}) = \sum_{n=c,v}\sum_{\mathbf{k}} \phi_{n,\mathbf{k}}(\mathbf{r})\hat{e}_{n,\mathbf{k}} \tag{2.2}$$

where the Bloch wavefunction $\phi_{n,\mathbf{k}}(\mathbf{r}) = e^{i\mathbf{k}\cdot\mathbf{r}}u_{n,\mathbf{k}}(\mathbf{r})$ is an eigenstate of electron in the periodic crystal field, and $\hat{e}_{n,\mathbf{k}}$ is the corresponding fermionic annihilation operator. The relevant states in a semiconductor are the conduction(c) and valence(v) bands. The index for spin is absorbed in the band states as they already take into account the spin-orbital coupling corrections. The background dielectric constant ε_B is attributed to the ions formed by nuclei and deeply bounded electrons, which effectively weaken the Coulomb interaction among the excited electrons.

In the jellium model[19], the ions form a uniform background of positive charge, which gives an attractive potential acting on electrons, canceling out the long wavelength divergence in electron-electron interactions. Therefore, the total Hamiltonian of (2.1) can be Fourier transformed into momentum space.

$$\begin{aligned} H_e = &\sum_{n=c,v}\sum_{\mathbf{k}} E_{n\mathbf{k}}\hat{e}^\dagger_{n,\mathbf{k}}\hat{e}_{n,\mathbf{k}} + \frac{1}{2}\sum_{n=c,v}\sum_{\mathbf{k},\mathbf{k}',\mathbf{q}\neq 0} V_{\mathbf{q}}\hat{e}^\dagger_{n,\mathbf{k}+\mathbf{q}}\hat{e}^\dagger_{n,\mathbf{k}'-\mathbf{q}}\hat{e}_{n,\mathbf{k}'}\hat{e}_{n,\mathbf{k}} \\ &+ \sum_{\mathbf{k},\mathbf{k}',\mathbf{q}\neq 0} V_{\mathbf{q}}\hat{e}^\dagger_{c,\mathbf{k}+\mathbf{q}}\hat{e}^\dagger_{v,\mathbf{k}'-\mathbf{q}}\hat{e}_{v,\mathbf{k}'}\hat{e}_{c,\mathbf{k}} \end{aligned} \tag{2.3}$$

where the second term represents the intra-band interaction between electrons, and the

third term represents the inter-band interaction between electrons, which is responsible for forming excitons.

Using the fact that a hole is the absence of an electron, one can rewrite the Hamiltonian of (2.3) focusing on the inter-band Coulomb interaction.

$$H_{e-h} = \sum_{\mathbf{k}} \left(E_e(\mathbf{k}) \hat{e}^\dagger_{\mathbf{k}} \hat{e}_{\mathbf{k}} + E_h(\mathbf{k}) \hat{h}^\dagger_{\mathbf{k}} \hat{h}_{\mathbf{k}} \right) - \sum_{\mathbf{k},\mathbf{k}',\mathbf{q}\neq 0} V_{\mathbf{q}} \hat{e}^\dagger_{\mathbf{k}+\mathbf{q}} \hat{h}^\dagger_{-\mathbf{k}'-\mathbf{q}} \hat{h}_{-\mathbf{k}'} \hat{e}_{\mathbf{k}} \tag{2.4}$$

where the dispersion relation $\epsilon_{e/h}(\mathbf{k})$ can be found for conduction/valence band states with corrections arising from intra-band interactions, and $\hat{h}_{\mathbf{k}}$ is the fermionic annihilation operator for holes. In conventional semiconductors with a direct gap at the Γ point, the electrons and holes can be approximated by free particles with their effective masses $m_{e/h}$ and the energy offset ϵ_g extracted from band states,

$$E_e(\mathbf{k}) = E_g + \frac{(\hbar|\mathbf{k}|)^2}{2m_e}, \qquad E_h(\mathbf{k}) = \frac{(\hbar|\mathbf{k}|)^2}{2m_h} \tag{2.5}$$

Note that $\hat{e}_{\mathbf{k}} = \hat{h}^\dagger_{-\mathbf{k}}$ means annihilating an electron is equivalent to creating a hole in the opposite momentum, and the normal ordering of the $\hat{h}$ operators is reversed compared to the $\hat{e}$ operators, the interaction term thus takes a minus sign, which also agrees with the fact that the Coulomb potential between a electron and a hole is attractive.

Defining state vector $|\nu, \mathbf{K}\rangle$ as an exciton in bound orbital ν with the center of mass momentum $\mathbf{K}$, and $|0\rangle$ as the vacuum of the exciton(fermi sea), one can construct the exciton creation operator $\hat{b}^\dagger_{\nu\mathbf{K}} = |\nu, \mathbf{K}\rangle \langle 0|$ and expand it in the electron and hole momentum basis,

$$\hat{b}^\dagger_{\nu\mathbf{K}} = \sum_{\mathbf{k},-\mathbf{k}'} |\mathbf{k}, -\mathbf{k}'\rangle \langle \mathbf{k}, -\mathbf{k}'|\nu, \mathbf{K}\rangle \langle 0| \tag{2.6}$$

therefore it is a superposition of pair creating operators $|\mathbf{k}, -\mathbf{k}'\rangle \langle 0| = \hat{e}^\dagger_{\mathbf{k}} \hat{h}^\dagger_{-\mathbf{k}'}$ and the

associated coefficient is,

$$\begin{aligned}
\langle \mathbf{k}, -\mathbf{k}'|\nu, \mathbf{K}\rangle &= \int d^d\mathbf{r} \int d^d\mathbf{r}' \, \langle \mathbf{k}, -\mathbf{k}'|\mathbf{r}, \mathbf{r}'\rangle \, \langle \mathbf{r}, \mathbf{r}'|\nu, \mathbf{K}\rangle \\
&= \int d^d\mathbf{r} \int d^d\mathbf{r}' e^{-i\mathbf{k}\cdot\mathbf{r}} e^{i\mathbf{k}'\cdot\mathbf{r}'} e^{i\mathbf{K}\cdot\mathbf{R}} \psi_\nu(\mathbf{r}-\mathbf{r}') \\
&= \int d^d(\mathbf{r}-\mathbf{r}') e^{-i\mathbf{k}\cdot(\mathbf{r}-\mathbf{R})} e^{ik'\cdot(\mathbf{r}'-\mathbf{R})} \psi_\nu(\mathbf{r}-\mathbf{r}') \int d^d\mathbf{R} e^{i(\mathbf{K}-\mathbf{k}+\mathbf{k}')\cdot\mathbf{R}} \\
&= \psi_\nu\bigg(\Big(\frac{m_h}{m_e+m_h}\Big)\mathbf{k} + \Big(\frac{m_e}{m_e+m_h}\Big)\mathbf{k}'\bigg)\delta(\mathbf{K}-\mathbf{k}+\mathbf{k}'),
\end{aligned} \tag{2.7}$$

where $\mathbf{r}$ and $\mathbf{r}'$ are real space positions of the electrons and hole pair, $\mathbf{R} = \frac{m_e\mathbf{r}+m_h\mathbf{r}'}{m_e+m_h}$ is their center of mass position. In conventional semiconductors, the electrons and holes can be treated as free particles that satisfy equation (2.5), therefore the wavefunction $\psi_\nu(\mathbf{r}-\mathbf{r}')$ of the bound state known as an exciton can be written in analogy to the bound orbitals of a hydrogen atom, with the substitution of semiconductor parameters. By the following convention of Fourier transform and inverse transform,

$$f(\mathbf{k}) = \int d^d\mathbf{r} \; f(\mathbf{r}) e^{i\mathbf{k}\cdot\mathbf{r}}, \quad f(\mathbf{r}) = \frac{1}{(2\pi)^d} \int d^d\mathbf{k} \; f(\mathbf{k}) e^{-i\mathbf{k}\cdot\mathbf{r}}, \tag{2.8}$$

The exciton orbital wavefunction can be written in the generalized momentum coordinates.

$$\tilde{\mathbf{k}} = \Big(\frac{m_h}{m_e+m_h}\Big)\mathbf{k} + \Big(\frac{m_e}{m_e+m_h}\Big)\mathbf{k}' \tag{2.9}$$

Finally, the exciton operator as a summation in momentum space can be simplified as,

$$\begin{aligned}
\hat{b}^\dagger_{\nu\mathbf{K}} &= \sum_{\mathbf{k},\mathbf{k}'} \psi_\nu\bigg(\Big(\frac{m_h}{m_e+m_h}\Big)\mathbf{k} + \Big(\frac{m_e}{m_e+m_h}\Big)\mathbf{k}'\bigg)\delta(\mathbf{K}-\mathbf{k}+\mathbf{k}')\hat{e}^\dagger_{\mathbf{k}}\hat{h}^\dagger_{-\mathbf{k}'} \\
&= \sum_{\mathbf{k}} \psi_\nu\left(\mathbf{k} - \frac{m_e}{m_e+m_h}\mathbf{K}\right)\hat{e}^\dagger_{\mathbf{k}}\hat{h}^\dagger_{\mathbf{K}-\mathbf{k}}
\end{aligned} \tag{2.10}$$

In a Wannier-Mott exciton, the electron and hole inherit the effective mass from their band states, which are usually asymmetric in conventional zinc-blende and würtzite semiconductors. In 2D materials, for example the transition metal dichalcogenides, one may find effective masses closer to ideal "particle-hole" symmetry, with non-zero crystal

momentum $\mathbf{K}$ near the band gap, hence the exciton creation operator,

$$\hat{b}^{\dagger}_{\nu\mathbf{K}} = \sum_{\mathbf{k}} \psi_{\nu}(\mathbf{k} - \mathbf{K}/2)\hat{e}^{\dagger}_{\mathbf{k}}\hat{h}^{\dagger}_{\mathbf{K}-\mathbf{k}} \tag{2.11}$$

In the new notation, one can write the Hamiltonian for excitons as,

$$H_{\text{exc}} = \sum_{\nu,\mathbf{K}} E_{\nu\mathbf{K}}\ \hat{b}^{\dagger}_{\nu\mathbf{k}}\hat{b}_{\nu\mathbf{K}} \tag{2.12}$$

where $E_{\nu\mathbf{K}} = E_{\nu} + \frac{(\hbar|\mathbf{K}|)^2}{2(m_e+m_h)}$ stands for the energy needed to excite such an exciton from the zero-temperature fermi sea of electrons.

The commutation relation of this exciton operator can be evaluated as follows,

$$\begin{aligned}
\left[\hat{b}_{\nu\mathbf{K}}, \hat{b}^{\dagger}_{\nu\mathbf{K}}\right] &= \sum_{\mathbf{k},\mathbf{q}} \psi^{*}_{\nu}(\mathbf{q},\mathbf{K})\psi_{\nu}(\mathbf{k},\mathbf{K})\left[\hat{h}_{\mathbf{K}-\mathbf{q}}\hat{e}_{\mathbf{q}}, \hat{e}^{\dagger}_{\mathbf{k}}\hat{h}^{\dagger}_{\mathbf{K}-\mathbf{k}}\right] \\
&= \sum_{\mathbf{k},\mathbf{q}} \psi^{*}_{\nu}(\mathbf{q},\mathbf{K})\psi_{\nu}(\mathbf{k},\mathbf{K})\left(1 - \hat{h}^{\dagger}_{\mathbf{K}-\mathbf{k}}\hat{h}_{\mathbf{K}-\mathbf{q}} - \hat{e}^{\dagger}_{\mathbf{k}}\hat{e}_{\mathbf{q}}\right) \\
&= \sum_{\mathbf{k}} |\psi_{\nu}(\mathbf{k},\mathbf{K})|^2\left(1 - \hat{h}^{\dagger}_{\mathbf{K}-\mathbf{k}}\hat{h}_{\mathbf{K}-\mathbf{k}} - \hat{e}^{\dagger}_{\mathbf{k}}\hat{e}_{\mathbf{k}}\right)
\end{aligned} \tag{2.13}$$

Because ψ_{ν} is a normalized single exciton orbital wavefunction, and the density of excited electrons and holes is sufficiently low, $\left\langle [\hat{b}_{\nu\mathbf{K}}, \hat{b}^{\dagger}_{\nu\mathbf{K}}] \right\rangle \approx 1$ is satisfied, therefore the exciton is considered as a bosonic quasi-particle in common physical scenarios.

2.2 Quasi-2D State of Quantum Well Excitons

Although the theory of excitons presented above is general and applies to any dimensionality, this dissertation focuses on 2D quantum fluid formed by exciton-photon strong coupling, and the quasi-2D excitons confined in quantum wells are an essential part of their composition . [20].

Starting with the Hamiltonian for an electron and a hole in the presence of the con-

finement potential, one could write down the time-independent Schrödiger equation,

$$\left(-\frac{\hbar^2}{2m_e}\nabla^2_{\mathbf{q_e}} - \frac{\hbar^2}{2m_h}\nabla^2_{\mathbf{q_h}} + V_e(z_e) + V_h(z_h) - \frac{e^2}{\varepsilon_B|\mathbf{q_e} - \mathbf{q_h}|}\right)\Psi = E\Psi \tag{2.14}$$

where the potential function $V_e(z_e)$ and $V_h(z_h)$ only vary along the z-direction perpendicular to the plane of active semiconducting layer, which can be modeled as a quantum well; the effective mass m_e/m_h is derived from the dispersion relation in the conduction/valence band, and ε_B is the dielectric constant of the material forming this quantum well.

Separating the z-direction as $\mathbf{q} = (\mathbf{r}, z)$ so that $\mathbf{r}$ is the in-plane position vector, and adopting the following coordinate system in 2-D,

$$\mathbf{R} = \frac{m_e\mathbf{r_e} + m_h\mathbf{r_h}}{m_e + m_h}, \quad \mathbf{r} = \mathbf{r_e} - \mathbf{r_h} \tag{2.15}$$

An ansatz for the state of interest can be expressed as,

$$\Psi(\mathbf{r_e}, \mathbf{r_h}) \approx F(\mathbf{R})\phi(\mathbf{r})f_e(z_e)f_h(z_h) \tag{2.16}$$

where the separated wavefunctions are normalized, respectively. Because $\mathbf{R}, \mathbf{r}$ and z are not exactly separable, in general one should get a summation of orthogonal functions of z as the 1D bound states of the quantum well, each multiplied by its corresponding center of mass function $\psi(\mathbf{R})$ and orbital function $\phi(\mathbf{r})$. But in practice, the energy difference between the ground state and the first excited state of a narrow quantum well is large enough (order of 0.1-1 eV) so that the z degree of freedom is not excited for either the electron or the hole; therefore it is a valid approximation to only consider the "channel" that $f_e(z_e)$ and $f_h(z_h)$ are in their 1D ground states.

Inserting the wave function into the Schrödinger equation, applying $F^*(\mathbf{R})$ to the left of equation(2.14), and integrating over $\mathbf{R}$, one should get a equation in the new

coordinates,

$$\Big(-\frac{\hbar^2}{2m_e}\frac{\partial^2}{\partial z_e^2} - \frac{\hbar^2}{2m_h}\frac{\partial^2}{\partial z_h^2} - \frac{\hbar^2}{2m}\nabla_{\mathbf{r}}^2 + V_e(z_e) + V_h(z_h) - \frac{e^2}{\varepsilon_B\sqrt{\mathbf{r}^2+(z_e-z_h)^2}}\Big) \phi(\mathbf{r})f_e(z_e)f_h(z_h) = (E - E_{\text{com}})\phi(\mathbf{r})f_e(z_e)f_h(z_h) \tag{2.17}$$

where the center of mass kinetic energy $E_{\text{com}} = \frac{P^2}{2M}$ is subtracted off, leaving behind a 2-body problem of reduced mass m in relative coordinates $\mathbf{r}$.

To extract the z-dependent part of the electron wavefunction, one can apply $\phi^*(\mathbf{r})f_h^*(z_h)$ to the left of equation(2.17) and integrate over $\mathbf{r}$ and z_h.

$$\Big(-\frac{\hbar^2}{2m_e}\frac{d^2}{dz_e^2} + V_e(z_e) - \frac{e^2}{\varepsilon_B}\iint \frac{|\phi(\mathbf{r})|^2|f_h(z_h)|^2}{\sqrt{\mathbf{r}^2+(z_e-z_h)^2}}\, d\mathbf{r}\, dz_h\Big) f_e(z_e) = E_e f_e(z_e) \tag{2.18}$$

The z-dependent part of the hole wavefunction can be obtained in the same manner.

To extract the equation in the 2D space parallel to the plane, one can apply $f_e^*(z_e)f_h^*(z_h)$ to the left of (2.17) and integrate over z_e and z_h,

$$\Big(-\frac{\hbar^2}{2m}\nabla_{\mathbf{r}}^2 - \frac{e^2}{\varepsilon_B}\iint \frac{|f_e(z_e)|^2|f_h(z_h)|^2}{\sqrt{\mathbf{r}^2+(z_e-z_h)^2}}\, dz_e dz_h\Big)\phi(\mathbf{r}) = -E^{QW}\phi(\mathbf{r}) \tag{2.19}$$

where $E^{QW} > 0$ is the binding energy of the electron-hole pair in the quantum well.

In the limit $|\phi_{e,h}(z_{e,h})|^2 \to \delta(z_{e,h})$, it reduces to the Schrödinger equation for in the ideal 2D space,

$$\Big(-\frac{\hbar^2}{2m}\nabla_{\mathbf{r}}^2 - \frac{e^2}{\varepsilon_B}\frac{1}{r}\Big)\phi(\mathbf{r}) = E\phi(\mathbf{r}) \tag{2.20}$$

which is essentially a 2D hydrogen atom model(2.D) with parameters for semiconductor excitons. The bound states have discrete energy levels labeled by a principal quantum number n.

$$E_n^{2D} = -\frac{1}{2(n-\frac{1}{2})^2}\frac{me^4}{\varepsilon_B^2\hbar^2} \tag{2.21}$$

and the wavefunction in general are labeled by n and an angular quantum number l,

$$\phi_{nl}(r,\theta) = R_{nl}(r)\Theta_l(\theta) \tag{2.22}$$

In the ground state $n = 1, l = 0$,

$$\phi_{10}(\rho) = \sqrt{\frac{2}{\pi}}\frac{1}{a_x}\exp\left(-r/a_x\right), \tag{2.23}$$

where $a_x = \varepsilon_B\hbar^2/2me^2$ the "Bohr radius" of this 2D system.

This implies the binding is tighter in the 2D system; unsurprisingly, its ground state energy,

$$E_{10} = -\frac{\hbar^2}{2ma_x^2} = -2\frac{me^4}{\varepsilon_B^2\hbar^2} \tag{2.24}$$

is equal to four times the ground state energy of the 3D system.

The binding energy of a real system varies between the ideal 2D and 3D cases as one tunes the thickness of the quantum well, which can be estimated using a variational method. Assume a separable trial wavefunction with the 2D part.

$$\tilde{\phi}_a(r) = \sqrt{\frac{2}{\pi}}\frac{1}{a}\exp(-r/a) \tag{2.25}$$

and apply it to the exact expression in Eq.(2.19), the bound state energy can be estimated as,

$$E^L(a) = -\frac{\hbar^2}{2ma^2} - \frac{e^2}{\varepsilon_B}\iiint \frac{|\tilde{\phi}_a(r)|^2|f_e^L(z_e)|^2|f_h^L(z_h)|^2}{\sqrt{r^2+(z_e-z_h)^2}}2rdrdz_edz_h \tag{2.26}$$

This integral depends on the tuning parameter L, which represents the thickness of the quantum well, and the variational parameter a, which represents the "Bohr radius" of 2D exciton. For every L, one can search for the a that minimizes the bound state energy($E_L(a) < 0$). The trial function with the optimal a is considered a good approximation of the exact wavefunction. By comparing the results of different L, one can find a good range for the thickness of the quantum well such that the excitons are strongly bound and hence protected from thermal fluctuations in the electron gas.

With the 2D exciton orbitals defined, we could write down envelope wavefunction for the center of mass in terms of separable coordinates $\mathbf{Q} = (\mathbf{R}, Z)$.

$$F(\mathbf{R}, Z) = \sqrt{\frac{2}{L_{\mathrm{QW}}}}\sin\left(\frac{\pi(Z-Z_0)}{L_{\mathrm{QW}}}\right)\frac{e^{i\mathbf{K}\cdot\mathbf{R}}}{\sqrt{\mathcal{A}}} \tag{2.27}$$

In microcavity design, it is common to have multiple quantum wells, each with a different center Z_0 placed at one of the anti-nodes of the cavity photon mode. The result is an overall quasi-2D state of exciton with enhanced coupling to the photon mode.

2.3 Quantization of Electromagnetic Field

In quantum mechanics, light-matter interaction is usually described by a non-relativistic Hamiltonian. A compatible canonical quantization scheme for the electromagnetic field is summarized as follows.

From the standard Lagrangian of quantum electrodynamics, identify the part attributed to the free electromagnetic field.

$$\mathcal{L} = \frac{1}{2}\varepsilon \mathbf{E}^2 - \frac{1}{2\mu_0}\mathbf{B}^2 \tag{2.28}$$

where $\varepsilon = \varepsilon_0 \varepsilon_r$ takes into account an isotropic, dielectric, non-magnetic background medium inside the host material.

With the substitution of scalar and vector potentials,

$$\mathbf{B} = \nabla \times \mathbf{A}, \quad \mathbf{E} = -\nabla\phi - \frac{\partial \mathbf{A}}{\partial t} \tag{2.29}$$

The Lagrangian density in real space is,

$$\mathcal{L}[\mathbf{A}, \dot{\mathbf{A}}, \phi, \dot{\phi}] = \frac{1}{2}\varepsilon\big(- \nabla\phi(\mathbf{r}) - \dot{\mathbf{A}}(\mathbf{r}, t)\big)^2 - \frac{1}{2\mu_0}(\nabla \times \mathbf{A}(\mathbf{r}, t))^2 \tag{2.30}$$

By the spatial Fourier transformation,

$$\begin{aligned} \mathcal{A}(\mathbf{k}, t) &= \frac{1}{(2\pi)^{3/2}} \int d^3\mathbf{r}\ \mathbf{A}(\mathbf{r}, t) e^{-i\mathbf{k}\cdot\mathbf{r}} \\ \varphi(\mathbf{k}, t) &= \frac{1}{(2\pi)^{3/2}} \int d^3\mathbf{r}\ \phi(\mathbf{r}, t) e^{-i\mathbf{k}\cdot\mathbf{r}} \end{aligned} \tag{2.31}$$

one can write the Lagrangian density in $\mathbf{k}$ space in terms of general coordinates as paired complex conjugate, with the additional constraint $\mathcal{A}(\mathbf{k}) = \mathcal{A}^*(-\mathbf{k}),\ \phi(\mathbf{k}) = \phi^*(-\mathbf{k})$.

The derivatives with respect to $\mathcal{A}^*(\mathbf{k})$,

$$\frac{\partial \mathcal{L}}{\partial \mathcal{A}^*{}_i} = \varepsilon[\mathbf{k} \times (\mathbf{k} \times \mathcal{A})]_i, \quad \frac{\partial \mathcal{L}}{\partial \dot{\mathcal{A}}_i^*} = \varepsilon[\dot{A}_i + \mathrm{i}k_i\varphi] \tag{2.32}$$

lead to the Euler-Lagrangian equation,

$$\varepsilon[\ddot{\mathcal{A}}_i + \mathrm{i}k_i\dot{\varphi}] = -\varepsilon[\mathrm{i}\mathbf{k} \times (\mathrm{i}\mathbf{k} \times \mathcal{A})]_i \tag{2.33}$$

which is essentially the Ampere-Maxwell equation,

$$\nabla \times \mathbf{B} = \varepsilon \frac{\partial \mathbf{E}}{\partial t} \tag{2.34}$$

Canonical quantization requires each Cartesian component of the dynamical variables $A_i, i \in \{x, y, x\}$ be uniquely defined, therefore the potentials are fixed in the Coulomb gauge $\nabla \cdot \mathbf{A} = 0,\ \phi = 0$, and only the Laplancian operator in $\nabla \times (\nabla \times \mathbf{A}) = \nabla(\nabla \cdot \mathbf{A}) - \nabla^2 \mathbf{A}$ is kept for the transverse electromagnetic(TEM) modes. Equation (2.34) eventually leads to,

$$\nabla^2 \mathbf{A} - \frac{\varepsilon_c}{c^2} \frac{\partial^2 \mathbf{A}}{\partial t^2} = 0 \tag{2.35}$$

Separating the solution to equation (2.35) into positive and negative frequency components,

$$\mathbf{A}(\mathbf{r}, t) = \mathbf{A}^{+}(\mathbf{r}, t) + \mathbf{A}^{(-)}(\mathbf{r}, t) \tag{2.36}$$

where

$$\mathbf{A}^{(+)}(\mathbf{r}, t) = \sum_{\kappa} c_\kappa \mathbf{u}_\kappa(\mathbf{r}) e^{-i\omega_\kappa t}, \quad \mathbf{A}^{(-)} = \left(\mathbf{A}^{(+)}\right)^* \tag{2.37}$$

The spatial dependent part, each labeled by mode index κ, is a solution of the Helmholtz equation,

$$\left(\nabla^2 + \frac{\varepsilon_r \omega_\kappa^2}{c^2}\right) \mathbf{u}_\kappa(\mathbf{r}) = 0 \tag{2.38}$$

A quantized vector potential can be expanded in the spatial modes,

$$\hat{\mathbf{A}}(\mathbf{r},t)=\sum_{\kappa}\Big(\frac{\hbar}{2\varepsilon\omega_{\kappa}}\Big)^{1/2}\big(\hat{a}_{\kappa}\mathbf{u}_{\kappa}(\mathbf{r})e^{-i\omega_{\kappa}t}+\hat{a}_{\kappa}^{\dagger}\mathbf{u}_{\kappa}^{*}(\mathbf{r})e^{i\omega_{\kappa}t}\big) \tag{2.39}$$

and the corresponding electric field is,

$$\hat{\mathbf{E}}(\mathbf{r},t)=i\sum_{\kappa}\Big(\frac{\hbar\omega_{\kappa}}{2\varepsilon}\Big)^{1/2}\big(\hat{a}_{\kappa}\mathbf{u}_{\kappa}(\mathbf{r})e^{-i\omega_{\kappa}t}-\hat{a}_{\kappa}^{\dagger}\mathbf{u}_{\kappa}^{*}(\mathbf{r})e^{i\omega_{\kappa}t}\big) \tag{2.40}$$

where the dimensionless operators obey boson commutation relations,

$$[\hat{a}_{\kappa},\hat{a}_{k'}]=[\hat{a}_{\kappa}^{\dagger},\hat{a}_{k'}^{\dagger}]=0,\quad [\hat{a}_{\kappa},\hat{a}_{k'}^{\dagger}]=\delta_{kk'} \tag{2.41}$$

From the Lagrangian(2.30), the canonical momentum conjugate to $\mathbf{A}$ can be derived as,

$$\Pi_i=\frac{\partial\mathcal{L}}{\partial(\frac{\partial A_i}{\partial t})}=-\varepsilon E_i,\quad i\in\{x,y,z\}, \tag{2.42}$$

and the commutation relation

$$[A_i(\mathbf{r},t),\Pi_j(\mathbf{r}',t')]=i\hbar\ \delta_{ij}\ \delta^{(3)}(\mathbf{r}-\mathbf{r}')\ \delta(t-t') \tag{2.43}$$

is satisfied. Therefore, the quantization of the electromagnetic field can be rigorously defined in terms of $\mathbf{A}$ and $\mathbf{\Pi}=-\varepsilon\mathbf{E}$.

The total Hamiltonian of the quantized field can be evaluated as a summation of all spatial modes,

$$H=\sum_{\kappa}\hbar\omega_{\kappa}\big(\hat{a}_{\kappa}^{\dagger}\hat{a}_{\kappa}+\frac{1}{2}\big) \tag{2.44}$$

while the fluctuations in the field are represented by the creation and annihilation of a type of bosonic particles called “photons”.

2.4 Photon Modes in Microcavity

The solution of equation (2.38) depends on the boundary conditions, and the distinct solutions for a specific cavity are regarded as the cavity photon modes. In conventional open cavities, the distance between the two mirrors is much longer than the wavelength of light; therefore, the propagation of light is treated as a Fresnel-Kirchhoff(scalar field) diffraction problem, and an integral equation is formulated in search of the "self-reproducing mode," that is, a specific periodic boundary condition where the stationary distribution in the plane perpendicular to the optical axis is maintained through each optical cycle. Analytical solutions in general exist for stable cavities (rays confined in the geometric optics limit) in the form of orthonormal special functions, for example, Hermite-Gaussian modes in square confocal cavities and Laguerre-Gaussian modes in circular confocal cavities[48].

A Fabry-Perot cavity formed by two parallel mirrors is an unstable cavity, where rays diverge in the geometric optics limit. In the limit of infinite surface area, any transverse electromagnetic wave can exist in the cavity as long as it satisfies,

$$r\mathrm{e}^{ik_\perp L_c} = \pm 1 \tag{2.45}$$

where r is the reflection coefficient of a single mirror, $k_\perp$ is the wavevector perpendicular to the mirror surface, and L_c is the cavity thickness measured against the inner side of the mirrors. However, diffraction on finite-size mirrors can transform a plane wavefront into a curved wavefront after multiple optical cycles; therefore, a "stationary mode" still exists for this unstable cavity, which can be found by numerical iterations and verified by experiments[48].

A planar microcavity is an extremely small Fabry-Perot cavity, where the semiconducting and dielectric inserts are sandwiched between a pair of parallel distributed Bragg reflectors(DBRs). The wavelength of light resonating with the semiconductor is comparable to the thickness of the cavity; therefore, the "stationary mode" found by the far-field diffraction approach is inappropriate. Instead, optical modes can be described in the plane wave basis, knowing that the total wavevector $k = \sqrt{k_\perp^2 + k_\parallel^2}$ can be de-

composed into a well-defined perpendicular component $k_\perp$ and a continuously varying in-plane component $k_\parallel$.

The cavity photon energy can be expanded in a Taylor series near $k_\parallel/k_\perp \approx 0$,

$$E_{\text{pho}}(k_\parallel) = \frac{\hbar c k_\perp}{n_c}\left(1 + \frac{k_\parallel^2}{2k_\perp^2} + \cdots\right) \approx E_{\text{pho}}(k_\parallel = 0) + \frac{\hbar^2 k_\parallel^2}{2m_{\text{pho}}} \tag{2.46}$$

This means at small oblique angles, the photon mode can be approximated as a free particle in a 2D space, where

$$E_{\text{pho}}(0) = \frac{\hbar c k_\perp}{n_c}, \quad m_{\text{pho}} = \frac{n_c \hbar k_\perp}{c} \tag{2.47}$$

are its "potential energy" and "effective mass", respectively, and $n_c = \sqrt{\varepsilon_c}$ is the index of refraction for the material inserted in the cavity, implying a reduced speed of light.

Therefore, the complete photon mode in 3D space can be described by a wavefunction,

$$\mathbf{u}_\lambda(\mathbf{r}_\parallel, z) = \sqrt{\frac{2}{L_c}} \sin\left(\frac{n\pi z}{L_c}\right) \frac{e^{i\mathbf{k}_\parallel \cdot \mathbf{r}_\parallel}}{\sqrt{\mathcal{A}}} \mathbf{e}^{(\lambda)} \tag{2.48}$$

where the perpendicular wavevector takes value $\mathbf{k}_\perp = n\pi/L_c,\ n \in \mathbb{Z}^+$ for standing waves between the two reflectors, which can be loosely defined as the "longitudinal mode", and $\mathbf{e}^{(\lambda)}$ is a unit vector with $\lambda = 1, 2$ labeled for two orthogonal optical polarizations. The plane wave phase factor describes the cavity photons as free particles in the 2D space, and the area $\mathcal{A}$ guarantees the single photon state is normalized for a finite-size system. The smallest choice of cavity thickness is half of the optical wavelength($L_C = \lambda/2$) that energetically resonates with the exciton. It is also common to choose a large thickness, where the standing wave has multiple antinodes between the reflectors, each overlapping with an active layer, resulting in a quasi-2D state with enhanced coupling to excitons. In either case, the thickness of the cavity determines the effective potential energy possessed by a 2D photon.

A slightly altered geometry of the planar cavity can be treated as a perturbation to the cavity photon mode. For example, the "mesa" geometry [49] as a local variation in the

cavity thickness alters the potential energy landscape of the 2D photon. In comparison, a micropillar cavity combines the geometric elements of a cylindrical waveguide with the planar cavity, resulting in two types of eigenmodes[20]. The "guided modes" in the limit $k_\perp \geq \omega/c$ propagate on the cylindrical walls have partially longitudinal electromagnetic fields. Only the "Fabry-Perot modes" in the limit $0 \leq k_\perp \leq \omega/c$ are completely TEM fields that can be properly quantized as cavity photons. The additional tight confinement in 2D space results in a set of bound states with vastly discrete energy levels, among them only a few can couple to excitons. Later chapters will revisit this topic and emphasize the consequences of choosing different geometries for polariton junctions.

2.5 Strong Coupling and Exciton Polaritons

In previous sections, the 2D states of excitons and photons are rigorously derived for the specific confining geometry of planar microcavities. Combining them, one can write down the system Hamiltonian in a 2D momentum space,

$$H = \sum_{\mathbf{k}} \left(\hat{b}^\dagger_{\mathbf{k}}, \hat{a}^\dagger_{\mathbf{k}} \right) \begin{pmatrix} E_{\mathrm{ex}}(\mathbf{k}) & \Omega(\mathbf{k}) \\ \Omega(\mathbf{k}) & E_{\mathrm{ph}}(\mathbf{k}) \end{pmatrix} \begin{pmatrix} \hat{b}_{\mathbf{k}} \\ \hat{a}_{\mathbf{k}} \end{pmatrix} \tag{2.49}$$

where the bosonic operator defined as $\hat{a}$ for the photon, $\hat{b}$ for exciton, and the in-plane wavevectors span the 2-D $\mathbf{k}$ space. In the rotating wave approximation, the "counter-rotating" terms $\hat{a}\hat{b}$ and $\hat{b}^\dagger\hat{a}^\dagger$ are neglected; the remaining Hamiltonian should give rise to new normal modes via linear coupling. The energy dispersion relations of exciton and photon are given as,

$$E_{\mathrm{ex}}(\mathbf{k}) = E_{\mathrm{ex}}(0) + \frac{\hbar^2 k^2}{2m_{\mathrm{ex}}}, \quad E_{\mathrm{ph}}(\mathbf{k}) = E_{\mathrm{ph}}(0) + \frac{\hbar^2 k^2}{2m_{\mathrm{ph}}}$$

, which are plotted in Fig.2.1 as dashed parabolas, showing the large difference in effect mass between exciton($\sim 10^{-1} m_0$) and photon($\sim 10^{-5} m_0$), where m_0 is the mass of a bare electron. A rigorous derivation of coupling strength $\Omega(\mathbf{k})$ can be discussed in the appendix

based on [19, 50]. The variation of photon energy along a small in-plane component is negligible compared to the constant offset; therefore, we can replace the function with a constant $\Omega \approx \Omega(\mathbf{k} = 0)$.

In the strong-coupling limit, the normal modes are found following a Hopfield transformation,

$$\begin{pmatrix} \hat{P}_{\mathbf{k}} \\ \hat{Q}_{\mathbf{k}} \end{pmatrix} = \begin{pmatrix} X_{\mathbf{k}} & C_{\mathbf{k}} \\ -C_{\mathbf{k}} & X_{\mathbf{k}} \end{pmatrix} \begin{pmatrix} \hat{b}_{\mathbf{k}} \\ \hat{a}_{\mathbf{k}} \end{pmatrix} \tag{2.50}$$

where $\hat{P}_{\mathbf{k}}, \hat{Q}_{\mathbf{k}}$ are annihilation operators for lower polariton(LP) and upper polariton(UP), respectively, $X_{\mathbf{k}}$ and $C_{\mathbf{k}}$ are complex amplitudes of exciton and photon in the composition of a polariton, named as "Hopfield coefficients" after the original 1958 paper[42].

The unitary condition $|X_{\mathbf{k}}|^2 + |C_{\mathbf{k}}|^2 = 1$, $-X_{\mathbf{k}}C_{\mathbf{k}}^* + C_{\mathbf{k}}X_{\mathbf{k}}^* = 0$ are satisfied, so that the polariton operators $P_{\mathbf{k}}, Q_{\mathbf{k}}$ obey the bosonic commutation relations. One can choose real-valued coefficients

$$X_{\mathbf{k}} = \sqrt{\frac{1}{2}\left(1 + \frac{\Delta_{\mathbf{k}}}{\sqrt{\Delta_{\mathbf{k}}^2 + 4\Omega^2}}\right)}, \quad C_{\mathbf{k}} = \sqrt{\frac{1}{2}\left(1 - \frac{\Delta_{\mathbf{k}}}{\sqrt{\Delta_{\mathbf{k}}^2 + 4\Omega^2}}\right)},$$

where $\Delta_{\mathbf{k}} = E_{\mathrm{ph}}(\mathbf{k}) - E_{\mathrm{ex}}(\mathbf{k})$, the detuning is usually defined as $\Delta_{\mathbf{k}=0}$.

The Hamiltonian in Eq.(2.49) can be rewritten in the polariton basis,

$$H = \sum_{\mathbf{k}} \begin{pmatrix} \hat{P}_{\mathbf{k}}^\dagger & \hat{Q}_{\mathbf{k}}^\dagger \end{pmatrix} \begin{pmatrix} E_{\mathrm{LP}}(\mathbf{k}) & 0 \\ 0 & E_{\mathrm{UP}}(\mathbf{k}) \end{pmatrix} \begin{pmatrix} \hat{P}_{\mathbf{k}} \\ \hat{Q}_{\mathbf{k}} \end{pmatrix} \tag{2.51}$$

where the dispersion relations,

$$E_{\mathrm{LP(UP)}}(\mathbf{k}) = \frac{1}{2}\Big\{E_{\mathrm{ex}}(\mathbf{k}) + E_{\mathrm{ph}}(\mathbf{k}) - (+)\sqrt{4\Omega^2 + \Delta_{\mathbf{k}}^2}\Big\} \tag{2.52}$$

are plotted as the colored curves in Fig.2.1, showing the exciton/photon fraction for the zero-detuning case.

In a real physical scenario, excitons and photons interact with their environment and have finite lifetimes. Photons leak out of the cavity due to partial reflecting/transmitting

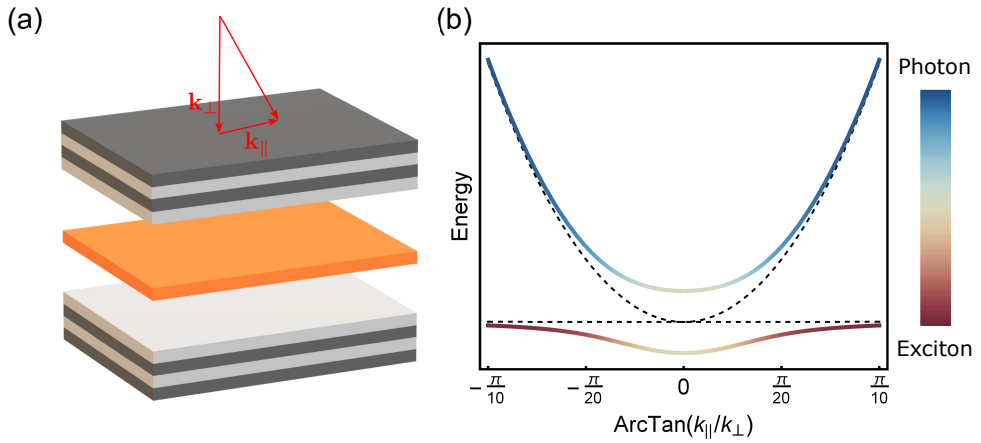

Figure 2.1: Plannar cavity and polariton dispersion relation (a) Schematics of a planner cavity and definition of wavevectors, the alternating grey layers symbolically represent(repeat 10-20 times) the distributed Bragg reflectors, the orange layer represents the quantum well confining the 2D exciton, the space between each reflector and the quantum well is filled with dielectric material or wide gap semiconductors (b) Typical energy dispersions of cavity polariton along in-plane momentum of incident light $k_\parallel$. Upper and lower polariton branches are formed due to strong exciton-photon hybridization at $k_\parallel = 0$. The color codes of the lower (upper) branch represent the weight of exciton (photon).

and imperfection diffractions at the reflectors, and excitons can decay through non-radiative mechanisms even though the radiative decay is suppressed by strongly coupling to the cavity photons.

In the simplest case, the fluctuation in the exciton/photon amplitude induced by the environment is a Markov process, which can be modeled with a pair of coupled quantum Langevin equations, in other words, the Heisenberg equations of motion for the annihilation operators with stochastic noise arising from the environment,

$$\begin{aligned} i\hbar\frac{\mathrm{d}\hat{b}}{\mathrm{d}t} &= E_{\mathrm{ex}}\hat{b} + \Omega\hat{a} + i\gamma_{\mathrm{ex}}\hat{b} + F_{\mathrm{ex}} \\ i\hbar\frac{\mathrm{d}\hat{a}}{\mathrm{d}t} &= E_{\mathrm{ph}}\hat{a} + \Omega\hat{b} + i\gamma_{\mathrm{ph}}\hat{a} + F_{\mathrm{ph}} \end{aligned} \tag{2.53}$$

where Ω is the overall coupling strength integrated over a localized wavepacket in the 2D space, γ_{ex} indicates non-radiative decay of excitons and γ_{ph} indicates the loss of cavity photon due to partial transmission and imperfect diffraction at the reflectors; the noise terms $F_{\mathrm{ex/ph}}$ are required in order to preserve the commutation relations for $\hat{a}/\hat{b}$ but negligible in the calculation of the spectrum. The coupled modes of finite lifetime can be

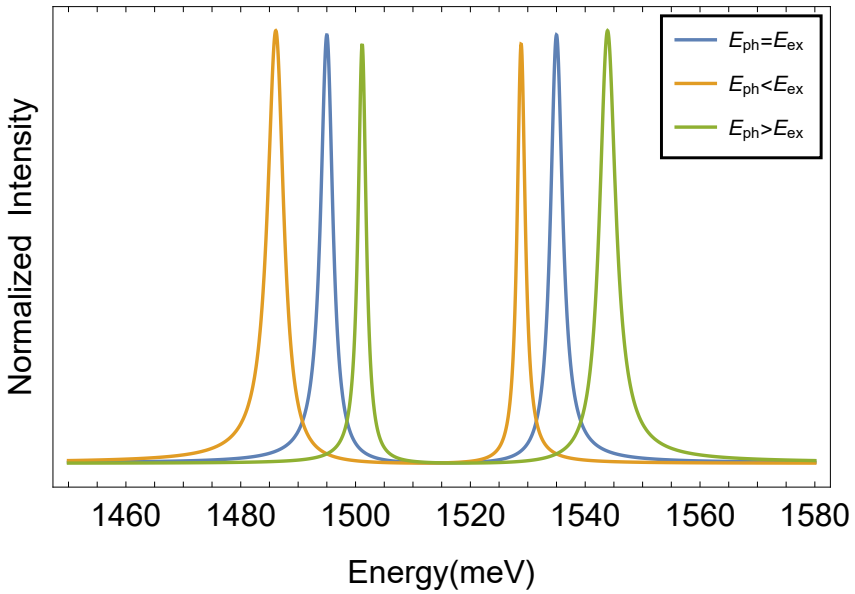

Figure 2.2: The power spectrum of polariton emission calculated based on Eq.(2.54) and typical parameters of GaAs

described with complex energy eigenvalues,

$$E_{\pm} = \frac{1}{2}\Big\{[E_{\rm ex} + E_{\rm ph} + i(\gamma_{\rm ph} + \gamma_{\rm ex}) \pm \sqrt{4\Omega^2 + [E_{\rm ex} - E_{\rm ph} + i(\gamma_{\rm ph} - \gamma_{\rm ex})]^2}\Big\} \tag{2.54}$$

which means the quantum state of the coupled exciton and photon evolves at a frequency determined by its real part and decays at a rate determined by its imaginary part.

In the limit $\Omega \gg (\gamma_{\rm ph} - \gamma_{\rm ex})/2$, a power spectrum of emitted photons can be calculated from the complex-valued eigenmodes, where the Rabi-Splitting of the real-valued closed system is reproduced along with the Lorentzian lineshapes arising from the finite lifetimes, therefore this limit is known as the strong-coupling condition. A typical microcavity exciton-polariton system usually has $\gamma_{\rm ex} \ll \gamma_{\rm ph} \ll \Omega$, meaning the lifetime of a polariton is determined by its photon component. In comparison, semiconductor lasers can have a similar cavity structure, but work in the weak coupling limit $\gamma_{\rm ph} \gg \Omega$, where the photons do not strongly couple back to the semiconductor but rather strongly radiate in a single mode.

It is also noteworthy that potential disorder and thermal fluctuation are inevitable in real semiconductors, therefore the exciton potential energy $E_{\rm ex}$ and decay $\gamma_{\rm ex}$ can vary over a small distance($\sim 10^0 - 10^1 nm$), often resulting in the inhomogeneous broadening

of absorption and photoluminescence spectrum. However, in the strong coupling limit of microcavities, the excitons are coupled to a photon mode with an extended coherence length($\sim 10^2 nm$) in the 2D space, therefore the lifetime is determined by the relatively homogeneous γ_{ph}, and hence result in the Lorantizan lineshape in the power spectrum. This is known as the "motional narrowing" effect of exciton-polaritons [20, 51], even though it is more of a spatial-averaging effect than the true motional-averaging effect in nuclear magnetic resonance. This effect gives an advantage to exciton-polaritons, for they can overcome the potential disorder that may trap the uncoupled excitons, in the meantime any effective engineering of the potential needs to be at least comparable in size with the coherence area of the photon mode, so that the intended potential variation is not averaged out by coupling to the photon mode.

2.A Theory of Exciton-Photon Coupling Strength

In multipole expansion of energy, the leading contribution next to static potential comes from light waves via electric dipole interactions, therefore the $\mathbf{r} \cdot \mathbf{E}$ Hamiltonian,

$$H_{\mathbf{r}\cdot\mathbf{E}} = \int d^d r \hat{\Psi}^\dagger(\mathbf{r})(-e\hat{\mathbf{r}}) \cdot \mathbf{E}(\mathbf{r}, t)\hat{\Psi}(\mathbf{r}) \tag{2.55}$$

is introduced in addition to Eq.(2.1), such that,

$$H_{\text{tot}} = H_e + H_{\mathbf{r}\cdot\mathbf{E}} \tag{2.56}$$

In this semiclassical formalism, the electron gas is second-quantized, and the electrical field of the light wave is kept as a classical amplitude, which can be further quantized as the "photon" field.

Assuming the light field has a constant amplitude and a varying phase across the semiconductor,

$$\mathbf{E}(\mathbf{r}, t) = \frac{1}{2}\mathbf{E}(t)\Big(e^{i\mathbf{k}\cdot\mathbf{r}} + e^{-i\mathbf{k}\cdot\mathbf{r}}\Big) \tag{2.57}$$

and using the definition of field operator in Eq.(2.2), the $\mathbf{r} \cdot \mathbf{E}$ Hamiltonian can be written

as,

$$H_{\mathbf{r}\cdot\mathbf{E}} = -\sum_{\mathbf{k}} \mathcal{E}(t)(\hat{e}^{\dagger}_{c,\mathbf{k}}\hat{e}_{v,\mathbf{k}}d_{cv} + \hat{e}^{\dagger}_{v,\mathbf{k}}\hat{e}_{c,\mathbf{k}}d_{vc}) \tag{2.58}$$

where $\mathbf{d}_{cv} = e\langle c|\hat{\mathbf{r}}|v\rangle$, $\mathcal{E}(t)$ and d_{cv} are the amplitudes projected in the direction of the external field, therefore taking scalar forms. The dipole matrix element d_{cv} between the conduction and valence band is an average value over spatially extended Bloch wavefunctions, which is often estimated using the relation,

$$\hat{\mathbf{p}} \approx \frac{d}{dt}\hat{\mathbf{r}} = \frac{m}{i\hbar}[\hat{\mathbf{r}}, \hat{H}] \tag{2.59}$$

where $p_{cv} = \langle c|\hat{\mathbf{p}}|v\rangle$, known as the optical matrix element in the equivalent $\mathbf{p}\cdot\mathbf{A}$ Hamiltonian, is characterized and documented for a wide range of semiconductors [52].

Define a dimensionless correlation function in momentum space using electron fermionic operators,

$$P_{vc,\mathbf{k}}(t) = \left\langle \hat{e}^{\dagger}_{v,\mathbf{k}}\hat{e}_{c,\mathbf{k}}(t) \right\rangle, \tag{2.60}$$

such that the macroscopic polarization is,

$$P(t) = \sum_{\mathbf{k}} \left(P_{cv,\mathbf{k}}d_{vc} + P_{vc,\mathbf{k}}d_{cv} \right) \tag{2.61}$$

The Heisenberg equation of motion

$$\frac{d\hat{e}^{\dagger}_{v,\mathbf{k}}\hat{e}_{c,\mathbf{k}}}{dt} = \frac{[\hat{e}^{\dagger}_{v,\mathbf{k}}\hat{e}_{c,\mathbf{k}}, H_{\text{tot}}]}{i\hbar} \tag{2.62}$$

leads to,

$$\left(i\hbar\frac{d}{dt} - (\tilde{\omega}_{c,k} - \tilde{\omega}_{v,k}) \right) P_{cv,\mathbf{k}}(t) = \left(n_{c,k}(t) - n_{v,k}(t) \right) \left(d_{cv}\mathcal{E}(t) + \sum_{q\neq k} V_{|k-q|}P_{vc,q} \right) \tag{2.63}$$

where the random phase approximation is applied such that the expectation value of density and correlation function are given as,

$$n_{\lambda,k} = \left\langle \hat{e}^{\dagger}_{\lambda,k}\hat{e}_{\lambda,k} \right\rangle, \quad \left\langle \hat{e}^{\dagger}_{c,k'+q}\hat{e}^{\dagger}_{v,k-1}\hat{e}_{c,k'}\hat{e}_{c,k} \right\rangle \approx P_{cv,k'}\ n_{c,k}\ \delta_{k-q,k'} \tag{2.64}$$

Note the eigenenergy of conduction and valance band are renormalized by intra-band Coulomb interaction,

$$\hbar\tilde{\omega}_{\lambda,k} = \hbar\omega_{\lambda,k} - \sum_{q\neq k} V_{|k-q|} n_{\lambda,q} \tag{2.65}$$

In thermal equilibrium, we expect the Fermi-Dirac distribution,

$$n_{c,k}(t) \to f_{c,k}, \quad n_{v,k}(t) \to f_{v,k} \tag{2.66}$$

in particular near zero temperature $f_{c,k} = 0, \quad f_{v,k} = 1$, equation (2.63) after a Fourier transform to frequency domain reduces to,

$$\left(\hbar(\omega + i\delta) - E_g - \frac{\hbar^2 k^2}{2\mu}\right) P_{vc,k}(\omega) = -d_{cv}E(\omega) + \sum_{q\neq k} V_{|k-q|} P_{vc,q}(\omega) \tag{2.67}$$

This expression allows us to focus on the responses at an optical frequency near interband transition, where the infinitesimal δ is added to keep causality in the time response.

Following the convention defined by (2.8), a Fourier transform from momentum to real space leads to,

$$\left(\hbar(\omega + i\delta) - E_g + \frac{\hbar^2 \nabla_{\mathbf{r}}^2}{2\mu} + V(\mathbf{r})\right) P_{cv}(\mathbf{r}, \omega) = -d_{cv}E(\omega)\delta(\mathbf{r})\Omega^3 \tag{2.68}$$

which is an inhomogeneous differential equation of the variable $\mathbf{r}$, and a particular solution as the response to electrical field $E(\omega)$ can be found in the superposition of the solutions to the homogeneous differential equation,

$$\left(-\frac{\hbar}{2\mu}\nabla_{\mathbf{r}}^2 + V(\mathbf{r})\right)\psi_\nu(r) = E_\nu \psi_\nu(\mathbf{r}) \tag{2.69}$$

The reduced electron-hole two-body equation, generally known as the Wannier equation, in this case, resembles the Shrödinger equation for a hydrogen atom.

Expanding the correlation function in the exciton orbital basis,

$$P_{vc}(\mathbf{r}, \omega) = \sum_\nu c_\nu \psi_\nu(\mathbf{r}) \tag{2.70}$$

leads to response function,

$$P_{vc}(\mathbf{r},\omega) = -\sum_{\nu} E(\omega)\frac{d_{cv}\Omega^3\psi_\nu^*(\mathbf{r}=0)}{\hbar(\omega+i\delta)-E_g-E_\nu}\psi_\nu(\mathbf{r}) \tag{2.71}$$

the frequency dependence means excitons are only created in response to certain optical frequencies.

Consider the macroscopic polarization is related to the correlation function according to equation(2.61), in the frequency domain it is,

$$P(\omega) = \sum_{\mathbf{k}} \Big(P_{cv,\mathbf{k}}(\omega)d_{vc} + P_{vc,\mathbf{k}}(-\omega)d_{cv} \Big) \tag{2.72}$$

which eventually leads to the susceptibility function,

$$\chi(\omega) = -2\sum_{\nu} |d_{cv}|^2 |\psi_{cv}(\mathbf{r}=0)|^2 \times \left[\frac{1}{\hbar(\omega+i\delta)-E_g-E_\nu} - \frac{1}{\hbar(\omega+i\delta)+E_g+E_\nu} \right] \tag{2.73}$$

following the definiton,

$$\chi(\omega) = \frac{\mathcal{P}(\omega)}{\mathcal{E}(\omega)} \tag{2.74}$$

where $\mathcal{P}(\omega)$ is the macroscopic polarization density averaged over the integrated volume.

From the response equation(2.73), and the relation for induced dipole energy,

$$E_{\text{ex-ph}}(\omega) = \frac{1}{2}\chi(\omega)\mathcal{E}(\omega)^2 \tag{2.75}$$

therefore the coupling strength between a ν-orbital exciton and a plane wave photon mode can be extracted as,

$$\Omega = \psi_\nu(\mathbf{r}=0)|d_{cv}|\bar{\mathcal{E}} \tag{2.76}$$

where the quantized increment in the electrical field $\bar{\mathcal{E}}$ is determined by single photon energy(SI units),

$$E_{\text{ph}} = \hbar\omega_{\text{ph}} = \frac{1}{2}\varepsilon_0\varepsilon_r\bar{\mathcal{E}}^2 \tag{2.77}$$

2.B $\mathbf{p}\cdot\mathbf{A}$ Hamiltonian and Optical Matrix Element

Besides the intuitive $\mathbf{d}\cdot\mathbf{E}$, the $\mathbf{p}\cdot\mathbf{A}$ Hamiltonian origins from a gauge theory is also widely used in light-matter interaction problems.

Starting from the minimal coupling Hamiltonian,

$$\mathcal{H} = \frac{\big(\hat{\mathbf{p}} - e\mathbf{A}(\mathbf{r},t)\big)^2}{2m} + eV(\mathbf{r},t) \tag{2.78}$$

simply expanding the square term and neglecting the A^2 term leads to the well known $\mathbf{p}\cdot\mathbf{A}$ Hamiltonian,

$$H_{\mathbf{p}\cdot\mathbf{A}} = -\frac{e}{m}\hat{\mathbf{p}}\cdot\mathbf{A}(\mathbf{r},t) \tag{2.79}$$

Describing the light as a plane wave with constant amplitude,

$$\mathbf{A}(\mathbf{r},t) = \frac{\mathbf{A}}{2}e^{i(\mathbf{k}_o\cdot\mathbf{r}-\omega_o t)} \tag{2.80}$$

the matrix element of the $\mathbf{p}\cdot\mathbf{A}$ Hamiltonian can be evaluated in the interaction picture as follows,

$$-\frac{e}{2m}\mathbf{A}\cdot\left\langle\phi_{c\mathbf{k}}\middle|e^{i\omega_c t}\hat{\mathbf{p}}e^{-i\omega_v t}\middle|\phi_{v\mathbf{k}}\right\rangle = -\frac{e}{2m}e^{i(\omega_c-\omega_v-\omega_o)t}\mathbf{A}\cdot\int_V d^3\mathbf{r}\ e^{i\mathbf{k}_o\cdot\mathbf{r}}\phi^*_{c\mathbf{k}}(\mathbf{r})\hat{\mathbf{p}}\phi_{v\mathbf{k}}(\mathbf{r}) \tag{2.81}$$

Recall the definition of Bloch wavefunction,

$$\phi_{n\mathbf{k}}(\mathbf{r}) = \frac{1}{\sqrt{V}}u_{n\mathbf{k}}(\mathbf{r})e^{i\mathbf{k}\cdot\mathbf{r}} \tag{2.82}$$

and momentum operator $\hat{\mathbf{p}} = -i\hbar\nabla_{\mathbf{r}}$, the spatial integral can be evaluated as,

$$\begin{aligned}
&\int\frac{d^3\mathbf{r}}{V}\ e^{-i\mathbf{k}_o\cdot\mathbf{r}}u^*_c(\mathbf{r})e^{-i\mathbf{k}_c\cdot\mathbf{r}}\Big[\big(-i\hbar\nabla_{\mathbf{r}}u_v(\mathbf{r})\big)e^{i\mathbf{k}_v\cdot\mathbf{r}} + \hbar\mathbf{k}_v u_v(\mathbf{r})e^{i\mathbf{k}_v\cdot\mathbf{r}}\Big]\\
\approx&\int\frac{d^3\mathbf{r}}{\Lambda}u^*_c(\mathbf{r})\Big(-i\hbar\nabla_{\mathbf{r}}\Big)u_v(\mathbf{r})\sum_m e^{i(\mathbf{k}_o+\mathbf{k}_v-\mathbf{k}_c)\cdot\mathbf{r}}\delta(\mathbf{r}-m\mathbf{R})\\
=&\mathbf{p}_{cv}\ \delta(k_o+k_v-k_c)
\end{aligned} \tag{2.83}$$

where $\mathbf{p}_{cv}$ is the optical matrix element defined as an integral over the unit cell Λ, and

the summation over lattice site m leads to the δ-function, indicating the phase-matching condition for this optically induced transition process, implying momentum conservation between initial and final states.

In a finite-size system with physical boundary and potential variation, either the electron or the hole can be described by its Bloch wavefunction convolved with a slow-varying spatial envelope function. However, the minimal coupling Hamiltonian in Eq.(2.78) only works conveniently for the free electron transition. The expression for exciton as a many-electron excitation is a little cumbersome, namely,

$$\Psi_{\text{ex}} = \sum_{j,j'} F_n(\mathbf{R})\phi(\mathbf{r}_i - \mathbf{r}_j)W_j^c(\mathbf{R}, \mathbf{r}_j) \prod_{i \neq j'} W_i^v(\mathbf{R}, \mathbf{r}_i) \tag{2.84}$$

where $F(\mathbf{R})$ is a slowly varying wavefunction across the host material for the center of mass of the exciton, $\phi(\mathbf{r}_j - \mathbf{r}_{j'})$ is the orbital wavefunction in relative coordinates, and $W_j^c(\mathbf{R}, \mathbf{r})$ is the Wannier function centered at lattice site $\mathbf{R}$ as the Fourier transform of the Bloch wavefunction,

$$W_{n\mathbf{k}}(\mathbf{R}, \mathbf{r}) = \frac{1}{\sqrt{N}} \sum_{\mathbf{k}} e^{-i\mathbf{k}\cdot\mathbf{R}} \psi_{n\mathbf{k}}(\mathbf{r}) \tag{2.85}$$

such that the optical matrix element can also be defined as,

$$\mathbf{p}_{cv} = \left\langle W_j^c(\mathbf{R}, \mathbf{r}_j) \middle| \hat{\mathbf{p}}_j \middle| W_j^v(\mathbf{R}, \mathbf{r}_j) \right\rangle \tag{2.86}$$

for jth electron. The exciton is written as a Slater determinant representing one electron excited into the conduction band and all others remaining in the valence band. The second-quantized formalism with $\mathbf{r} \cdot \mathbf{E}$ is now connected to the first-quantized formalism with $\mathbf{p} \cdot \mathbf{A}$ Hamiltonian. The optical matrix element p_{cv} is considered a property of the host material, which justifies the use of average dipole moment d_{cv}. In the meantime, the inhomogeneous external field and electron/hole densities are described by their envelope functions.

In the case of microcavity polariton, one can extract the center of mass envelope

function of exciton(2.27) and calculate its overlap with the cavity photon mode(2.48), to evaluate the overall coupling strength in the cavity,

$$\Omega(\mathbf{k}) = d_{cv}\ \phi_{10}(\mathbf{r}=0)\ \sqrt{\frac{E_{\mathrm{ph}}(\mathbf{k})}{2\varepsilon_0\varepsilon_r}} \int dz d^2\mathbf{r}\ F_n^*(\mathbf{r},z) u_\lambda(\mathbf{r},z) \tag{2.87}$$

where $d_{cv} = |\mathbf{d}_{cv}|$ is projected in the polarization direction of the photon mode, $\phi_{10}(\mathbf{r})$ is the 2D exciton wave function in the ground orbital($n=1, l=0$), $E_{\mathrm{ph}}(\mathbf{k})$ is the photon energy dispersion relation in the $\mathbf{k}$ plane.

It is noteworthy that the Schrödinger equation based on minimal coupling Hamiltonian(2.78) is covariant under a gauge transform,

$$\begin{aligned} &\mathbf{A}(\mathbf{r},t) \to \mathbf{A}(\mathbf{r},t) + \frac{\hbar}{e}\nabla\chi(\mathbf{r},t) \\ &V(\mathbf{r},t) \to V(\mathbf{r},t) - \frac{\hbar}{e}\frac{\partial\chi(\mathbf{r},t)}{\partial t} \\ &\psi(\mathbf{r},t) \to \psi(\mathbf{r},t)e^{i\chi(\mathbf{r},t)} \end{aligned} \tag{2.88}$$

while the physical quantities such as the mechanical momentum $\hat{\mathbf{p}} - e\mathbf{A}$ and local probability density $P(\mathbf{r},t) = |\psi(r,t)|^2$ are gauge invariant. However, the time-dependent Schödinger equation is usually fixed in the Coulomb gauge,

$$i\hbar\frac{\partial\psi(\mathbf{r},t)}{\partial t} = \Big(-\frac{\hbar^2}{2m}\Big(\nabla - i\frac{e\mathbf{A}(\mathbf{r},t)}{\hbar}\Big)^2 + eV(\mathbf{r})\Big)\psi(\mathbf{r},t) \tag{2.89}$$

such that the scalar potential $V(\mathbf{r})$ is time-independent and only attributed to the static crystal field, while $\mathbf{A}(\mathbf{r},t)$ accounts for the time-dependent light waves.

The $\mathbf{r}\cdot\mathbf{E}$ Hamiltonian, once put in a quantum mechanical form, implies a different gauge. One should find a gauge transformation,

$$\phi(\mathbf{r},t) = \exp\Big(-\frac{e\mathbf{A}(\mathbf{r},t)\cdot\mathbf{r}}{\hbar}\Big)\psi(\mathbf{r},t) \tag{2.90}$$

applied to Eq.(2.89) leads to the Schrödinger equation for the $\mathbf{r}\cdot\mathbf{E}$ Hamiltonian,

$$i\hbar\frac{d}{dt}\phi(\mathbf{r},t)=\left(\frac{\hat{\mathbf{p}}^2}{2m}+V(\mathbf{r})-e\mathbf{r}\cdot\mathbf{E}\right)\phi(\mathbf{r},t) \tag{2.91}$$

Note that the system before being perturbed by the light-matter interaction is described by the Hamiltonian,

$$H_0=\frac{\hat{\mathbf{p}}^2}{2m}+V(\mathbf{r}) \tag{2.92}$$

which implies the time-dependent wavefunctions evolving under the $\mathbf{r}\cdot\mathbf{E}$ Hamiltonian are defined in the same gauge as the unperturbed wavefunctions. Meanwhile, the basis wavefunctions must be consistently transformed to the Coulomb gauge if the time-evolution is calculated based on the $\mathbf{p}\cdot\mathbf{A}$ Hamiltonian, especially in those problems involving transition probability and gauge field effects.

2.C Spin-Orbit Coupling and Semiconductor Bands

The spin-orbit coupling effect and its impact on the semiconductor band structure can be understood in the Luttinger-Kohn model [53]. For pedagogical purposes, one could start by applying the $\mathbf{k}\cdot\mathbf{p}$ method to a spinless model.

Recall the time-independent Shrödinger equation describing an electron in the presence of a periodic crystal field,

$$H\phi(\mathbf{r})=\Big(\frac{\hat{\mathbf{p}}^2}{2m}+V(\mathbf{r})\Big)\phi(r),\quad V(\mathbf{r})=V(\mathbf{r}+\mathbf{R}) \tag{2.93}$$

According to Bloch's theorem, the wavefunction takes the form,

$$\phi_{n\mathbf{k}}(\mathbf{r})=\exp(i\mathbf{k}\cdot\mathbf{r})u_{n\mathbf{k}}(\mathbf{r}),\quad u_{n\mathbf{k}}(\mathbf{r}+\mathbf{R})=u_{n\mathbf{k}}(\mathbf{r}) \tag{2.94}$$

The momentum operator $\hat{\mathbf{p}}=-i\hbar\nabla_{\mathbf{r}}$ acting on the Bloch wavefunction effectively extracts the crystal wavevector $\mathbf{k}$ and the spatial gradient in $u_{n\mathbf{k}}(\mathbf{r})$, therefore Eq. (2.93)

can be rewritten as eigenvalue equation of $u_{n\mathbf{k}}(\mathbf{r})$,

$$\left(\frac{\hat{\mathbf{p}}^2}{2m} + \frac{\hbar}{m}\mathbf{k}\cdot\hat{\mathbf{p}} + \frac{\hbar^2k^2}{2m} + V(\mathbf{r})\right) u_{n\mathbf{k}}(\mathbf{r}) = E_{n\mathbf{k}}u_{n\mathbf{k}}(\mathbf{r}) \tag{2.95}$$

where the states at the Γ point($\mathbf{k} = 0$ in reciprocal space) satisfying,

$$\left(\frac{\hat{\mathbf{p}}^2}{2m} + V(\mathbf{r})\right) u_{n\mathbf{0}}(\mathbf{r}) = E_{n\mathbf{0}}u_{n\mathbf{0}}(\mathbf{r}) \tag{2.96}$$

serve as the unperturbed basis. The parabolic term $\frac{\hbar^2k^2}{2m}$ can be directly calculated for any given $k = |\mathbf{k}|$, and the $\mathbf{k}\cdot\hat{\mathbf{p}}$ term can be treated as a perturbation.

For an ideal model consisting of only non-degenerate states, the energy with perturbative correction can be evaluated as,

$$E_{n\mathbf{k}} = E_{n\mathbf{0}} + \frac{\hbar^2k^2}{2m} + \frac{\hbar^2}{m^2}\sum_{n'\neq n}\frac{|\mathbf{k}\cdot\langle u_{n\mathbf{0}}|\hat{\mathbf{p}}|u_{n'\mathbf{0}}\rangle|^2}{E_{n\mathbf{0}} - E_{n'\mathbf{0}}} \tag{2.97}$$

where the n' runs over all the other unperturbed energy bands, $\hat{\mathbf{p}}$ is a quantum operator, and its matrix element$\langle u_{c\mathbf{0}}|\hat{\mathbf{p}}|u_{n\mathbf{0}}\rangle$ evaluated between the conduction and the valence band is a general property of the host material, usually characterized in experiments and documented as the optical matrix element. Therefore the $\mathbf{k}\cdot\hat{\mathbf{p}}$ term makes the dispersion relation deviate from the parabola of free particles, but in the vicinity of the Γ point, the energy band can still be described by an effective mass m^* that satisfies,

$$\frac{1}{m^*} = \frac{1}{m} + \frac{2}{m^2k^2}\sum_{n'\neq n}\frac{|\mathbf{k}\cdot\langle u_{n\mathbf{0}}|\hat{\mathbf{p}}|u_{n'\mathbf{0}}\rangle|^2}{E_{n\mathbf{0}} - E_{n'\mathbf{0}}} \tag{2.98}$$

Once the spin is included, the $\mathbf{k}\cdot\mathbf{p}$ model needs to be solved in degenerate perturbation theory, and the spin-orbit coupling will lift the degeneracy and define the energy bands. By reducing the Dirac equation to the non-relativistic limit [54], the spin-orbit coupling Hamiltonian

$$H_{SO} = \frac{\hbar}{4m^2c^2}(\nabla V \times \hat{\mathbf{p}})\cdot\hat{\sigma} \tag{2.99}$$

is identified as a correction to the Schrödinger equation, where the Cartesian components

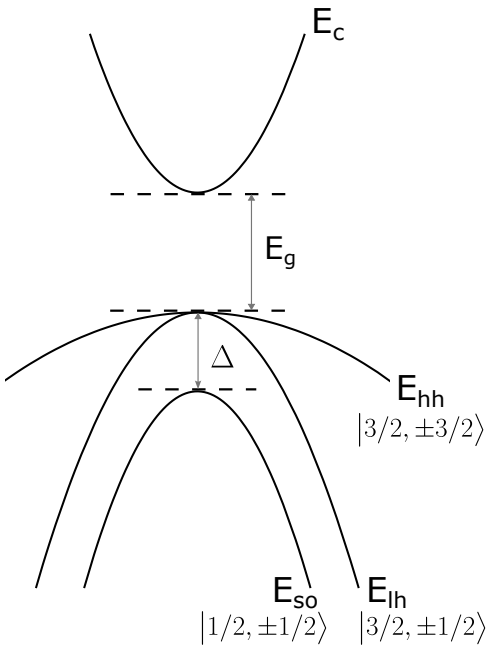

Figure 2.3: Energy band structure of zinc blende crystals near the Γ-point, $E_{\mathbf{c}}$ represents conduction band, $E_{\mathbf{hh}}$ represents heavy hole, $E_{\mathbf{lh}}$ represents light hole, $E_{\mathbf{so}}$ represents split-off bands.

of operator $\hat{\sigma}$ are represented by the Pauli matrices.

Considering a crystal field sharing the discrete symmetry of the lattice and being spherical symmetric within the unit cell, using $\nabla V = \frac{1}{r}\frac{\partial V}{\partial r}\mathbf{r}$, $\mathbf{l} = \mathbf{r} \times \mathbf{p}$, and recognizing $\mathbf{s} = \frac{\hbar}{2}\sigma$, one should find the effective Hamiltonian at the Γ point,

$$H_0 = \frac{\hat{\mathbf{p}}^2}{2m} + V(\mathbf{r}) + \frac{1}{2m^2c^2}\frac{1}{r}\frac{\partial V}{\partial r}\hat{\mathbf{l}} \cdot \hat{\mathbf{s}} \tag{2.100}$$

The spin-orbit coupling term has a similar effect as it does in alkali atoms, which can be described by the orbital angular quantum number l and the spin quantum number s, and diagonalized in the space of the joint angular quantum number $j = l + s$.

Common semiconductors used in exciton-polariton research are zincblende crystals such as GaAs and CdTe, where the conduction band has an s-like($l = 0$) $u_{c0}(\mathbf{r})$ wavefunction and the valence bands have p-like($l = 1$) $u_{v0}(\mathbf{r})$ wavefunctions. The basis function for the six valence bands can be written as $\left|j, j_m\right\rangle$, or in the combinations of spherical

harmonics $Y_{l,m}$ and spin polarizations($\big|\uparrow\big\rangle, \big|\downarrow\big\rangle$), in this case,

$$\begin{aligned}
\left\langle \mathbf{r}\middle|\frac{3}{2},\frac{3}{2}\right\rangle &\propto Y_{1,1}\big|\uparrow\big\rangle \\
\left\langle \mathbf{r}\middle|\frac{3}{2},\frac{1}{2}\right\rangle &\propto \sqrt{\frac{1}{3}}Y_{1,1}\big|\downarrow\big\rangle + \sqrt{\frac{2}{3}}Y_{1,0}\big|\uparrow\big\rangle \\
\left\langle \mathbf{r}\middle|\frac{3}{2},-\frac{1}{2}\right\rangle &\propto \sqrt{\frac{1}{3}}Y_{1,-1}\big|\uparrow\big\rangle + \sqrt{\frac{2}{3}}Y_{1,0}\big|\downarrow\big\rangle \\
\left\langle \mathbf{r}\middle|\frac{3}{2},-\frac{3}{2}\right\rangle &\propto Y_{1,-1}\big|\downarrow\big\rangle \\
\left\langle \mathbf{r}\middle|\frac{1}{2},\frac{1}{2}\right\rangle &\propto -\sqrt{\frac{2}{3}}Y_{1,1}\big|\downarrow\big\rangle + \sqrt{\frac{1}{3}}Y_{1,0}\big|\uparrow\big\rangle \\
\left\langle \mathbf{r}\middle|\frac{1}{2},-\frac{1}{2}\right\rangle &\propto \sqrt{\frac{2}{3}}Y_{1,-1}\big|\uparrow\big\rangle - \sqrt{\frac{1}{3}}Y_{1,0}\big|\downarrow\big\rangle
\end{aligned} \tag{2.101}$$

and the two spin degenerate conduction bands are $Y_{0,0}\big|\uparrow\big\rangle$ and $Y_{0,0}\big|\downarrow\big\rangle$. In the end, the new eigenstates serve as the basis for the $\mathbf{k}\cdot\mathbf{p}$ calculation.

The perturbation Hamiltonian can also take in the spin-orbit correction by using a modified momentum operator such that,

$$H' = \frac{\hbar}{m}\mathbf{k}\cdot\hat{\mathbf{\Pi}}, \quad \hat{\mathbf{\Pi}} = \hat{\mathbf{p}} + \frac{1}{4mc^2}\hat{\sigma}\times\nabla V \tag{2.102}$$

The general idea of the Luttinger-Kohn model is to reduce the $\mathbf{k}\cdot\mathbf{\Pi}$ Hamiltonian to a subspace consisting of a few bands near the band gap, and treat the effective coupling between them as second-order perturbations mediated by the bands beyond the subspace, then diagonalize the reduced Hamiltonian to find the eigenstates as the final result of energy bands. A practical calculation based on the band gap and inter-band matrix elements can be carried out using Löwdin's perturbation method [52].

Based on a general symmetry argument, an effective total Hamiltonian can be written as,

$$\begin{aligned}
H &= \frac{\hbar^2}{2m}\gamma_1\mathbf{k}^2 - \frac{\hbar^2}{9m}\sum_{\alpha,\beta}[\gamma_3 - (\gamma_3-\gamma_2)\delta_{\alpha,\beta}]K_{\alpha,\beta}J_{\alpha,\beta} \\
K_{\alpha,\beta} &= 3k_\alpha k_\beta - \delta_{\alpha,\beta}k^2, \\
J_{\alpha,\beta} &= \frac{3}{2}(j_\alpha j_\beta + j_\beta j_\alpha) - \delta_{\alpha,\beta}j^2
\end{aligned} \tag{2.103}$$

where $K_{\alpha,\beta}$ and $J_{\alpha,\beta}$ are tensors constructed with crystal momenta and joint angular quantum number, respectively, and $\gamma_1, \gamma_2, \gamma_3$ are called Luttinger parameters, often characterized by experimentally measured effective masses.

However, for most conventional materials with $\gamma_1 > \gamma_2 \approx \gamma_3$, it is sufficient to use a simplified Hamiltonian with spherical symmetry. The six valence bands, denoted by the joint angular quantum number and polarization, are categorized based on energy offset and the band dispersion relation as follows: $\left|3/2, \pm 3/2\right\rangle$ have a larger effective mass, hence are known as "heavy hole" bands, $\left|3/2, \pm 1/2\right\rangle$ have a smaller effective mass, hence are known as the "light hole" bands. The top of the heavy hole and light hole bands are degenerate, which, against the bottom of the two degenerate conduction bands, defines the band gap. $\left|1/2, \pm 1/2\right\rangle$ are degenerate but farther away from the bottom of the conduction bands, hence known as "split-off" bands.

Low-dimension confinement, for example, a quantum well, would reduce the symmetry of the crystal field and further lift the degeneracy between the heavy holes and light holes; therefore, the single word "exciton" in the context of planar microcavities usually refers to the type formed by one electron and one heavy hole.

The dipole field interaction does not flip the spin, therefore an optically excited electron-hole pair must have matched spin polarization, which defines the "bright exciton". In contrast, a "dark exciton" has opposite spin polarizations in its electron and hole components, which leads to a vanishing transition dipole moment, eventually results in negligible radiative recombination and a long lifetime. An exciton-polariton is formed by a "bright exciton" with its corresponding circularly polarized photon, for example, $Y_{1,1}\left|\uparrow\right\rangle$ is coupled to $Y_{0,0}\left|\uparrow\right\rangle$ via a left-hand circularly polarized photon, and $Y_{1,-1}\left|\downarrow\right\rangle$ is coupled to $Y_{0,0}\left|\downarrow\right\rangle$ via a right-hand circularly-polarized photon. A hole is an absence in the valence band and takes the opposite sign in j_m, therefore the heavy hole excitons can be written as $\left|1, \pm 1\right\rangle$ in the joint quantum numbers, while the corresponding dark exciton can be written as $\left|2, \pm 2\right\rangle$. Considering the photon is also a boson with integer spin 1, indicating its polarization, the strong coupling process converting between exciton and photon is thus spin-conserved, and the exciton-polariton inherits the pseudo spin of

the bright exciton. The time evolution of the polariton pseudo spin can lead to interesting macroscopic phenomena revealed in the polarization of the photon field.

2.D Two-dimensional Hydrogen Atom

This subsection presents important results from [55] related to exciton quasi-2D state and Stark effect calculation.

The Hamiltonian of a 2D hydrogen atom consists of an isotropic Coulomb potential.

$$H = \frac{\hbar^2}{2m}\nabla^2 - \frac{e^2}{r} \tag{2.104}$$

The time-independent Schrödinger equation in polar coordinates $\mathbf{r} = (r, \theta)$ reads,

$$\left\{ -\frac{\hbar^2}{2m}\Big(\frac{1}{r}\frac{\partial}{\partial r}\big(r\frac{\partial}{\partial r}\big) + \frac{1}{r^2}\frac{\partial^2}{\partial\theta^2}\Big) - \frac{e^2}{r}\right\}\phi(r,\theta) = E\phi(r,\theta) \tag{2.105}$$

In the 2D system, the angular momentum is perpendicular to the plane and commutes with the Hamiltonian; therefore, a general solution to the Schrödinger equation can be obtained by separation of variables, where the angular wavefunction

$$\Theta(\theta) = \frac{1}{\sqrt{2\pi}}e^{il\theta}, \quad l = 0, \pm1, \pm2, \dots \tag{2.106}$$

is characterized by the "winding quantum number" l, which is the eigenvalue of the angular momentum operator,

$$\hat{L}_z = -i\hbar\frac{\partial}{\partial\theta} \tag{2.107}$$

Therefore, the radial equation can be written as,

$$\frac{d^2}{dr^2}R(r) + \frac{1}{r}\frac{d}{dr}R(r) + \left\{\frac{2m}{\hbar^2}\Big(E + \frac{e^2}{r}\Big) - \frac{l^2}{r^2}\right\}R(r) = 0 \tag{2.108}$$

It is convenient to choose the energy scale and length scale jointly such that both are

related to a dimensionless coefficient N,

$$E = -\frac{1}{2N^2}\frac{m_e e^4}{\hbar^2}, \quad r = N\frac{\hbar^2}{2m_e e^2}x = \frac{x}{\beta_N} \tag{2.109}$$

Also by the change of variables,

$$R(x) = x^{|l|}e^{-x/2}G(x), \tag{2.110}$$

The radial equation is converted to the confluent hypergeometric equation,

$$x\frac{d^2G(x)}{dx^2} + \Big((2|l|+1) - x\Big)\frac{dG(x)}{dx} - \Big(-N + |l| + \frac{1}{2}\Big)G(x) = 0 \tag{2.111}$$

which has a regular singular point at $x = 0$, and an irregular singular point at $x = \infty$.

In order to keep the asymptotic solution finite at $r = \infty$, the coefficient $-N+|l|+1/2$ has to be a non-positive integer value. Therefore, a positive integer "principle quantum number" $n = N + 1/2$ can be chosen such that,

$$n = 1, 2, 3, \ldots \tag{2.112}$$

and $|l|$ is bounded below n,

$$|l| = 0, 1, 2, \ldots, n-1 \tag{2.113}$$

The general form of wavefunction for a bound state is then,

$$\phi(r, \theta) = R_{nl}(r)\Theta_l(\theta) \tag{2.114}$$

With the normalized radial wavefunction

$$R_{nl}(r) = \frac{\beta_n}{(2|l|)!}\left[\frac{(n+|l|-1)!}{(2n-1)(n-|l|-1)!}\right]^{1/2}(\beta_n r)^{|l|}e^{-\beta_n r/2}\,{}_1F_1(-n+|l|+1,\ 2|l|+1,\ \beta_n r) \tag{2.115}$$

where ${}_1F_1(a, b, x)$ is a hypergeometric series known as Kummer's function of the first kind[56].

Recalling the definition (2.109), we have the eigenenergies related to the principal quantum number,

$$E_n = -\frac{1}{2(n-\frac{1}{2})^2}\frac{m_e e^4}{\hbar^2}, \tag{2.116}$$

And the parameter for the length scale is,

$$\beta_n = \frac{2}{n-\frac{1}{2}}\frac{m_e e^2}{\hbar} \tag{2.117}$$

In particular, we can write down the wavefunction for the ground state,

$$\phi_{10}(r) = R_{10}(r)\Theta_0(\theta) = \sqrt{\frac{1}{a_{2\mathrm{D}}}}e^{-r/a_{2\mathrm{D}}}, \quad E_0 = -\frac{\hbar^2}{2m_e a_{2\mathrm{D}}^2} = -2\frac{m_e e^4}{\hbar^2} \tag{2.118}$$

where $a_{2\mathrm{D}} = 2a_0$ is the most probable distance between the electron and the nucleus for a 2D hydrogen atom, which is half of the 3D Bohr radius, while the ground energy E_0 is four times that of the 3D hydrogen atom.

The dipole matrix elements are important for evaluating the Stark effect. We note the parity of the total wavefunction is given by $(-1)^l$, and the dipole operator within the 2D plane has odd parity, resulting in a selection rule that changes the winding number l by ± 1 each time. Therefore, the non-vanishing dipole matrix elements related to the ground state are,

$$\begin{aligned}\big\langle R_{10}\big|r\big|R_{n1}\big\rangle &= \int_0^\infty R_{10}(r) r R_{n1}(1) r dr \\ &= \frac{1}{4}\frac{(2n-1)^{5/2}(n-1)^{n-5/2}}{n^{n+3/2}}\end{aligned} \tag{2.119}$$

where the expression in terms of n is obtained by expanding the excited radial wavefunctions in their series form.

Chapter 3

Exciton-Polariton Condensates

Generally speaking, a condensate can be the macroscopic occupation of any state by bosonic particles. By the conventional definition, a Bose-Einstein condensate(BEC) is the occupation of the ground state emerging in the thermal equilibrium of a homogeneous quantum gas. Given the fact that the microcavity polariton system is inherently 2D, which has a density of states accommodating infinite particles in the long wavelength limit, it is not possible to form an infinite-size condensate at any finite temperature. The modern definition of BEC is associated with a macroscopic wavefunction with non-zero mean value $\langle\psi(\mathbf{r})\rangle$, where the transition criterion,

$$\lim_{|\mathbf{r}-\mathbf{r}'|\to\infty} \langle\psi^\dagger(\mathbf{r})\psi(\mathbf{r}')\rangle \sim \langle\psi(\mathbf{r}')\rangle^* \langle\psi(\mathbf{r})\rangle \tag{3.1}$$

is also known as "off-diagonal long-range order"(ODLRO) [57]. However, by the well-known Mermin-Wagner theorem [58], thermal fluctuations destroy long-range order in any system with lower dimensionality than two, which means phase coherence and superfluidity of the polariton condensate can only be found at a finite length scale [28].

Experimentally, it is possible to create a homogeneous polariton gas with ODLRO at a finite size [27, 59], as it is possible to create an inhomogeneous polariton gas occupying the bound ground state in a trap [47]. The latter is inspired by the dipole trap technique from atomic condensate experiments and is closely related to the first conceptualization of the boson Josephson junctions[12]. It is also possible to create a thermal condensate

in an excited state, for example, using a periodic photonic structure to create an energy band gap, hence accumulating polaritons in the state at the bottom of the upper band [26]. The ground state can also be coherently injected, which is known as the resonant pumping scheme of polariton condensate. For example, the micropillar structure in [60] is specially designed, such that the pumping laser is energetically resonant and spatially matched with the polariton state.

To explore spontaneous quantum coherence, the polariton condensate must be created using a non-resonant pumping scheme, in which the relaxation process plays a crucial role.

3.1 Relaxation of Non-Resonantly Pumped Polariton Gases

The relaxation process in a non-resonantly pumped polariton gas can be described as follows(Fig.3.1). After absorbing the energy from the incident light, a free electron/hole gas is created instantly, which quickly loses energy due to electron-phonon interaction and forms bound excitons with net kinetic energy. These excitons further interact with the lattice and lose kinetic energy to phonons. As the excitons approach the anti-crossing region of exciton-photon coupling, they are scattered into polaritons, the true normal modes of the system, and gain a much longer lifetime due to the spontaneously arising optical coherence in the microcavity. It is also in this region that the exciton-phonon scattering becomes less efficient below a certain momentum known as the "phonon bottleneck" due to the less matched phase-space cross section, and the polariton-polariton scattering takes over for the relaxation towards the zero momentum ground state, to eventually form the Bose-Einstein condensate. Therefore, a realistic physical picture should include the condensate and the non-condensate polariton reservoir below the bottleneck.

The laser spot determines the initially excited area, but the spontaneous coherence does not immediately occur across the whole area. As pointed out above, the excitons are relaxed and scattered into polaritons over an inhomogeneous semiconductor sample, which can be considered as many localized wavepackets, resembling droplets formed by

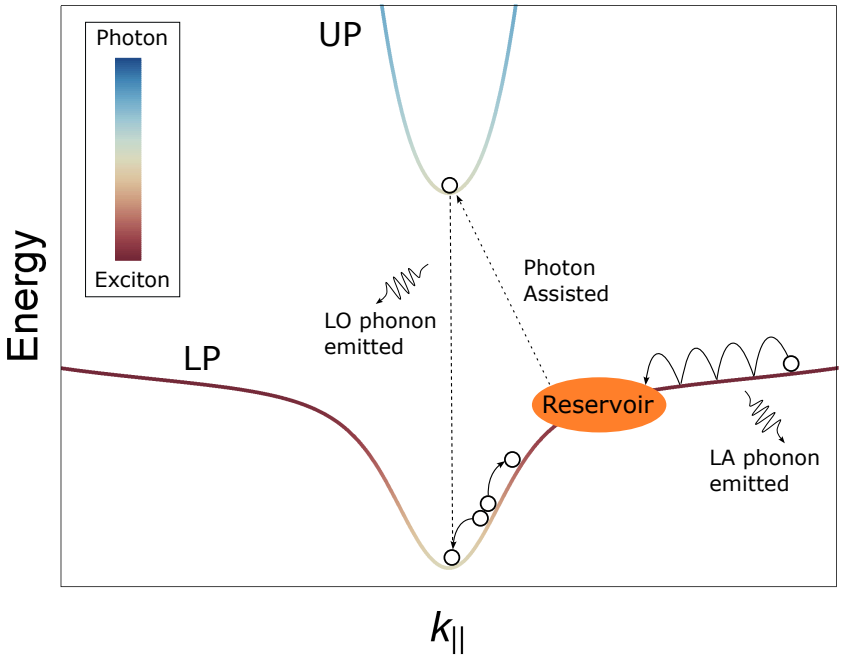

Figure 3.1: Relaxation process in a non-resonantly pumped polariton gas, the solid curves with arrows represented widely accepted mechanisms, while the dashed straight lines represent the mechanisms explored in recent research [61]

individual particles with finite momentum in the 2D space, and are only coherent within each wavepacket. The detailed condensing mechanism that may be described by the nucleation of these polariton droplets is beyond the scope of this dissertation. A semi-classical statistical model describing the reservoir and a mean-field equation describing the condensate should suffice for the main topic of the Josephson effect.

3.2 Semiclassical Boltzmann Equations

By modifying the classical Boltzmann equation with the bosonic particle exchange rule, one can formulate a rate equation for a polariton momentum state[20],

$$\frac{dn_{\mathbf{k}}}{dt} = P_{\mathbf{k}} - \Gamma_{\mathbf{k}} n_{\mathbf{k}} - n_{\mathbf{k}} \sum_{\mathbf{k}'} W_{\mathbf{k}\to\mathbf{k}'}(1+n_{\mathbf{k}'}) + (1+n_{\mathbf{k}}) \sum_{\mathbf{k}'} W_{\mathbf{k}'\to\mathbf{k}} n_{\mathbf{k}'} \tag{3.2}$$

where $P_{\mathbf{k}}$ and $\Gamma_{\mathbf{k}}$ are the pump rate and decay rate at this momentum, attributed to non-resonant laser excitation and cavity photon leaking, respectively. Considering the averaging effect of the photon mode, the convection and diffusion terms are neglected,

making the model spatially homogeneous. Note that the rate of creating or annihilating polaritons in a certain momentum state depends on the transition rate $W_{i\to f}$ and the population in the initial and final states, which shows the unique signature of bosonic quantum gas, in contrast to a classical system. The overall transition rate accounts for both polariton-phonon and polariton-polariton interactions.

A simulation based on this model has successfully predicted the time-dependent photoluminescence of excitons[62] and condensation time for polaritons [63]. The entropy product is also a good indicator of how the system approaches true thermal equilibrium.

For a selective parametric scattering process such as polariton lasing, a seeding population in the desired final state $\mathbf{k}'$ can enhance the transition rate; therefore, the following two equations,

$$\frac{dn_{\mathbf{k}}}{dt} = P_k - \Gamma_{\mathbf{k}} n_k - n_{\mathbf{k}} W^{pol-ph}_{\mathbf{k}\to\mathbf{k}'}(1+n_{\mathbf{k}'}) - n_{\mathbf{k}} W^{pol-pol}_{\mathbf{k}\to\mathbf{k}'}(1+n_{\mathbf{k}'}) \tag{3.3}$$

and

$$\frac{dn_{\mathbf{k}'}}{dt} = -\Gamma_{\mathbf{k}'} n_{\mathbf{k}'} + n_{\mathbf{k}} W^{pol-ph}_{\mathbf{k}\to\mathbf{k}'}(1+n_{\mathbf{k}'}) + n_{\mathbf{k}} W^{pol-pol}_{\mathbf{k}\to\mathbf{k}'}(1+n_{\mathbf{k}'}) \tag{3.4}$$

can effectively describe a closed system formed between the input and output states, and the light emitted by the $\mathbf{k}'$ polariton is coherent radiation without a population inversion in the semiconductor conduction and valence bands.

To reconcile with the 2D nature of the polariton gas, a long-wavelength cutoff is required to define the "ground state" for the condensate. Although this model still cannot explain the condensing mechanism, as the scattering rate into the ground state would be zero if there is no population seeding in the first place, it is useful in describing how a condensate coexists with the thermal particles.

3.3 Elementary Excitations in BEC

A real Bose-Einstein condensate can be treated as a weakly interacting Bose gas by a special perturbation theory. Consider the total Hamiltonian,

$$\hat{H} = \int \frac{\hbar^2}{2m}\big(\nabla\hat{\Psi}^\dagger(\mathbf{r})\nabla\hat{\Psi}(\mathbf{r}')\big)d^d\mathbf{r} + \frac{1}{2}\int \hat{\Psi}^\dagger(\mathbf{r}')\hat{\Psi}^\dagger(\mathbf{r})V(\mathbf{r}'-\mathbf{r})\hat{\Psi}(\mathbf{r}')\hat{\Psi}(\mathbf{r})d^d\mathbf{r}d^d\mathbf{r}' \tag{3.5}$$

where the $V(\mathbf{r}'-\mathbf{r})$ is a repulsive potential that effectively describes the interaction between two bosons.

The total Hamiltonian can be Fourier transformed into momentum space,

$$\hat{H} = \sum_{\mathbf{k}} \frac{\hbar^2k^2}{2m}\hat{a}^\dagger_{\mathbf{k}}\hat{a}_{\mathbf{k}} + \frac{1}{2}\sum_{\mathbf{k},\mathbf{k}',\mathbf{q}} V_{\mathbf{q}}\hat{a}^\dagger_{\mathbf{k}+\mathbf{q}}\hat{a}^\dagger_{\mathbf{k}'-\mathbf{q}}\hat{a}_{\mathbf{k}'}\hat{a}_{\mathbf{k}} \tag{3.6}$$

where $\hat{a}_{\mathbf{k}}$ is a bosonic operator, associated with a plane wave normalized on the volume of the system. By replacing the operator in the ground state with a c-number related to particle density N_0,

$$\hat{a}_0 = \sqrt{N_0} \tag{3.7}$$

and approximated the interaction potential with its average strength($V_{\mathbf{q}=0}$ component), one should find an effective Hamiltonian,

$$\hat{H} = N_0V_0 + \sum_{\mathbf{k}} \frac{\hbar^2k^2}{2m}\hat{a}^\dagger_{\mathbf{k}}\hat{a}_{\mathbf{k}} + \frac{V_0}{2}\big(2\hat{a}^\dagger_{\mathbf{k}}\hat{a}_{\mathbf{k}} + \hat{a}^\dagger_{\mathbf{k}}\hat{a}^\dagger_{-\mathbf{k}} + \hat{a}_{\mathbf{k}}\hat{a}_{-\mathbf{k}}\big) \tag{3.8}$$

Given the isotropic nature of the interaction potential, it is common to describe the interaction strength with an s-wave scattering parameter $g_s = 4\pi\hbar a_s^2/m$, where a_s is the scattering length characterizing the scattered asymptotic wavefunction. By calculating the a_s up to the quadratic order in V_0 in the Born approximation, one should find the following relation,

$$V_0 = g_s\left(1 + g_s\sum_{\mathbf{k}\neq 0}\frac{m}{(\hbar k)^2}\right) \tag{3.9}$$

Using the normalization condition on total particle density $N = N_0 + \sum_{\mathbf{k}\neq 0}\langle\hat{a}^\dagger_{\mathbf{k}}\hat{a}_{\mathbf{k}}\rangle$ and keep up to the first order of $\hat{a}^\dagger_{\mathbf{k}}\hat{a}_{\mathbf{k}}$, the reduced effective Hamiltonian can be written

as,

$$\hat{H} = \frac{1}{2} g_s N^2 + \sum_{\mathbf{k}} \frac{\hbar^2 k^2}{2m} \hat{a}^\dagger_{\mathbf{k}} \hat{a}_{\mathbf{k}} + \frac{1}{2} g_s N \Big(2\hat{a}^\dagger_{\mathbf{k}} \hat{a}_{\mathbf{k}} + \hat{a}^\dagger_{\mathbf{k}} \hat{a}^\dagger_{-\mathbf{k}} + \hat{a}_{\mathbf{k}} \hat{a}_{-\mathbf{k}} + g_s N \frac{m}{(\hbar k)^2} \Big) \tag{3.10}$$

where each pair in the momentum space

$$\hat{H}_{\mathbf{k},-\mathbf{k}} \doteq \begin{pmatrix} \hat{a}^\dagger_{\mathbf{k}} & \hat{a}_{-\mathbf{k}} \end{pmatrix} \begin{pmatrix} \frac{\hbar^2 k^2}{2m} + g_s N & \frac{1}{2} g_s N \\ \frac{1}{2} g_s N & \frac{\hbar^2 k^2}{2m} + g_s N \end{pmatrix} \begin{pmatrix} \hat{a}_{\mathbf{k}} \\ \hat{a}^\dagger_{-\mathbf{k}} \end{pmatrix} \tag{3.11}$$

can be diagonalized by a Bogoliubov transformation,

$$\begin{pmatrix} \hat{a}_{\mathbf{k}} \\ \hat{a}^\dagger_{-\mathbf{k}} \end{pmatrix} = \begin{pmatrix} u_k & v_k \\ v_k^* & u_k^* \end{pmatrix} \begin{pmatrix} \hat{B}_{\mathbf{k}} \\ \hat{B}^\dagger_{-\mathbf{k}} \end{pmatrix} \tag{3.12}$$

The condition $|u_k|^2 - |v_k|^2 = 1$ is satisfied such that the newly defined operators obey the commutation relation $[\hat{B}_{\mathbf{k}}, \hat{B}^\dagger_{\mathbf{k}}] = 1$.

Finally, the total Hamiltonian takes the form,

$$\hat{H} = E_0 + \sum_{\mathbf{k}} E_{\mathrm{Bog}}(\mathbf{k}) \hat{B}^\dagger_{\mathbf{k}} \hat{B}_{\mathbf{k}} \tag{3.13}$$

The elementary excitations in a real condensate, taking into account the interactions, can be described by the bosonic Bogoliubov quasiparticles, where the free particle dispersion $E(\mathbf{k}) = \frac{\hbar^2 |\mathbf{k}|^2}{2m}$ is modified into,

$$E_{\mathrm{Bog}}(\mathbf{k}) = \sqrt{E(\mathbf{k}) \big[E(\mathbf{k}) + 2 g_s N \big]} \tag{3.14}$$

and the corrected total energy in the ground state can be written as,

$$E_0 = \frac{1}{2} g_s N^2 + \frac{1}{2} (g_s N)^2 \sum_{\mathbf{k} \neq 0} \frac{m}{\hbar^2 k^2} + \sum_{\mathbf{k} \neq 0} \left(E(\mathbf{k}) - \Big(\frac{\hbar^2 k^2}{2m} + g_s N \Big) \right) \tag{3.15}$$

The summation in the momentum space results in an expression in terms of the "gas parameter" $N(a_s)^d$, where N is the total particle density and a_s is the scattering length

in the d-dimensional space, and therefore is negligible in a dilute boson gas [64].

An angle-resolved photoluminescence measurement tracks the polariton density and energy over the in-plane wavevector $\mathbf{k}$, which describes the actual dispersion relation and can be used to extract the quasiparticle parameters. The scattering strength g_s can be characterized by a blue shift at the bottom of the lower polariton dispersion curve, since the energy correction to the mean-field single polariton state is approximated by the chemical potential.

$$\mu = \frac{\partial E_0}{\partial N} \approx g_s N \tag{3.16}$$

According to a recent experiment [65], the linear energy-to-density relation is obeyed by a homogeneous microcavity polariton gas at a dilute density($< 10^0 \mu m^{-2}$); once past that density, it starts to curve down, which means the physical predictions based on the quasi-particles need to be corrected by the stronger interaction.

3.4 Mean-Field Wavefunction and Gross-Pitaevskii Equation

An inhomogeneous finite-size condensate can be described by its mean-field wavefunction. Consider a system of N identical bosons condensed into the same single-particle state,

$$\Psi(\mathbf{r}_1, \mathbf{r}_2, \ldots, \mathbf{r}_N) = \psi(\mathbf{r}_1)\psi(\mathbf{r}_2)\ldots\psi(\mathbf{r}_2) \tag{3.17}$$

and the many-body Hamiltonian,

$$H = \sum_{i=1}^{N} \Big(-\frac{\hbar^2}{2m}\nabla_i^2 + V(\mathbf{r}_i) \Big) + \sum_{i<j} g_s \delta(\mathbf{r}_i - \mathbf{r}_j) \tag{3.18}$$

where g_s is the parameter indicating the s-wave scattering strength.

In the second quantized form, the condensate wavefunction is $\Psi(\mathbf{r}) = \sqrt{N}\psi(r)$, a

Hartree-Fock ground state should minimize local energy density

$$\mathcal{E} = \frac{\hbar^2}{2m}|\nabla\Psi(\mathbf{r})|^2 + V(\mathbf{r})|\Psi(\mathbf{r})|^2 + \frac{1}{2}g_s|\Psi(\mathbf{r})|^4 \tag{3.19}$$

with respect to $\Psi^*(\mathbf{r})$, which leads to the Gross-Pitaevskii(GP) equation,

$$\mu\Psi(\mathbf{r}) = \Big(-\frac{\hbar^2}{2m}\nabla^2 + V(\mathbf{r}) + g_s|\Psi(\mathbf{r})|^2\Big)\Psi(\mathbf{r}) \tag{3.20}$$

where the chemical potential μ describes the energy needed to add a single boson to this system at constant entropy.

The phase evolution of this ground state is described by the time-dependent Gross-Pitaevskii equation,

$$i\hbar\frac{\partial\Psi(\mathbf{r},t)}{\partial t} = \Big(-\frac{\hbar^2}{2m}\nabla^2 + V(\mathbf{r}) + g_s|\Psi(\mathbf{r},t)|^2\Big)\Psi(\mathbf{r},t) \tag{3.21}$$

In the physical limit where the boson gases adiabatically adjust to the minimal energy in the presence of a slow-varying external potential $V(\mathbf{r},t)$, the system obeys the time-dependent GP equation, which can lead to rich phenomena including dynamical control of the Josephson effect.

3.5 Generalized Gross-Pitaevskii Equation for Open System

Given the very short life($\sim 10^1 - 10^2 ps$) of polariton due to cavity photon leaking, its population has to be replenished by a pump laser, and the condensed polariton gas can be described as a steady state established in this driven-dissipation open system. To keep track of the condensate coherence in the presence of a time-dependent particle reservoir, a theoretical model was first proposed in [66], where a generalized Gross-Pitaevskii

equation,

$$i\frac{\partial\psi(\mathbf{r},t)}{\partial t} = \Big\{ -\frac{\hbar}{2m_{\mathrm{LP}}}\nabla^2 + \frac{i}{2}\Big(R\big[n_R(\mathbf{r},t)\big] - \gamma\Big) + g|\psi(\mathbf{r},t)|^2 + 2gn_R(\mathbf{r},t)\Big\}\psi(\mathbf{r},t) \quad (3.22)$$

is coupled to a rate equation accounting for the particle density in the reservoir,

$$\frac{\partial n_R(\mathbf{r},t)}{\partial t} = P - \gamma_R n_R(\mathbf{r},t) - R\big[n_R(\mathbf{r},t)\big]|\psi(\mathbf{r},t)|^2 + D\nabla^2 n_R(\mathbf{r},t) \quad (3.23)$$

Among the newly defined parameters, $R[n_R]$ is the overall replenishing rate contributed by all relaxation mechanisms, written as a functional of reservoir particle density, P is the pump rate of adding particles to the reservoir, γ and γ_R are the respective decay rates integrated over the states in the condensate and the reservoir, D is the spatial diffusive rate of the reservoir polaritons. This model has been successfully applied to interpret various phenomena, especially the experiment where a laminar flow of polaritons passes through a potential disorder without being scattered, demonstrating polariton condensates as "quantum fluids of light" [29].

In most microcavities, the individual lifetime of a polariton is shorter than the thermalization time($\sim$ 30ps), which means the polariton gas is not in thermal equilibrium. Therefore, the condensation process is not defined by a critical temperature, but rather by a threshold laser power that makes the polariton gas exceed the critical density [28]. The particle exchange rate $R[n_R]$ depends on the instant distribution in the reservoir, and therefore is very unpredictable in the non-equilibrium limit. A recent experiment [67] proves that true thermal equilibrium can develop in polariton gases with long individual lifetimes($\sim 270ps$). Thus, it is possible to maintain a particle-conserved polariton condensate by balanced pump and decay.

3.6 Monitoring Condensate Coherence via Emitted Photons

Based on the definition of off-diagonal long-range order, a condensed polariton gas with partial phase coherence can be described by a spatial correlation function,

$$g(\mathbf{r},\mathbf{r}') = \frac{\langle \psi^\dagger(\mathbf{r})\psi(\mathbf{r}')\rangle}{\langle \psi(\mathbf{r}')\rangle^* \langle \psi(\mathbf{r})\rangle} \tag{3.24}$$

This correlation can be extracted from the optical coherence of the photon field. As shown in the linear coupling model, the superposition of exciton and photon evolves at the frequency defined by the polariton eigenenergies; therefore, the partially transmitted cavity photons inherit the frequency and coherence from the polaritons. The spatial correlation in the polariton condensate can be indirectly measured via the emitted photons without collapsing the quantum state of the condensate.

Recall the positive and negative frequency components of a quantized photon field,

$$E^{(+)}(\mathbf{r},t) = \sum_{\mathbf{k},\lambda} E_{\mathbf{k}} \hat{a}_{\mathbf{k}} e^{i(\mathbf{k}\cdot\mathbf{r}-\omega_{\mathrm{pl}}t)}\mathbf{e}^{(\lambda)}, \quad E^{(-)}(\mathbf{r},t) = \sum_{\mathbf{k},\lambda} E_{\mathbf{k}} \hat{a}^\dagger_{\mathbf{k}} e^{-i(\mathbf{k}\cdot\mathbf{r}-\omega_{\mathrm{pl}}t)}\mathbf{e}^{(\lambda)} \tag{3.25}$$

where ω_{pl} is the frequency determined by the polariton energy. The intensity of the light is the expectation value at the same space-time point,

$$I(\mathbf{r},t) = \langle \hat{E}^{(-)}(\mathbf{r},t)\hat{E}^{(+)}(\mathbf{r},t)\rangle \tag{3.26}$$

and the first-order correlation in the photon field is generally defined as,

$$g^{(1)}(\mathbf{r}_1,\mathbf{r}_2;t_1,t_2) = \frac{\langle \hat{E}^{(-)}(\mathbf{r}_1,t_1)\hat{E}^{(+)}(\mathbf{r}_2,t_2)\rangle}{\sqrt{\langle \hat{E}^{(-)}(\mathbf{r}_1,t_1)\hat{E}^{(+)}(\mathbf{r}_1,t_1)\rangle\langle \hat{E}^{(-)}(\mathbf{r}_2,t_2)\hat{E}^{(+)}(\mathbf{r}_2,t_2)\rangle}} \tag{3.27}$$

Either can be calculated as an ensemble average for a partially coherent light source.

This information contained in the photon field can be extracted in an interference measurement. One way is to produce two enlarged images of the condensate using a

Michelson interferometer and overlap them at the measured plane [27], with a small displacement $\mathbf{d}$ in the plane perpendicular to the optical axis. The optical field at the measured plane can be described as,

$$\hat{E}(\mathbf{r}) = \hat{E}(\mathbf{r}) + \hat{E}(\mathbf{r}+\mathbf{d}) \tag{3.28}$$

where variable t is suppressed since there is no time delay. The light intensity is then described by the quantum expectation value,

$$\big\langle I(\mathbf{r})\big\rangle = \big\langle I(\mathbf{r})\big\rangle + \big\langle I(\mathbf{r}+\mathbf{d})\big\rangle + 2\sqrt{\big\langle I(\mathbf{r})\big\rangle\big\langle I(\mathbf{r}+\mathbf{d})\big\rangle}\mathrm{Re}[g^{(1)}(\mathbf{r},\mathbf{r}+\mathbf{d})] \tag{3.29}$$

The phase variation in the complex-valued correlation function $g^{(1)}$ leads to a sinusoidal modulation function, resulting in the parallel fringes in the interference pattern. The visibility of the fringes is defined with maximum and minimum light intensity, in this case,

$$U = \frac{\big\langle I\big\rangle_{\max} - \big\langle I\big\rangle_{\min}}{\big\langle I\big\rangle_{\max} + \big\langle I\big\rangle_{\min}} = \frac{2\sqrt{\big\langle I(\mathbf{r})\big\rangle\big\langle I(\mathbf{r}+\mathbf{d})\big\rangle}}{\big\langle I(\mathbf{r})\big\rangle + \big\langle(\mathbf{r}+\mathbf{d})\big\rangle}\big|g^{(1)}(\mathbf{r},\mathbf{r}+\mathbf{d})\big| \tag{3.30}$$

from which the correlation function can be extracted.

An alternative method uses a set of double slits with various spacings to characterize the correlation between two spatial points on the condensate [68], In this case, the photon field at the measured plane can be described by

$$\hat{E}(\mathbf{r},t) = K_1\hat{E}_1(\mathbf{r}_1,t-t_1) + K_2\hat{E}_2(\mathbf{r}_2,t-t_2) \tag{3.31}$$

where $\hat{E}_1, \hat{E}_2$ are the photon field at the two slits, t_1, t_2 are the times required for light to travel to the measured plane, K_1, K_2 are the phase factors picked up on the optical paths, taking into account the finite aperture effect. Similar to the first method, a series of point-to-point correlation strengths can be extracted from the double-slit interference pattern, showing dependence on distance $\mathbf{r} = \mathbf{r}_1 - \mathbf{r}_2$, which in the uncondensed phase

can be characterized with a function using the thermal wavelength Λ_T,

$$g^{(1)}(r) = e^{-r^2/\Lambda_T^2}, \quad \Lambda_T = \sqrt{\frac{2\pi\hbar^2}{mk_BT}} \tag{3.32}$$

It is reported in the same experiment that the correlation length goes under a transition, from the scale of thermal wavelength($\sim 3\mu m$) to the scale of the finite-size condensate($\sim 20\mu$m), as the pumping laser exceeds the threshold power for condensation.

Furthermore, the condensate and the thermal polaritons are distinguishable by their optical signal in the momentum space [67]. Consider a lens system that transforms the field distribution from object plane U_o to the image plane U_i, described by the following diffraction integration [69],

$$U_i(u,v) = \frac{\exp\left(i\frac{\pi}{\lambda f}(u^2+v^2)\right)}{i\lambda f}\iint U_o(x,y)\exp\Big[-i\frac{2\pi}{\lambda f}(ux+vy)\Big]dxdy \tag{3.33}$$

where f is the effective focal length, λ is the optical wavelength. The output signal at the image plane is effectively a 2D Fourier transform of the input signal at the object plane, with rescaled wavevectors $k_x = \frac{2\pi}{\lambda}\frac{u}{f}, k_y = \frac{2\pi}{\lambda}\frac{v}{f}$, which reveal the momentum space correlation of the condensate,

$$\hat{E}(u,v) \propto \hat{\psi}(k_x,k_y) \tag{3.34}$$

Flip the image and overlap it with the original, such that the momentum space function is,

$$\hat{\psi}(\mathbf{k}) = \hat{\psi}(k_x,k_y) + \hat{\psi}(-k_x,k_y) \tag{3.35}$$

The partial coherence in the polariton gas can be revealed in the interference fringes by fitting to the following function,

$$I(k) = N(k)[1+\alpha e^{-k/\kappa}\cos(\beta k)] \tag{3.36}$$

along with a Gaussian profile function in momentum space,

$$N(k) = Be^{-k^2/\sigma_k^2} \tag{3.37}$$

where α takes a value between 0 and 1 and accounts for overall coherence, β accounts for the rescaling of momentum space in the image, and κ characterizes typical coherent lengths for the finite-size condensate.

Using the extracted fitting parameters and the density function $N(k)$, the coherent fraction of the condensed polariton gas can be estimated as,

$$\frac{n_0}{n_{\text{tot}}} = \frac{\alpha \int d^2k\ N(k)e^{-k/\kappa}}{\int d^2k\ N(k)} \tag{3.38}$$

3.A Polariton-Phonon Interaction

An exciton-polariton inherits the interaction with the crystal lattice from its exciton component. Lattice vibrations, also known as phonons, deform the crystal and change the electrical field acting on the electron and hole wavefunctions. The matrix elements of electron/hole-phonon interaction can be derived from a perturbation theory [70], in this case, based on the deformation potential,

$$U(\mathbf{r}_e, \mathbf{r}_h) = \Delta(\mathbf{r}_e)a_e - \Delta(\mathbf{r}_h)a_h \tag{3.39}$$

where $\Delta(\mathbf{r_e}), \Delta(\mathbf{r_h})$ are the relative positions and spatial profiles of the deformation, a_e, a_r are the deformation intensity in energy units characterized by experiments.

Following the review paper[71], the method originally developed for excitons [62] can be adapted for polaritons. The Hamiltonian for the lower polariton relaxation process from mode $\mathbf{k}$ to mode $\mathbf{k}-\mathbf{q}$ is,

$$H^{pol-ph} = \sum_{\mathbf{k},\mathbf{q},q_z} X^*_{\mathbf{k}-\mathbf{q}} X_{\mathbf{k}} \langle \mathbf{k}-\mathbf{q}|H^{\text{exc-ph}}(\mathbf{q}, q_z)|\mathbf{k}\rangle \times (\hat{c}^\dagger_{\mathbf{q},q_z} - \hat{c}_{-\mathbf{q},-q_z})\hat{b}^\dagger_{\mathbf{k}-\mathbf{q}}\hat{b}_{\mathbf{k}} \tag{3.40}$$

where $H^{\text{exc-ph}}$ is an effective Hamiltonian written in terms of exciton-phonon interaction, $X_{\mathbf{k}}$ is the Hopfield coefficient that accounts for the exciton proportion in the polariton. The total phonon wave vector is decomposed into ($\mathbf{q}$ in the plane of the quantum well and q_z perpendicular to the plane; the in-plane momentum of the exciton-phonon system is conserved, but phonon can transfer the m, so there is a sum over all possible q_z values.

Using the quantum well envelope function $F(\mathbf{R})f_e(z_e)f_h(z_h)$ the plane wave phonon function in mode $(\mathbf{q}, q_z)$, the deformation $\Delta(\mathbf{r}_e)/\Delta(\mathbf{r}_h)$ over the distribution of $\mathbf{r}_e/\mathbf{r}_h$ to evaluate the deformation energy, and through this, evaluate the interaction coefficient,

$$G(\mathbf{q}, q_z) = \langle \mathbf{k} - \mathbf{q}|H^{\text{exc-ph}}(\mathbf{q}, q_z)|\mathbf{k}\rangle = i\sqrt{\frac{\hbar(q^2 + q_z^2)^{1/2}}{2\rho V u}}[a_e I_e^{\parallel}(\mathbf{q})I_e^z(q_z) - a_h I_h^{\parallel}(\mathbf{q})I_h^z(q_z)] \tag{3.41}$$

The square root term originates from phonon quantization, where ρ is the mass density of the crystal, V is the quantization volume of the phonon, u is the longitudinal sound velocity. The overall integral is separated into two superposition integrals, the in-plane part and the z-direction part,

$$\begin{aligned} I_{e/h}^{\parallel}(|\mathbf{q}|) &= [1 + (\frac{m_{h/e}}{2M}|\mathbf{q}|a_B)^2]^{-3/2} \\ I_{e/h}^{z}(q_z) &= \int_0^{L_{QW}} \mathrm{d}z\, |f_{e/h}(z)|^2 \exp(iq_z z) \end{aligned} \tag{3.42}$$

The average transition rate of the polariton by emitting a phonon in mode $(\mathbf{q}, q_z)$ can be calculated in Fermi's golden rule,

$$W_{\mathbf{k}\to\mathbf{k}-\mathbf{q}}^{pol-ph} = \frac{2\pi}{\hbar}\sum_{q_z}|X_{\mathbf{k}-\mathbf{q}}|^2|X_{\mathbf{k}}|^2|G(\mathbf{q}, q_z)|^2\delta(E_{\mathbf{k}-\mathbf{q}} - E_{\mathbf{k}} + \hbar\omega_{\mathbf{q},q_z}) \tag{3.43}$$

Summing over the initial and final states of phonons and assuming the vibrating lattice is a heat reservoir at a certain temperature, the total transition rate by emitting phonons is,

$$W_{\mathbf{k}\to\mathbf{k}-\mathbf{q}}^{pol-ph} = \frac{2\pi}{\hbar}|X_{\mathbf{k}-\mathbf{q}}|^2|X_{\mathbf{k}}|^2|G(\mathbf{q}, q_z^0)|^2\left(N_B(\hbar\omega_{\mathbf{q},q_z^0}) + 1\right) \tag{3.44}$$

where $(\mathbf{q}, q_z^0)$ represents a phonon mode that satisfies both the conservation of in-plane

momentum and conservation of the total energy, and $N_B(\hbar\omega_{\mathbf{q},q_z^0})$ is a Bose-Einstein distribution of such phonons.

3.B Polariton-Polariton Interaction

Exciton-polaritons also inherit the interaction among their exciton components, which in turn can be attributed to their composition parts, the electrons and holes. The exchange interaction between pairs of these fermionic particles plays an important part in the elastic scattering of excitons [72].

In a quantum well, the scattering process can be described in the 2D momentum space using the matrix element $\langle \mathbf{K_1}+\mathbf{Q}, \mathbf{K_2}-\mathbf{Q}|V_{\text{tot}}|\mathbf{K_1}, \mathbf{K_2}\rangle$ where V_{tot} is the Fourier transform of the real space potential, taking into account the direct and exchange interaction among the electrons and holes out of the two excitons.

Recall that the exciton state in momentum space can be written as pair creation states in the electron/hole space,

$$|\mathbf{K_1}, \mathbf{K_2}\rangle = \hat{b}_{\mathbf{K_1}}\hat{b}_{\mathbf{K_2}}|0\rangle_B = \sum_{\mathbf{k}_1,\mathbf{k}_2} \psi_\nu^*(\mathbf{k_1} - \alpha\mathbf{K_1})\psi_\nu^*(\mathbf{k_2} - \alpha\mathbf{K_2})\hat{e}^\dagger_{\mathbf{k_1}}\hat{h}^\dagger_{\mathbf{K_1}-\mathbf{k_1}}\hat{e}^\dagger_{\mathbf{k_2}}\hat{h}^\dagger_{\mathbf{K_2}-\mathbf{k_2}}|0\rangle_F \tag{3.45}$$

where $|0\rangle_B$ represents the vacuum in exciton space, $|0\rangle_F$ represents the fermi sea, $\alpha = m_e/(m_e + m_h)$.

The matrix elements between momentum states are derived in detail by reference [73]. In the limit $K_1, K_2, Q \ll a_B^{-1}$, meaning the center of mass kinetic energy is much smaller than the exciton binding energy. The matrix element is estimated for electron-electron, hole-hole exchange interaction,

$$\langle \mathbf{K_1} + \mathbf{Q}, \mathbf{K_2} - \mathbf{Q}|V_{\text{ee}} + V_{\text{hh}}|\mathbf{K_1}, \mathbf{K_2}\rangle \sim -4 \sum_{\mathbf{k_1},\mathbf{k_2}} V_{\mathbf{k_1}-\mathbf{k_2}}|\psi(\mathbf{k_1})|^2|\psi(\mathbf{k_2})|^2 \tag{3.46}$$

and for electron-hole exchange interaction,

$$\left\langle \mathbf{K_1}+\mathbf{Q},\mathbf{K_2}-\mathbf{Q}\middle|V_{\mathrm{eh}}\middle|\mathbf{K_1},\mathbf{K_2}\right\rangle \sim 4\sum_{\mathbf{k_1},\mathbf{k_2}} V_{\mathbf{k_1}-\mathbf{k_2}}|\psi(\mathbf{k_1})|^2\psi(\mathbf{k_2})\psi^*(\mathbf{k_1}) \tag{3.47}$$

where the $V_{\mathbf{k}}$ is the Fourier transform of the Coulomb potential, $\psi(\mathbf{k})$ is the Fourier transform of the exciton orbital wavefunction, following convention defined in Eq.(2.8), the orbital ν and center of mass momentum $\mathbf{K}$ is drop from the index for ground orbital and low kinetic energy.

Summing up the two parts gives the matrix element for exciton-exciton scattering,

$$M \sim 2\sum_{\mathbf{k},\mathbf{k}'} V_{\mathbf{k}-\mathbf{K}'}\psi(\mathbf{k})\psi(\mathbf{k}')\Big(|\psi(\mathbf{k})|^2-\psi(\mathbf{k})\psi(\mathbf{k}')\Big) \sim 6E_B\frac{a_B^2}{S} \tag{3.48}$$

where E_B is the bounding energy, a_B is the "Bohr radius" for 2D exciton, and S is the homogeneous area in which the envelope wavefunction is normalized. This expression is a good theoretical estimation of the s-wave scattering strength between two excitons, which can be inherited by polariton-polariton interaction. The transition rate $W^{pol-pol}_{\mathbf{k}\to\mathbf{k}'}$ used in the Boltzmann equation can also be estimated as the ensemble average of this four-wave scattering process, with a partial trace focus on the scattered down state $\mathbf{k}'$.

A real quantum well usually contains local disorders($\sim 10-100$ nm) known as "natural quantum dots", which act on the center of mass of excitons as weak trapping potentials. The exchange interaction between two excitons confined on such a quantum dot is strongly affected by the overlap of their wavefunctions, which gives rise to fine structure splitting within the respectively degenerate "bight exciton" and "dark exciton" states [74]. However, the spatial averaging effect of the photon field makes exciton-polaritons insensitive to these potential disorders, therefore the major consequences of polariton-polariton interaction are sufficiently accounted for by the s-wave scattering picture.

Chapter 4

Josephson Effect in Dilute Boson Gases

The original work of Josephson is based on the Bardeen-Cooper-Schrieffer(BCS) theory of superconductivity and the correlated tunneling of Cooper pairs. However, its essential idea of broken symmetry, that two areas with macroscopic coherence and independent phases can spontaneously arise from thermal equilibrium, applies not only to superconducting systems. The Ginzburg-Landau phenomenological theory, which was rigorously proved by Gor'kov [36] to be a physical limit of BCS theory, captures this main idea and has great similarity to the mean-field theory of dilute boson gases, and therefore bridges superconductivity and superfluidity despite their different microscopic mechanisms. I will discuss the Josephson effect in this chapter using the Ginzburg-Landau theory, naturally followed by the discussion of exploring it in dilute bosonic gases consisting of excitons and exciton-polaritons.

4.1 Ginzburg-Landau Theory

The Ginzburg-Landau theory is formulated in terms of the free energy,

$$F[\psi, \mathbf{A}] = F_n + \alpha|\psi|^2 + \frac{\beta}{2}|\psi|^4 + \frac{1}{2m^*}\Big|\Big(-i\hbar\nabla - e^*\mathbf{A}\Big)\psi\Big|^2 + \frac{|\mathbf{B}|^2}{2\mu_0} \tag{4.1}$$

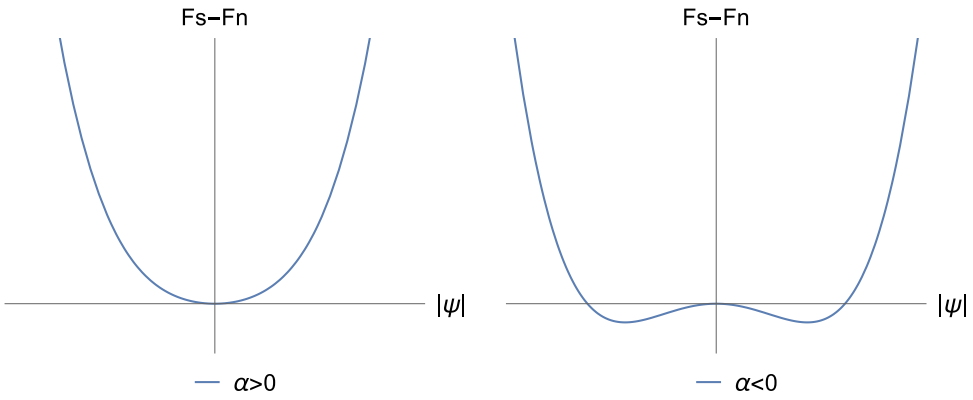

Figure 4.1: Ginzburg Laudau free energy for $\alpha > 0$ and $\alpha < 0$

where a complex-valued pseudo wavefunction $\psi(\mathbf{r})$ is introduced as the order parameter, F_n accounts for the free energy of the normal conducting state, and vector potential $\mathbf{A}$ and magnetic field $\mathbf{B}$ account for the interaction with the external magnetic field, keeping the theory in a gauge-invariant form.

Assuming that F is an analytic function of ψ, and that $\psi(\mathbf{r})$ is small and slowly varying in space, it should suffice to expand F in a series of ψ only to the 4th order,

$$F_s[\psi] - F_n = \alpha|\psi|^2 + \frac{1}{2}\beta|\psi|^4 \tag{4.2}$$

The phenomenological parameter $\alpha(T)$ and $\beta(T)$ account for the change over varying temperature, β has to remain positive to give a reasonable potential term at large ψ; a positive α gives a minimum at $|\psi| = 0$ while a negative α gives two minima at $|\psi|^2 = -\alpha/\beta$, which implies a non-vanishing superconducting density(see figure 4.1). Therefore, the occurrence of superconducting density or current signals a second-order phase transition in this model.

In a spatially inhomogeneous problem, the order parameter $\psi(\mathbf{r})$ adjusts itself to minimize the local free energy density. The Euler-Lagrangian equation with respect to ψ^* is satisfied everywhere across the real space, which leads to the first Ginzburg-Landau equation,

$$\alpha\psi + \beta|\psi|^2\psi + \frac{1}{2m^*}\Big(-i\hbar\nabla - e^*\mathbf{A}\Big)^2\psi = 0 \tag{4.3}$$

The order parameter is related to the superconducting density $\rho = |\psi|^2$, so charge

continuity requires,

$$\nabla \cdot \mathbf{j} + e^* \frac{\partial |\psi|^2}{\partial t} = 0 \tag{4.4}$$

which leads to the second Ginzburg-Landau equation,

$$\mathbf{j} = \frac{e^*}{m^*} Re\Big\{ \psi^* \big(-i\hbar\nabla - e^* \mathbf{A} \big) \psi \Big\} \tag{4.5}$$

Substituting $\psi = \sqrt{\rho} e^{i\varphi}$ and assuming that ρ is nearly constant, one will find that the supercurrent is proportional to the gradient of phase,

$$\mathbf{j} = \rho \frac{e^*}{m^*} \Big(\hbar\nabla\varphi - e^* \mathbf{A} \Big) \tag{4.6}$$

which is invariant under gauge transformation,

$$\mathbf{A} \to \mathbf{A} + \nabla\chi, \quad \varphi \to \varphi + \frac{e^*}{\hbar}\chi \tag{4.7}$$

By choosing the London Gauge $\nabla \cdot \mathbf{A_s} = 0,\ \mathbf{A_s} = 0$ (bulk), $\mathbf{A_s} \cdot \hat{n} = 0$ (surface) allows us to identify the spatially homogeneous contribution,

$$\mathbf{j_s} = -\frac{(e^*)^2 \rho}{m^*} \mathbf{A_s} \tag{4.8}$$

which leads to the famous London equations describing perfect conductivity and the Meissner effect,

$$\frac{\partial \mathbf{j_s}}{\partial t} = \frac{n_s e^2}{m} \mathbf{E}, \quad \nabla \times \mathbf{j_S} = -\frac{n_s e^2}{m} \mathbf{B} \tag{4.9}$$

where the parameter choice $e^* = 2e,\ m^* = 2m_e,\ \rho = \frac{1}{2} n_s$ agrees with the microscopic picture of Cooper pairs.

4.2 Coherence Length and Superfluid Stiffness

To examine the possible mechanisms that break the phase continuity and give rise to the Josephson effect, one should take a closer look at the spatial variation in (4.3),

$$\frac{\hbar^2}{2m^*|\alpha(T)|}\nabla^2 f + f - |f|^2 f = 0 \tag{4.10}$$

where $f = \psi/\psi_\infty$ is a normalized pseudo wavefunction, ψ_∞ represents the ideal homogeneous order parameters buried at infinite depth in contrast to the inhomogeneous ψ sensitive to boundary conditions. It is natural to characterize the spatial gradient of f with the Ginzburg-Landau coherent length,

$$\xi(T) = \frac{\hbar}{\sqrt{2m^*|\alpha(T)|}} \tag{4.11}$$

In particular, the superfluid stiffness can be defined as $\gamma = 2\xi^2(T)\rho$, such that the local free energy density varies with the phase $\mathcal{F}(\mathbf{r}) = \frac{1}{2}\gamma|\nabla\varphi(\mathbf{r})|^2$.

Therefore, a weak link that suppresses the superconducting density ρ, be it a thin insulator, a normal metal, or a constriction in the superconductor, can reduce the phase stiffness between the two superconducting leads, which is essential for a Josephson junction.

Considering the axial symmetry of the junction, it suffices to model it with the one-dimensional case,

$$\xi^2\frac{d^2 f}{dx^2} + f - |f|^2 f = 0 \tag{4.12}$$

In a typical setup of a Josephson junction, it is safe to assume the two bulk superconductors have reached thermal equilibrium, each satisfying $|f| = 1$ but possibly with a phase difference between the two sides of the junction. In the weak link with length $L \ll \xi$, the change in the first term dominates the balance of equation(4.12), which allow us to use a simplified ansartz in the form of $f = a + bx$, using the boundary condition

$f = 1$ at $x = 0$, and $f = e^{i\Delta\varphi}$ at $x = L$, we arrive at the solution,

$$f = (1 - x/L) + (x/L)e^{i\Delta\varphi} \tag{4.13}$$

Substituting it in (4.5) leads to the equation for supercurrent,

$$I_s = I_0 \sin(\Delta\varphi) \tag{4.14}$$

The characteristic current can be evaluated as,

$$I_0 = \frac{e^* \hbar \psi_\infty^2}{m^*} \frac{\mathcal{A}}{L} \tag{4.15}$$

where $\mathcal{A}$ is the cross-section area of the weak link. As we can see from (4.15), the geometry of the superconducting electrodes is not important, as long as they are much smaller than the Ginzburg-Landau coherent length; the deciding factor of the Josephson current is the geometry of the weak link.

By the same principle, the weak coupling between two homogeneous Bose-Einstein condensates can give rise to the Josephson effect. From (3.20) we evaluated the superfluidity stiffness of a Bose-Einstein condensate described by a mean field wavefunction $\Psi(\mathbf{r}) = \sqrt{N(\mathbf{r})}e^{i\theta(\mathbf{r})}$,

$$\gamma = \frac{\hbar^2 N}{2m} \tag{4.16}$$

such that the energy density over the phase gradient $\mathcal{E} = \frac{1}{2}\gamma|\nabla\theta|^2$.

Therefore, lowering the condensate density could effectively reduce the phase stiffness and form a weak link between two homogenous Bose-Einstein condensates.

4.3 Josephson Equations

An intuitive derivation of Josephson equations based on a "two-state system" was given by Feynman in 1965 [75]. Consider the "small junction" case, where the coherence length ξ is much larger than the dimension of the device so that the density and phase variation

within each superconductor is negligible and represented by a constant order parameter, $\psi_\sigma = \sqrt{\rho_\sigma} e^{i\phi_\sigma}, \sigma \in \{L, R\}$.

Consider the junction subject to a total Hamiltonian,

$$H = H_L + H_R + H_T \tag{4.17}$$

where the projection on superconducting electrodes gives

$$H_L = E_L \big|L\big\rangle\big\langle L\big|, \quad H_R = E_R \big|R\big\rangle\big\langle R\big|, \tag{4.18}$$

and the tunneling between left and right gives,

$$H_T = -J\Big(\big|L\big\rangle\big\langle R\big| + \big|R\big\rangle\big\langle L\big|\Big) \tag{4.19}$$

An arbitrary state vector is in a superposition of the left and right,

$$\big|\Psi\big\rangle = \psi_L \big|L\big\rangle + \psi_R \big|R\big\rangle \tag{4.20}$$

where $\psi_{L/R}$ are the order parameters that carry the superconducting density.

The time-evolution of the junction can be written in the Schrödinger-like equation,

$$i\hbar \frac{d}{dt}\big|\Psi\big\rangle = H\big|\Psi\big\rangle \tag{4.21}$$

In particular, when the energy difference is introduced by a voltage source $E_L - E_R = 2eV$, we arrive at the coupled Josephson equations,

$$i\hbar \frac{d}{dt} \begin{pmatrix} \psi_L \\ \psi_R \end{pmatrix} = \begin{pmatrix} eV & -J \\ -J & -eV \end{pmatrix} \begin{pmatrix} \psi_L \\ \psi_R \end{pmatrix} \tag{4.22}$$

This formalism is in agreement with Ginzburg-Landau theory, given the potential acting on a single charged particle would raise the free energy locally by $e^* V |\psi|^2$.

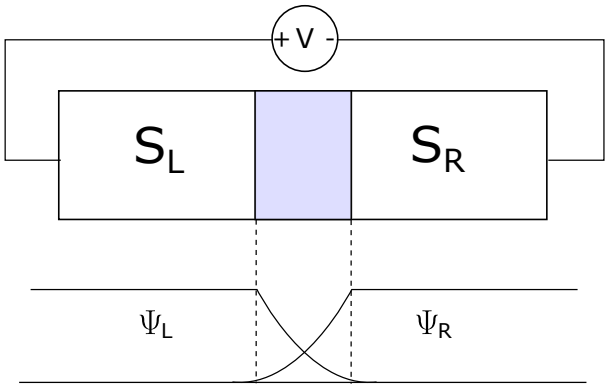

Figure 4.2: Josephson Junction connected to a voltage source.

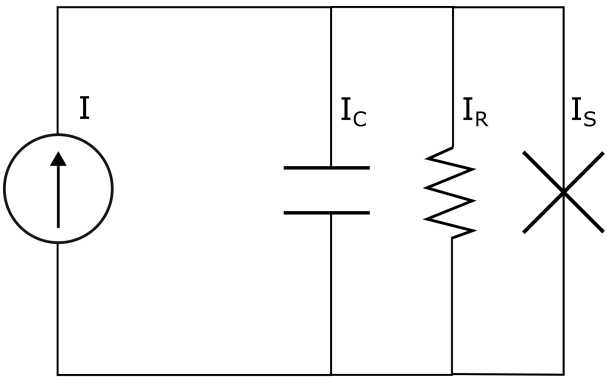

Figure 4.3: Symbolic Circuit of the Resistively Capacitively Shunted Junction(RCSJ) model.

By matching the real and imaginary parts, one can reorganize the equations into:

$$\begin{aligned} \frac{d\rho_R}{dt} = -\frac{d\rho_L}{dt} &= \frac{2J}{\hbar}\sqrt{\rho_L\rho_R}\sin\phi \\ \frac{d\phi}{dt} &= \frac{2eV}{\hbar} + \frac{J}{\hbar}\Big(\sqrt{\frac{\rho_L}{\rho_R}} - \sqrt{\frac{\rho_R}{\rho_L}}\Big) \end{aligned} \tag{4.23}$$

where $\phi = \phi_R - \phi_L$ is the phase difference. The first equation gives the amplitude of supercurrent, while the second equation gives the rate of phase evolution, which can account for AC Josephson effect. In typical Josephson junctions, the oscillations in superconducting density are negligible compared to their average amplitude, therefore,

$$\frac{d\phi}{dt} \approx \frac{2eV}{\hbar} \tag{4.24}$$

decouples the second equation from the first.

A particularly interesting aspect of the Josephson junction lies in the resistively and capacitively shunted junction(RCSJ) model(see figure 4.3). This model is also a realistic description of any superconducting junction, for it takes into account the intrinsic normal current and the capacitance arising from the junction structure. The total current that runs through the parallel shunted circuits consists of three parts,

$$I = C\frac{dV(t)}{dt} + \frac{V(t)}{R} + I_0 \sin\phi(t), \tag{4.25}$$

where

$$I_0 = \frac{4eJ\sqrt{\rho_L \rho_R}}{\hbar} \tag{4.26}$$

is the upper limit of supercurrent that can be supported by the junction. Using approximation (4.24), it becomes a second-order differential equation in ϕ,

$$I = \frac{\hbar}{2e}C\frac{d^2\phi(t)}{dt^2} + \frac{\hbar}{2e}\frac{1}{R}\frac{d\phi(t)}{dt} + I_0 \sin\phi(t) \tag{4.27}$$

With the rescaling of time and change of variables,

$$\tau = \omega_0 t, \quad \omega_0 = \left(\frac{2eI_0}{\hbar C}\right)^{1/2}, \alpha = \frac{I}{I_0}, \quad \beta = \frac{1}{RC}\frac{1}{\omega_0} \tag{4.28}$$

the dimensionless equation reads,

$$\alpha = \frac{d^2\phi}{dt^2} + \beta\frac{d\phi}{dt} + \sin(\phi) \tag{4.29}$$

which can be broken down into two first-order differential equations,

$$\frac{d\phi}{dt} = z, \quad \frac{dz}{dt} = \alpha - \beta z + \sin(\phi) \tag{4.30}$$

and analyzed in the phase space of (ϕ, z).

In an analogy to a mechanical system, the potential function U is determined by the sinusoid term arising from the supercurrent. In the case of no driving current and

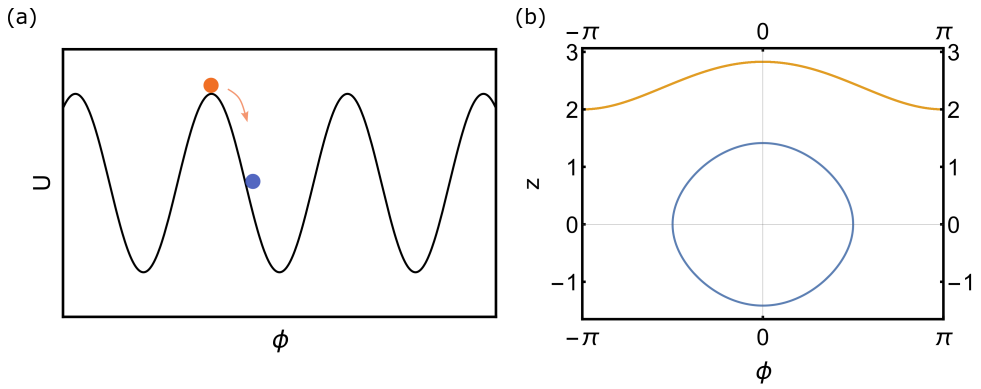

Figure 4.4: Capacitively Shunted Junction with no external driving current (a)potential function and initial conditions (b)Corresponding trajectories in $(\phi, \dot{\phi})$ phase space

damping($\alpha = 0, \beta = 0$), the system has two types of periodic trajectories(see figure 4.4), the one starts at the top of the hill with non-zero velocity, would run over the next hill and goes on to enter next period of 2π, therefore is an open curve in the phase space; the one starts in the valley with zero velocity would swing back and oscillated around the same minimal energy point, therefore is a closed loop in the phase space. Note that z here is defined as the rate of change in phase angle, which is a velocity in the mechanical analog, hence unbounded.

With external driving current introduced, the potential function resembles a "tilted washboard", which can be tuned by the relative current amplitude $\alpha > 0$, and with the damping($\beta > 0$) the closed loop trajectory would reduce to the equilibrium position at its center, giving a vanishing phase angle velocity, and by (4.24) result in a vanishing average voltage; while the open curve trajectory running down the tilted washboard would eventually reach a steady velocity such that the energy gained each period of the sinusoidal potential is dissipated via the damping force during the same time, result in a nonzero constant voltage. Therefore, each damping coefficient corresponds to a $I - V$ characteristic curve, and at the limit $\alpha \gg 1$, the total current is dominated by the shunt resistor; therefore, they all asymptotically approach the straight line that agrees with Ohm's law.

The hysteresis is developed in the following procedure: The junction starts in thermal equilibrium with zero phase angle velocity, as the driving current increases, the initial

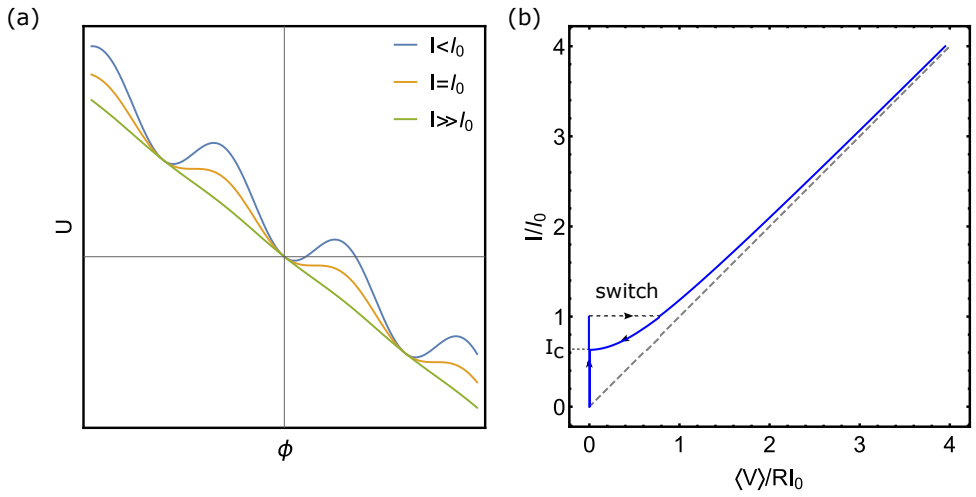

Figure 4.5: Bistability and Hysteresis of RCSJ model (a)potential function varying over driving current (b)$I-V$ characteristics for fixed damping coefficient β_J

state $\phi = 0$ remains a local minimum of the potential function and, therefore keeps giving zero voltage, until the driving current exceeds the upper limit of supercurrent($\alpha = 1$) the $\phi = 0$ is no longer a local minimum, and it starts to run down the potential and eventually reaches a constant velocity. On the time scale of experimental observation, the voltage is instantly switched from zero to the $I-V$ curve. From this point on, decreasing the current would not switch the junction back to zero voltage; rather, the voltage would follow the $I-V$ curve and gradually reduce to zero at the critical current I_c, which means at this tilted angle the damping force is sufficiently strong to stop a running state of the junction. Therefore, when the driving current is between I_c and I_0, the system shows bistability. This mechanism has been used to study ultrafast switching in conventional logic bits.

4.4 Boson Josephson Junctions

The boson Josephson junction was first proposed in the context of an atomic Bose-Einstein condensate[12, 76]. Inspired by the dipole trap, which acts like a harmonic potential, a double-well potential is formed by two dipole traps set close to each other.

Assuming that the elementary excitation in the trapped atomic gas only goes up to the two lowest bound states, and the probability of finding particles in the barrier is sufficiently low, one can project the total wavefunction into a time-dependent superposition

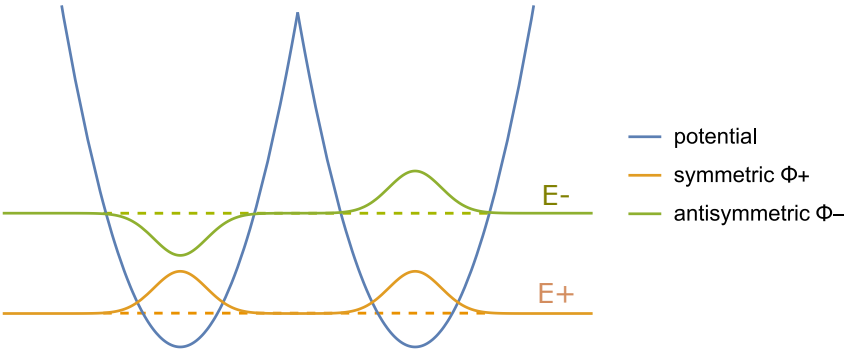

Figure 4.6: Double Harmonic potential and Wavefunctions

of two spatial modes, each defined by the ground state of a single well,

$$\Psi(\mathbf{r},t) = \psi_1(t)\Phi_1(\mathbf{r}) + \psi_2(t)\Phi_2(\mathbf{r}) \tag{4.31}$$

Defining the complex coefficient on each side with density and phase $\psi_\kappa = \sqrt{N_\kappa}\exp(i\phi_\kappa)$, in the same idea of (4.5), one should find a charge-neutral superfluid current, which is defined as the Josephson current of the boson junction,

$$I_s = I_0\sqrt{N_1 N_2}\sin(\phi_2 - \phi_1) \tag{4.32}$$

The most important difference compared to (4.15) is that the density oscillation in the dilute boson gas is not negligible and therefore needs to be tracked rather than absorbed in a constant parameter. The characteristic current I_0 can be calculated as an integration over the plane normal to the middle point $z = 0$ between the two single wells,

$$I_0 = \frac{\hbar}{m}\int_{z=0} d\sigma(\Phi_1^*\partial_z\Phi_2 - \Phi_2^*\partial_z\Phi_1) \tag{4.33}$$

Unlike in a superconducting junction, where the Josephson coupling strength is mainly determined by the geometry of the weak link, a dilute boson gas can be highly inhomogeneous over the whole trapping area, meaning this integral is sensitive to the changes in any part of the double-well potential.

Applying the (4.31) to (3.21), one should find the equations of motion for the complex

coefficients, which resemble the Josephson equations for the two-state model,

$$i\hbar\frac{d}{dt}\begin{pmatrix}\psi_1\\ \psi_2\end{pmatrix}=\begin{pmatrix}E_1+U_1|\psi_1|^2 & -J\\ -J & E_2+U_2|\psi_2|^2\end{pmatrix}\begin{pmatrix}\psi_1\\ \psi_2\end{pmatrix} \tag{4.34}$$

where $E_{1,2}$ is the ground state energies for each single well, $U_{1,2}=\int d^3r\ g|\Phi_{1,2}(\mathbf{r})|^4$ is the interaction energies normalized on the spatial mode within each side, and the Josephson energy can be estimated as, $J\approx\int d^3r\ \Phi_1^*(\mathbf{r})\Big(-\frac{\hbar^2}{2m}\nabla^2+V_{\text{ext}}(\mathbf{r})\Big)\Phi_2(\mathbf{r})$ given that the spatial wavefunction Φ_1 and Φ_2 are almost orthogonal. The two lowest bound states can be projected into the superposition the single-well ground state $\Phi_+=(\Phi_1+\Phi_2)/\sqrt{2}$ and $\Phi_-=(\Phi_1-\Phi_2)/\sqrt{2}$, which satisfy,

$$E_\pm=\int d^3r\ \Phi_\pm^*(r)\Big(-\frac{\hbar^2}{2m}\nabla^2+V_{\text{ext}}(\mathbf{r})\Big)\Phi_\pm(\mathbf{r}) \tag{4.35}$$

therefore the Josephson energy can be experimentally characterized as $J\approx(E_--E_+)/2$ by measuring the symmetric and antisymmetric states trapped in the double well.

Consider the total boson number N_T is conserved but oscillating between the two trapped condensates. By defining $z=(|\psi_2|^2-|\psi_1|^2)/N_T,\ \phi=\phi_2-\phi_1$, and applying change of variables

$$U=\frac{U_1+U_2}{2},\quad \Lambda=\frac{UN_T}{2J},\quad \Delta\mu=\frac{E_1-E_2}{2J}+\frac{U_1-U_2}{4J}N_T$$

to equation (4.34), one should find the dimensionless Hamiltonian,

$$H(z,\phi)=\Lambda\frac{z^2}{2}+\Delta\mu z-\cos\phi\sqrt{1-z^2}, \tag{4.36}$$

and the following equations of motion,

$$\dot{z}=-\frac{\partial H}{\partial\phi}=-\sqrt{1-z^2}\sin\phi,\quad \dot{\phi}=\frac{\partial H}{\partial z}=\Lambda z+\Delta\mu-\sqrt{1-z^2}\sin\phi \tag{4.37}$$

The interaction among the bosons gives rise to the z^2 term, which is analogous to

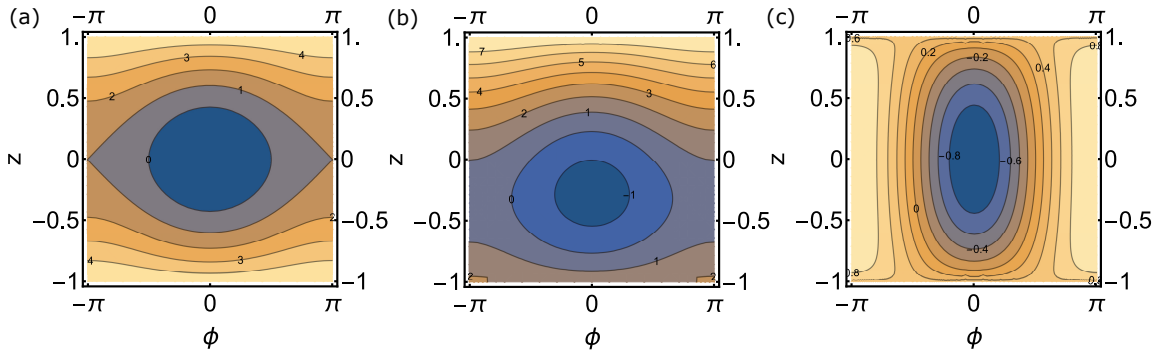

Figure 4.7: Isoenergy contours in the (z, ϕ) phase space for given parameters (a)$\Lambda = 10, \Delta\mu = 0$, (b)$\Lambda = 10, \Delta\mu = 3$,(c)$\Lambda = 1, \Delta\mu = 0$

kinetic energy in the mechanical model, and the capacitor charging energy in the RCSJ model. The dependence on z makes the boson junction resemble a non-linear pendulum with a varying length. Plotting the isoenergy contours in the (z, ϕ) phase space is straightforward given the explicit expression of Hamiltonian. Similar to RCSJ, there are two types of trajectories, open curves and closed loops. But z in the boson junction is a normalized density difference, therefore an open curve in the upper or lower plane of z implies a nonzero density bias between the two condensates(see figure4.7(a)), thus giving rise to a unique phenomenon, named macroscopic quantum self-trapping (MQST) after the original paper [12]. The impact of the parameters can be understood by comparing the isoenergy contours(figure 4.7). A larger Λ means a smaller effective mass in the mechanical analog, which means a larger fraction of the trajectories will be open curves representing the running phase where the pendulum swings over the top. A potential bias $\Delta\mu$ shifts the balance of density difference, and creates new isoenergy contours that intersect with multiple original contours without the bias.

Therefore, tuning the potential bias while maintaining the spacing of energy contours at a constant interaction strength is an effective method of switching between trajectories. Here I present an example generated by numerical simulation(figure 4.8). The blue contours represent the unbiased isoenergy surfaces at $\Lambda = 1, \Delta\mu = 0$, which will be replaced by the red contours once the bias potential $\Delta\mu = 1.2$ is turned on. The black dots represent the switching point between the two types of trajectories. In an ideal control sequence(figure 4.8b), the system starts in an oscillation phase with larger amplitude, fol-

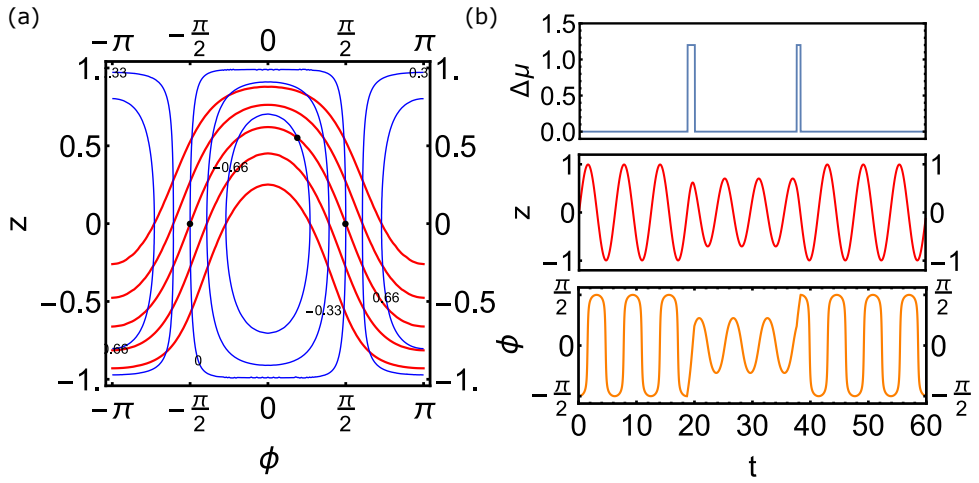

Figure 4.8: Showing a control sequence that switches the boson Josephson junction between two stable trajectories

lows the red contour after the first switching point until arriving at the second switching point on an energy surface of smaller amplitude, stays there for a few oscillation periods while the bias potential is off, then follows the red contour to reach the third switching point and return to the starting state of larger amplitude. The experimental realization depends on the ramping time of the control potential, and the coherent time of the condensates and needs to be discussed case by case based on microscopic mechanisms. I will revisit the issue of time scale in the context of electrically controlled polariton junctions.

4.5 Correlated Tunneling of Electron-Hole Pairs

Following the discussion of previous sections, a closer analog of a conventional superconducting junction can be formed by two coupled homogeneous exciton condensates, where the tunneling of an exciton can be considered as a second-order process, the correlated tunneling of an electron-hole pair. Here I present my original work on this theoretical model.

Recall in homogenous gases, the excitons are labeled by their bound orbitals ν and center of mass momentum $\mathbf{K}$(equation (2.10)), for both the left(L) and right(R) side of

the junction, hence the unperturbed Hamiltonian,

$$H_0 = \sum_{\nu\mathbf{K},\sigma} \epsilon_{\nu\mathbf{K},\sigma} \hat{b}^\dagger_{\nu\mathbf{K},\sigma} \hat{b}_{\nu\mathbf{K},\sigma}, \quad \sigma \in \{L, R\} \tag{4.38}$$

An effective tunneling Hamiltonian can be constructed in the bosonic operators,

$$H_T = \sum_{\nu\mathbf{K}} \Big(t_{\nu\mathbf{K}} \hat{b}^\dagger_{\nu\mathbf{K},R} \hat{b}_{\nu\mathbf{K},L} + t^*_{\nu\mathbf{K}} \hat{b}^\dagger_{\nu\mathbf{K},L} \hat{b}_{\nu\mathbf{K},R} \Big) \tag{4.39}$$

where $t_{\nu\mathbf{K}}$ can be evaluated in the correlated tunneling process.

The first-order tunneling Hamiltonian can be written in the joint plane-wave basis of electrons and holes,

$$H_T^{(1st)} = \sum_{\mathbf{k}} \Big(t_e \hat{e}^\dagger_{\mathbf{k},R} \hat{e}_{\mathbf{k},L} + t^*_e \hat{e}^\dagger_{\mathbf{k},L} \hat{e}_{\mathbf{k},R} \Big) + \sum_{\mathbf{k}'} \Big(t_h \hat{h}^\dagger_{\mathbf{k}',R} \hat{h}_{\mathbf{k}',L} + t^*_h \hat{h}^\dagger_{\mathbf{k}',L} \hat{h}_{\mathbf{k}',R} \Big) \tag{4.40}$$

where t_e and t_h are the single electron and hole tunneling strengths dependent on the geometry and potential landscape of the tunneling barrier.

The goal is to find the matrix element for single exciton tunneling,

$$t_{\nu\mathbf{K}} = \big\langle 0_L, 1_R \big| H_T^{(2nd)} \big| 1_L, 0_R \big\rangle_{\nu\mathbf{K}} \tag{4.41}$$

where the Dirac notations indicate the number of excitons in state $\nu\mathbf{K}$ on each side. For example, the ket state can be expanded in the electron-hole basis following the definition of equation(2.10),

$$\big| 1_L, 0_R \big\rangle = \hat{b}^\dagger_{\nu K,L} \big| 0_L, 0_R \big\rangle = \sum_{\mathbf{k}} \psi_\nu \Big(\mathbf{k} - \frac{m_e}{m_e + m_h} \mathbf{K} \Big) \hat{e}^\dagger_{\mathbf{k},L} \hat{h}^\dagger_{\mathbf{K}-\mathbf{k},L} \big| 0 \big\rangle \tag{4.42}$$

where $\big|0\big\rangle$ represents the unexcited fermi sea.

The effective second-order tunneling Hamilton can be derived from a perturbation

theory,

$$t_{\nu\mathbf{K}} = \frac{1}{2}\big\langle 0_L, 1_R\big|H_T^{(1st)}\sum_{\gamma}\big|\gamma\big\rangle\big\langle\gamma\big|H_T^{(1st)}\big|1_L, 0_R\big\rangle \times \left[\frac{1}{\epsilon_{\nu\mathbf{K},L}-\epsilon_\gamma}+\frac{1}{\epsilon_{\nu\mathbf{K},R}-\epsilon_\gamma}\right] \tag{4.43}$$

where the intermediate state $\big|\gamma\big\rangle$ represents an electron-hole pair separated by the tunneling barrier.

For demonstration, I write down the example where the separated electron and hole are free particles, each in its plane wave basis.

$$\big|\gamma_1\big\rangle = \big|0\big\rangle_{\mathbf{k}_1,L}\big|1\big\rangle_{-\mathbf{k}_2,L}\big|1\big\rangle_{\mathbf{k}_1,R}\big|0\big\rangle_{-\mathbf{k}_2,R} = \hat{e}^\dagger_{\mathbf{k}_1,R}\hat{h}^\dagger_{-\mathbf{k}_2,L}\big|0\big\rangle_{\mathbf{k}_1,L}\big|0\big\rangle_{-\mathbf{k}_2,L}\big|0\big\rangle_{\mathbf{k}_1,R}\big|0\big\rangle_{-\mathbf{k}_2,R} \tag{4.44}$$

following the momentum sign convention and completeness relation,

$$\hat{e}_{\mathbf{k}} = \hat{h}^\dagger_{-\mathbf{k}}, \quad \sum_{\mathbf{k}_1,\mathbf{k}_2}\big|\mathbf{k}_1,-\mathbf{k}_2\big\rangle\big\langle\mathbf{k}_1,-\mathbf{k}_2\big| = 1 \tag{4.45}$$

Therefore, each of those intermediate states can couple to a single exciton state by the first-order tunneling of an electron or a hole. The two intermediate matrix elements in equation(4.43) can be evaluated as follows,

$$\begin{aligned}
&\big\langle\gamma_1\big|H_T^{(1st)}\big|1_L,0_R\big\rangle\\
=&\Big(\big\langle 0\big|\hat{h}_{-\mathbf{k}_2,L}\hat{e}_{\mathbf{k}_1,R}\Big)\Big(\sum_{\mathbf{k}'}t_e\hat{e}^\dagger_{\mathbf{k}',R}\hat{e}_{\mathbf{k}',L}\Big)\Big(\sum_{\mathbf{k}}\psi_\nu(\mathbf{k},\mathbf{K})\hat{e}^\dagger_{\mathbf{k},L}\hat{h}^\dagger_{\mathbf{K}-\mathbf{k},L}\big|0\big\rangle\Big)\\
=&t_e\sum_{\mathbf{k},\mathbf{k}'}\psi_\nu(\mathbf{k},\mathbf{K})\big\langle 0\big|\hat{h}_{-\mathbf{k}_2,L}\ \hat{e}_{\mathbf{k}_1,R}\ \hat{e}^\dagger_{\mathbf{k}',R}\ \hat{e}_{\mathbf{k}',L}\ \hat{e}^\dagger_{\mathbf{k},L}\ \hat{h}^\dagger_{\mathbf{K}-\mathbf{k},L}\big|0\big\rangle\\
=&t_e\sum_{\mathbf{k},\mathbf{k}'}\psi_\nu(\mathbf{k},\mathbf{K})\delta_{-\mathbf{k}_2,\mathbf{K}-\mathbf{k}}\ \delta_{\mathbf{k}_1,\mathbf{k}'}\ \delta_{\mathbf{k},\mathbf{k}'}\\
=&t_e\psi_\nu(\mathbf{k}_1,\mathbf{K})\delta_{-\mathbf{k}_2,\mathbf{K}-\mathbf{k}_1}
\end{aligned} \tag{4.46}$$

and

$$
\begin{aligned}
&\big\langle 0_L, 1_R \big| H_T^{(1st)} \big| \gamma_1 \big\rangle \\
=&\Bigg(\sum_{\mathbf{k}} \langle 0 | \psi_\nu^*(\mathbf{k}, \mathbf{K}) \hat{h}_{\mathbf{K}-\mathbf{k},R} \hat{e}_{\mathbf{k},R} \Bigg) \Bigg(\sum_{\mathbf{k}'} t_h \hat{h}^\dagger_{\mathbf{k}',R} \hat{h}_{\mathbf{k}',L} \Bigg) \Big(\hat{e}^\dagger_{\mathbf{k}_1 R} \hat{h}^\dagger_{-\mathbf{k}_2,L} \big| 0 \big\rangle \Big) \\
=&t_h \sum_{\mathbf{k},\mathbf{k}'} \psi_\nu^*(\mathbf{k}, \mathbf{K}) \big\langle 0 \big| \hat{h}_{\mathbf{K}-\mathbf{k},R}\ \hat{e}_{\mathbf{k},R}\ \hat{h}^\dagger_{\mathbf{k}',R}\ \hat{h}_{\mathbf{k}',L}\ \hat{e}^\dagger_{\mathbf{k}_1,R}\ \hat{h}^\dagger_{-\mathbf{k}_2,L} \big| 0 \big\rangle \\
=&t_h \sum_{\mathbf{k},\mathbf{k}'} \psi_\nu^*(\mathbf{k}, \mathbf{K}) \delta_{\mathbf{K}-\mathbf{k},\mathbf{k}'}\ \delta_{\mathbf{k},\mathbf{k}_1}\ \delta_{-\mathbf{k}_2,\mathbf{k}'} \\
=&t_h \psi_\nu^*(\mathbf{k}_1, \mathbf{K}) \delta_{-\mathbf{k}_2,\mathbf{K}-\mathbf{k}_1}
\end{aligned}
\tag{4.47}
$$

Therefore the second-order matrix element mediated by $\big|\gamma_1\big\rangle$ is,

$$
\sum_{\mathbf{k}_1,\mathbf{k}_2} \big\langle 0_L, 1_R \big| H_T^{(1st)} \big| \gamma_1 \big\rangle \big\langle \gamma_1 \big| H_T^{(1st)} \big| 1_L, 0_R \big\rangle = t_e t_h \sum_{\mathbf{k}} \psi_\nu^*(\mathbf{k}, \mathbf{K}) \psi_\nu(\mathbf{k}, \mathbf{K}) \tag{4.48}
$$

Likewise, the other type of intermediate state is defined as,

$$
\big|\gamma_2\big\rangle == \big|1\big\rangle_{\mathbf{k}_1,L} \big|0\big\rangle_{-\mathbf{k}_2,L} \big|0\big\rangle_{\mathbf{k}_1,R} \big|1\big\rangle_{-\mathbf{k}_2,R} \tag{4.49}
$$

Summing over all possible intermediate states leads to the total matrix element,

$$
t_{\nu\mathbf{K}} = t_e t_h \sum_{\mathbf{k}} \psi_\nu^*(\mathbf{k}, \mathbf{K}) \psi_\nu(\mathbf{k}, \mathbf{K}) \times \left[\frac{1}{\epsilon_{\nu\mathbf{K}} - \epsilon_{\mathbf{k},\mathbf{K}-\mathbf{k}}} + \frac{1}{\epsilon_{\nu\mathbf{K}} - \epsilon_{\mathbf{k},\mathbf{K}-\mathbf{k}}} \right] \tag{4.50}
$$

where the energy of a bound exciton is estimated as,

$$
\epsilon_{\nu\mathbf{K}} = \epsilon_\nu + \frac{\hbar^2 |\mathbf{K}|^2}{2(m_e + m_h)} \tag{4.51}
$$

and the energy of a separated electron-hole pair is estimated as,

$$
\epsilon_{\mathbf{k},\mathbf{K}-\mathbf{k}} = \frac{\hbar^2 |\mathbf{k}|^2}{2m_e} + \frac{\hbar^2 |\mathbf{K}-\mathbf{k}|^2}{2m_h} \tag{4.52}
$$

A Bose-Einstein condensate consists of excitons near $\mathbf{K} = 0$, therefore the summation

is simplified as,

$$\sum_{\mathbf{k}} \left|\psi_\nu(\mathbf{k})\right|^2 \times \frac{1}{\epsilon_\nu - \frac{\hbar^2|\mathbf{k}|^2}{2\mu}}$$

where $\mu = m_e m_h/(m_e + m_h)$ is the reduced mass of the electron-hole pair.

In particular, the energy and wavefunction of a quasi-2D exciton in ground orbital state($\nu = 0$) can be written in terms of the 2D "Bohr radius" a and relative coordinates,

$$\epsilon_0 = -\frac{\hbar^2}{2\mu a^2}, \quad \psi_0(\mathbf{r} - \mathbf{r}') = \sqrt{\frac{2}{\pi}}\frac{1}{a}e^{-|\mathbf{r}-\mathbf{r}'|/a}, \tag{4.53}$$

Following the convention defined in equation (2.8), the Fourier transform of the wavefunction is,

$$\psi_0(\mathbf{k}) = \frac{\sqrt{2\pi}2a}{(1 + a^2|\mathbf{k}|^2)^{3/2}} \tag{4.54}$$

Carrying out the integration over a dimensionless momentum $\kappa = ak$ leads to the simple expression,

$$\left(\frac{\hbar^2}{2\mu a^2}\right)^{-1} \int_0^{2\pi} d\theta \int \left(\frac{2\sqrt{2\pi}}{(1+\kappa^2)^{3/2}}\right)^2 \times \frac{1}{-1-\kappa^2}\kappa d\kappa = -\frac{16\pi^2\mu a^2}{3\hbar^2} \tag{4.55}$$

Finally, the second-order tunneling energy of a ground state exciton is in a compact formula,

$$t_{00} = -\frac{16\pi^2}{3}\frac{t_e t_h}{|\epsilon_0|}. \tag{4.56}$$

Considering the Bose-Einstein condensate is a macroscopic occupation in the ground state, this single exciton tunneling energy can naturally give rise to the Josephson coupling energy in the two-state model(Eq.(4.34)). However, in an open quantum system, the bright excitons created by incident light also have short lifetimes due to radiative recombination; therefore are not able to fully thermalize to form a condensate. Nevertheless, this tunneling mechanism can create spatial correlations in the excitons, which could be inherited by higher-order nonlinear effects, potentially giving extra control over the correlated photon emitters, a type of device based on the principles of quantum optics and much desired in quantum communication and quantum computing.

The dark excitons due to unmatched spins between the electron and hole pair are inactive in light-matter interaction, therefore can have much longer lifetimes. In some tunneling barriers with weak screening, the spatially separated electron-hole pairs are still bound by their long-range Coulomb interaction, known as indirect excitons, which also have longer lifetimes due to suppressed recombination. The confinement effect of the quantum well acts as an effective magnetic field that flips the spins[77], which can convert between the bright and dark excitons. The interplay between the dark excitons and indirect excitons, taking into account the correlated tunneling mechanism, could be a promising topic for future research.

Chapter 5

Polariton Josephson Junctions based on Exciton Stark Effect

The pioneering experimental studies on the exciton-polariton(EP) Josephson effect are based on trapping polaritons via the photon component [78]. For example, [79] exploits the naturally occurring thickness variation in the inactive spacing layer of the planar cavity, which gives rise to a double-well potential only acting on the photon component. In comparison, [60] uses an etched-out double-micropillar structure, where the photon component, due to its smaller effective mass, is more sensitive to the confinement geometry and therefore determines the trapping potential.

In these systems, the initial state is prepared by large condensation imbalance [79] or by resonant laser pumping [60]. The EP Josephson energy is given by the inter-trap tunneling energy of the photonic modes, which is preset via the cavity material and geometry. Moreover, the chemical potential bias induced by non-resonantly pumped excitons is time-independent and indirectly determined by the dynamical balance of short-lived excitons [60]. The inability to set an arbitrary initial state or to control the dynamics in real-time are the major challenges that prevent the existing EP junctions from achieving their full potential as active quantum devices.

Trapping polaritons via the exciton component [78, 80, 81] allows an alternative, more flexible device design for non-resonantly pumped EP condensates. For example, stress

applied to the planar cavity can induce a significant change in the local crystal field with only minor variation in cavity thickness, resulting in a trapping potential acting on the exciton component, which allows an EP gas drift from the pumping laser spot to the trap and eventually form the condensate. [47]

In condensates dynamically maintained in thermal equilibrium [82, 59], it is feasible to control the chemical potential bias via the single-polariton potential energy. While indirect control on the photon component is made possible by introducing novel elements such as liquid crystals [83], directly manipulating the exciton component using electrical fields has been successfully applied to various physical scenarios. [84, 85, 86]. In particular, the exciton potential energy can be tuned locally via the exciton quadratic Stark effect [87, 88].

In this chapter, I present the original research based on the coauthored article[1]. An alternative design of a polariton junction is proposed, where electrical fields can control both the Josephson energy and potential energy bias.

5.1 Unified Model for Polariton Josephson Junction

In a generally defined polariton Josephson junction, it is equally reasonable to confine the polaritons via their exciton or photon component.

We start by recognizing the total Hamilton $H = H_0 + H_{\text{int}}$, which consists of the part that accounts for exciton-photon coupling and trapping potentials,

$$H_0 = \sum_{\mathbf{k},\mathbf{k}'} \left(\hat{b}^\dagger_{\mathbf{k}}, \hat{a}^\dagger_{\mathbf{k}}\right) \begin{pmatrix} E_{\text{ex}}(\mathbf{k})\delta_{\mathbf{k},\mathbf{k}'} + V_{\text{ex}}(\mathbf{k}'-\mathbf{k}) & \Omega\ \delta_{\mathbf{k},\mathbf{k}'} \\ \Omega\ \delta_{\mathbf{k},\mathbf{k}'} & E_{\text{ph}}(\mathbf{k})\delta_{\mathbf{k},\mathbf{k}'} + V_{\text{ph}}(\mathbf{k}'-\mathbf{k}) \end{pmatrix} \begin{pmatrix} \hat{b}_{\mathbf{k}'} \\ \hat{a}_{\mathbf{k}'} \end{pmatrix} \tag{5.1}$$

and the part that accounts for the interaction among excitons,

$$H_{\text{int}} = \frac{g_s}{\mathcal{A}} \sum_{\mathbf{k},\mathbf{k}',\mathbf{q}} \hat{b}^\dagger_{\mathbf{k}} \hat{b}^\dagger_{\mathbf{k}'} \hat{b}_{\mathbf{k}'+\mathbf{q}} \hat{b}_{\mathbf{k}-\mathbf{q}} \tag{5.2}$$

[1]Reproduced in part with permission from Nano Letters 2025, 25, 18, 7336–7342 Copyright 2025 American Chemical Society.

where $\mathbf{k}, \mathbf{k}'$ span the same 2D space shared by exciton and photon, the field operators and parameters are defined in Sec.(2.5).

Note that a local confinement potential in real space for either excitons or photons would transform into $\mathbf{k}$-space,

$$\begin{aligned}\int d^2\mathbf{r}\ \psi^*(\mathbf{r})V(\mathbf{r})\psi(\mathbf{r}) &= \int d^2\mathbf{r}\ \Big(\int d^2\mathbf{k}\psi^*(\mathbf{k})e^{-i\mathbf{k}\cdot\mathbf{r}}\Big)V(\mathbf{r})\Big(\int d^2\mathbf{k}'\psi(\mathbf{k}')e^{i\mathbf{k}'\cdot\mathbf{r}}\Big) \\ &= \iint d^2\mathbf{k}\ d^2\mathbf{k}'\ \psi^*(\mathbf{k})V(\mathbf{k}'-\mathbf{k})\psi(\mathbf{k}')\end{aligned} \tag{5.3}$$

implying off-diagonal coupling between different wavevectors.

The trapping should be introduced as a small potential variation over the well-defined exciton/photon states, therefore we treat them as perturbations to the polariton states, following the Hopfield transformation(2.50)

$$H' = \sum_{\mathbf{k},\mathbf{k}'} \begin{pmatrix} P_{\mathbf{k}}^\dagger & Q_{\mathbf{k}}^\dagger \end{pmatrix} \hat{O}_{\mathbf{k}} \begin{pmatrix} V_{\mathrm{ex}}(\mathbf{k}-\mathbf{k}') & 0 \\ 0 & V_{\mathrm{ph}}(\mathbf{k}-\mathbf{k}') \end{pmatrix} \hat{O}_{\mathbf{k}'}^\dagger \begin{pmatrix} P_{\mathbf{k}'} \\ Q_{\mathbf{k}'} \end{pmatrix} \tag{5.4}$$

In general, the potential terms after the transformation will mix different wavevectors and no longer in a simple form of $V(\mathbf{k}-\mathbf{k}')$, resulting in a non-local potential acting on the polaritons.

$$\begin{aligned}V(\mathbf{k},\mathbf{k}') = \sum_{\mathbf{k},\mathbf{k}'} \begin{pmatrix} \hat{P}_{\mathbf{k}}^\dagger & \hat{Q}_{\mathbf{k}}^\dagger \end{pmatrix} \Bigg[&\begin{pmatrix} X_{\mathbf{k}}X_{\mathbf{k}'} & X_{\mathbf{k}}C_{\mathbf{k}'} \\ C_{\mathbf{k}}X_{\mathbf{k}'} & C_{\mathbf{k}}C_{\mathbf{k}'} \end{pmatrix} V_{\mathrm{ex}}(\mathbf{k}-\mathbf{k}') \\ &+ \begin{pmatrix} C_{\mathbf{k}}C_{\mathbf{k}'} & -C_{\mathbf{k}}X_{\mathbf{k}'} \\ -X_{\mathbf{k}}C_{\mathbf{k}'} & X_{\mathbf{k}}X_{\mathbf{k}'} \end{pmatrix} V_{\mathrm{ph}}(\mathbf{k}-\mathbf{k}') \Bigg] \begin{pmatrix} \hat{P}_{\mathbf{k}'} \\ \hat{Q}_{\mathbf{k}'} \end{pmatrix}\end{aligned} \tag{5.5}$$

However, when we work with $\mathbf{k} \approx 0$ states in the finite-size polariton condensate, the approximation $X_{\mathbf{k}} \approx X_0, C_{\mathbf{k}} \approx C_0$ allows us to simplify it to a form in real space with local potentials,

$$H_0 = \int d^2\mathbf{r} \begin{pmatrix} \hat{P}^\dagger(\mathbf{r}) & \hat{Q}^\dagger(\mathbf{r}) \end{pmatrix} \begin{pmatrix} h_{\mathrm{LP}}(\mathbf{r}) & W(\mathbf{r}) \\ W(\mathbf{r}) & h_{\mathrm{UP}}(\mathbf{r}) \end{pmatrix} \begin{pmatrix} \hat{P}(\mathbf{r}) \\ \hat{Q}(\mathbf{r}) \end{pmatrix} \tag{5.6}$$

The diagonal terms are the effective Hamiltonian in each polariton branch,

$$h_\zeta(\mathbf{r}) = -\frac{\hbar^2\nabla^2}{2m_\zeta} + \epsilon_\zeta + V_\zeta(\mathbf{r}), \quad \zeta \in \{\mathrm{LP}, \mathrm{UP}\}$$

where $V_{\mathrm{LP}}(\mathbf{r}) = X_0^2 V_{\mathrm{ex}}(\mathbf{r}) + C_0^2 V_{\mathrm{ph}}(\mathbf{r})$, $V_{\mathrm{UP}} = C_0^2 V_{\mathrm{ex}}(\mathbf{r}) + X_0^2 V_{\mathrm{ph}}(\mathbf{r})$. and the energy offset of polaritons is

$$\varepsilon_{\mathrm{LP(UP)}} = \frac{\Delta - (+)\sqrt{\Delta^2 + 4\Omega^2}}{2} \tag{5.7}$$

where the detuning is defined as $\Delta = E_{\mathrm{ph}}(\mathbf{k} = 0) - E_{\mathrm{ex}}(\mathbf{k} = 0)$, while the off-diagonal term

$$W(\mathbf{r}) = X_0 C_0 V_{\mathrm{ex}}(\mathbf{r}) - X_0 C_0 V_{\mathrm{ph}}(\mathbf{r}) \tag{5.8}$$

represents the coupling energy between the lower and upper polaritons introduced by the external potentials.

5.2 Description of Proposed Device

We conclude from the previous section that a polariton junction can be formed by introducing a local double-well potential to either the photon or the exciton component. This naturally leads to the following proposal for an electrically controlled polariton junction.

In the semiconducting layer of the optical microcavity, we introduce a double-well potential to the excitons, which defines two polariton trapping areas. Each area is bracketed between two conducting wires (see Fig. 5.1), which generate an in-plane electric field controlled by an external voltage source.

We project the macroscopic wavefunction of the polariton condensate into the spatial modes defined by the trapping potentials in the polariton basis. The LP and UP condensates confined on the left and right side of the device can then be described by a four-component Gross-Pitaevskii (GP) equation. The detailed derivation is presented in Appendix 5.A. We introduce the complex variables ψ_κ and χ_κ to describe the macroscopic amplitude of the polariton ground state $\phi_\kappa(\mathbf{r})$ for the LP and UP condensates, respectively, where $\kappa \in \{L, R\}$ denotes the left (L) and right (R) side of the junction.

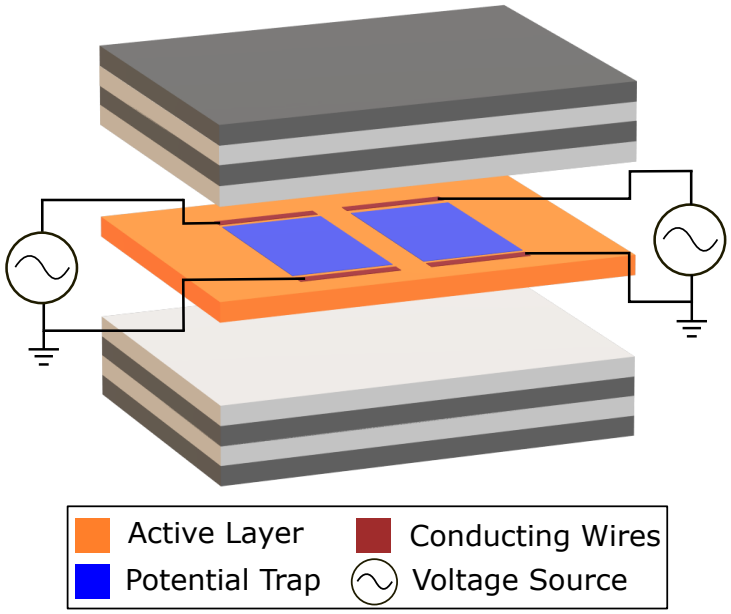

Figure 5.1: Schematic geometry of an EP junction. The two-dimensional device is defined via nanofabrication of a GaAs active layer embedded in an optical microcavity filled with AlAs, where the exciton potential wells(1-10meV) are formed by slightly mixing aluminum in the $\mathrm{GaAs/Al_xGa_{1-x}As}$ heterostructure. Two conducting nanowires bracket each potential well to apply an in-plane electric field, which polarizes the EP condensate as well as to measure the local capacitance.

The time evolution of the lower polariton condensates is described by

$$
\begin{aligned}
i\hbar\frac{d\psi_L}{dt} &= \Big(-\frac{\mu_{LR}+\mu_{UL}}{2} + \frac{U}{4}|\psi_L|^2 + \frac{U}{2}|\chi_L|^2 \Big)\psi_L - J\psi_R \\
&\quad + \Big\{ U\Big[\frac{1}{4}\psi_L^*\chi_L + \frac{1}{2}\Big(|\psi_L|^2 + |\chi_L|^2\Big)\Big] + I_1 \Big\}\chi_L + I_2\chi_R
\end{aligned}
\tag{5.9a}
$$

$$
\begin{aligned}
i\hbar\frac{d\psi_R}{dt} &= \Big(\frac{\mu_{LR}-\mu_{UL}}{2} + \frac{U}{4}|\psi_R|^2 + \frac{U}{2}|\chi_R|^2 \Big)\psi_R - J\psi_L \\
&\quad + \Big\{ U\Big[\frac{1}{4}\psi_R^*\chi_R + \frac{1}{2}\big(|\psi_R|^2 + |\chi_R|^2\big)\Big] + I_1 \Big\}\chi_R + I_2\chi_L
\end{aligned}
\tag{5.9b}
$$

$$
\begin{aligned}
i\hbar\frac{d\chi_L}{dt} &= \Big(-\frac{\mu_{LR}-\mu_{UL}}{2} + \frac{U}{4}|\chi_L|^2 + \frac{U}{2}|\psi_L|^2 \Big)\chi_L - J\chi_R \\
&\quad + \Big\{ U\Big[\frac{1}{4}\chi_L^*\psi_L + \frac{1}{2}\Big(|\chi_L|^2 + |\psi_L|^2\Big)\Big] + I_1 \Big\}\psi_L + I_2\psi_R
\end{aligned}
\tag{5.9c}
$$

$$
\begin{aligned}
i\hbar\frac{d\chi_R}{dt} &= \Big(\frac{\mu_{LR}+\mu_{UL}}{2} + \frac{U}{4}|\chi_R|^2 + \frac{U}{2}|\psi_R|^2 \Big)\chi_R - J\chi_L \\
&\quad + \Big\{ U\Big[\frac{1}{4}\chi_R^*\psi_R + \frac{1}{2}\big(|\chi_R|^2 + |\psi_R|^2\big)\Big] + I_1 \Big\}\psi_R + I_2\psi_L
\end{aligned}
\tag{5.9d}
$$

The energy difference μ_{UL} is determined by the vacuum Rabi splitting at $\mathbf{k}_\parallel = 0$. The left-right bias potential μ_{LR} is controlled by the in-plane electric fields applied to the two semiconductors via the exciton Stark effect. The exciton components polarizability α can be estimated by perturbation theory in terms of exciton orbital wavefunctions, which resembles that of a 2D hydrogen atom [55], where Φ_{nl} is the 2D electron-hole orbital wavefunction in principle quantum number n and angular quantum number l, and $E_{nl} < 0$ is the corresponding eigen-energy, $\hat{\mathbf{x}}$ is the e-h displacement operator in the direction of the applied electric field $\mathcal{E}_{L/R}$. This produces the energy difference $\mu_{LR} = \alpha\left(\mathcal{E}_L^2 - \mathcal{E}_R^2\right)/2$. Taking into account the dielectric constant of the host semiconductor, we estimate an electric field of $\sim 1\,V/\mu$m is needed to create a dipole energy of ~ 0.1 meV in the quasi-2D exciton of GaAs.

The Josephson energy J arises from the spatial overlapping of left and right trapped polariton states. Assuming that the excitons are confined in a double square well poten-

tial, we estimate the Josephson energy as a function of the exciton tunneling barrier

$$J \approx \pi^2 \frac{D_b}{D_w} E_0 e^{-D_b/\xi}, \tag{5.10}$$

where D_w and D_b are the widths of a single well and the tunneling barrier, respectively, $E_0 = \frac{\hbar^2\pi^2}{2mD_w^2}$ with m being the polariton effective mass, and $\xi = \hbar/\sqrt{mV_B}$ is the penetration depth with V_B being the tunneling barrier strength. The calculation is shown in the Appendix 5.C. We note that Eq. (5.10) is valid in the tunneling regime $D_b \gg \xi$. The Josephson energy tunability $|J(V_B + \delta V)/J(V_B) - 1| \sim \frac{D_b}{\xi}\frac{\delta V}{V_B}$ for $\delta V \ll V_B$, which can be of order of one due to the large prefactor D_b/ξ. In addition, the coupling energies between upper and lower polaritons $I_{1,2}$ are determined by the spatial overlap of the localized LP and UP wavefunctions, which can be neglected for strong Rabi splitting $\mu_{LR} \gg I_{1,2}$.

The interaction energy U arises from the s-wave scattering of the excitons. For the double-square-well potential we estimate $U \approx 3g_s/(2D_w)$, where $g_s = 6|E_{10}|a_{\mathrm{B}}^2$ is the contact interaction parameter predicted by theory [73] with a_{B} being the Bohr radius and E_{10} the $1s$ state energy. The magnitude of g_s is sensitive to confinement geometry and is usually characterized by the blue shift of LP dispersion. Based on the experimental results reported for GaAs [65, 89], we estimate g_s is of the order of $1 \sim 10\,\mu\mathrm{eV}\mu\mathrm{m}^2$ for an exciton potential trap with unspecified geometry between idea 1D and 2D. The tunability of the Josephson energy J in Eq. (5.10) makes it possible to study the interplay between the Josephson effect and the non-linearity induced by interactions.

To follow the dynamics of this polariton junction, we suggest measuring the phase and density evolution using methods based on optical coherence, as mentioned in Section3.6. The condensate densities in each trapping area can be indirectly measured via emitted photons and deduced from the transmission/reflection ratio at the surface of the cavity. The phase difference can be extracted from the shift in interference fringes, created by the Michelson interferometer method, where the image of one trapping area overlaps with the other, which has been successfully applied in existing experiments [79, 60]. The added electrical elements could also provide new methods to probe the system that complement the methods based on optical coherence, which will be discussed as a future direction of

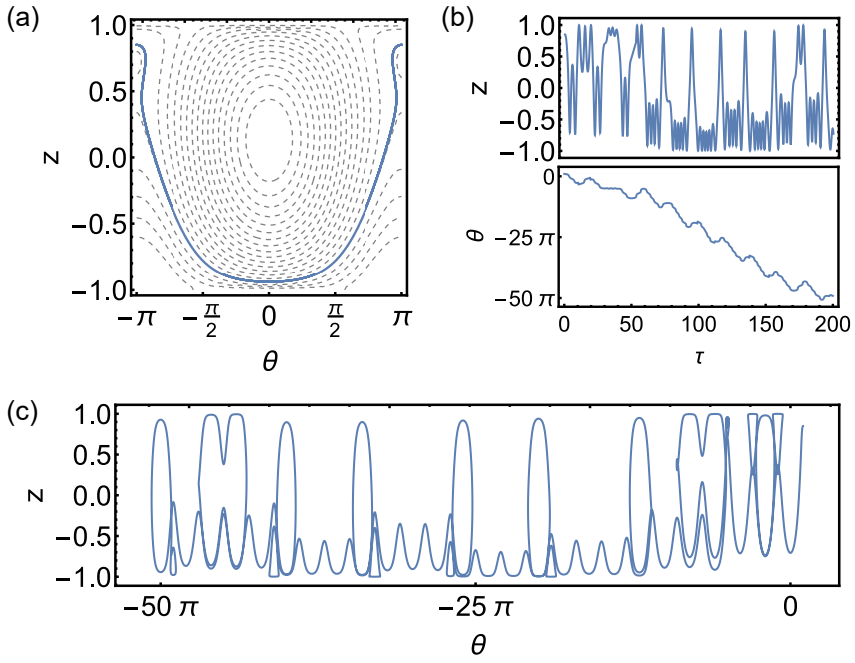

Figure 5.2: Stable and chaotic dynamics in LP-only Josephson junctions [Eq. (5.11)]. We take $\Lambda = 2$ and $z_0 = 0.2$. (a) Energy contour in phase space for static driving potential $z_1 = 0$. For the initial conditions $z(0) = 0.85$ and $\theta(0) = \pi$, the system follows the blue trajectory. (b) Time evolution of density (upper panel) and phase (lower panel) for dynamical driving potential $z_1 = 0.4$. The phase-space trajectory exhibits chaotic behavior as shown in (c).

study in the conclusion chapter.

5.3 Stable Trajectories and Chaos in Lower Polariton Branch

We consider two major cases. In the first, the coherent excitation in the upper polariton branch is negligible, and the coupled equations reduce to the two-component bosonic junction model that has been intensively studied [12]. Defining the dimensionless interaction strength $\Lambda = UN_T/2J$ and time $\tau = \frac{2J}{\hbar}t$ in LP parameters, where $N_T = |\psi_L|^2 + |\psi_R|^2$, and parametrizing $\psi_{L,R} = \sqrt{N_T(1 \pm z)/2}e^{i\theta_{L,R}}$ with $|z| \leq 1$, we transform Eq. (5.9)(a,b) to

$$\dot{\theta} = \Lambda\Big(z - z_b(\tau)\Big) + \frac{z\cos\theta}{\sqrt{1-z^2}}, \quad \dot{z} = -\sqrt{1-z^2}\sin\theta, \tag{5.11}$$

where $\theta = \theta_R - \theta_L$.

For a time-independent bias potential $z_b(\tau) = z_0$, such a system resembles an undriven, non-linear pendulum. Its dynamics fall into two categories: those for which the pendulum decelerates enough to turn around and swing back, where the trajectory is a closed loop in phase space; and those for which the pendulum would swing through the complete circle, where the trajectory is unbounded in phase space and enters the next cycle repeatedly. The latter are termed "macroscopic quantum self-trapping" modes [12], meaning the condensate density difference indicated by z remains non-zero. Both types of modes are present in the energy contours [Fig. 5.2(a)].

When the bias potential has a constant and an oscillating component $z_b(\tau) = z_0 + z_1 \sin(\Omega\tau)$, it is possible to switch between different trajectories within the same dynamical category. For example, a control sequence of voltage applied to the nanoelectric, by shifting the chemical potential bias, can drive the system between two stable trajectories.

However, the modes near the separatrix are unstable, and the dynamical potential can lead to chaotic behavior [Fig. 5.2(b)].

5.4 Intrinsic Chaos with Lower and Upper Polariton Branches

The second major case is that both the LP and UP condensates are non-negligible so the system must be described by the four-component model. Switching to the dimensionless variables $g = U/J$, $\delta = \mu_{LR}/J$, $\Delta = \mu_{UL}/J$, and $\lambda_{1,2} = I_{1,2}/J$, and performing a rotating-frame transformation (see appendix), we rewrite Eq. (5.9) in the matrix form

$$i\partial_\tau \begin{pmatrix} \tilde{\psi}_L \\ \tilde{\psi}_R \\ \tilde{\chi}_L \\ \tilde{\chi}_R \end{pmatrix} = \begin{pmatrix} h_{LP} & v \\ v^\dagger & h_{UP} \end{pmatrix} \begin{pmatrix} \tilde{\psi}_L \\ \tilde{\psi}_R \\ \tilde{\chi}_L \\ \tilde{\chi}_R \end{pmatrix} \tag{5.12}$$

where the blocks of the effective Hamiltonian read

$$h_{LP} = \begin{pmatrix} \frac{\delta}{2} + \frac{g}{4}|\tilde{\psi}_L|^2 + \frac{g}{2}|\tilde{\chi}_L|^2 & -1 \\ -1 & -\frac{\delta}{2} + \frac{g}{4}|\tilde{\psi}_R|^2 + \frac{g}{2}|\tilde{\chi}_R|^2 \end{pmatrix},$$

$$h_{UP} = \begin{pmatrix} \frac{\delta}{2} + \frac{g}{4}|\tilde{\chi}_L|^2 + \frac{g}{2}|\tilde{\psi}_L|^2 & -1 \\ -1 & -\frac{\delta}{2} + \frac{g}{4}|\tilde{\chi}_R|^2 + \frac{g}{2}|\tilde{\psi}_R|^2 \end{pmatrix},$$

$$v = e^{-i\Delta\tau} \begin{pmatrix} \frac{g}{2}n_L + \lambda_1 & \lambda_2 \\ \lambda_2 & \frac{g}{2}n_R + \lambda_1 \end{pmatrix} + e^{-i2\Delta\tau} \begin{pmatrix} \frac{g}{4}\tilde{\psi}_L^*\tilde{\chi}_L & 0 \\ 0 & \frac{g}{4}\tilde{\psi}_R^*\tilde{\chi}_R \end{pmatrix}$$

where $n_{L(R)}$ is the total particle number on the left (right) side.

In a typical polariton system, the LP-UP energy difference μ_{UL}, which is the Rabi-splitting determined by strong photon-exciton hybridization, is several orders of magnitude larger than the left-right energy difference μ_{LR}. In Eq. (5.12), for $\Delta \gg \delta, g, \lambda_{1,2}$, the inter-branch block v carries a fast oscillating phase. Under the random phase approximation, we neglect this inter-branch coupling and obtain a pair of two-component equations for upper and lower EP condensates,

$$i\partial_\tau \begin{pmatrix} \tilde{\psi}_L \\ \tilde{\psi}_R \end{pmatrix} = h_L \begin{pmatrix} \tilde{\psi}_L \\ \tilde{\psi}_R \end{pmatrix}, \quad i\partial_\tau \begin{pmatrix} \tilde{\chi}_L \\ \tilde{\chi}_R \end{pmatrix} = h_U \begin{pmatrix} \tilde{\chi}_L \\ \tilde{\chi}_R \end{pmatrix}. \tag{5.13}$$

We note that the polariton-exchange process between LP and UP branches is effectively absent, and the particle numbers of UP and LP branches are approximately conserved in the time scale much larger than the Rabi period. However, the existence of the upper polariton serves as a dynamical chemical potential to the lower polariton condensate, causing the density $n_{L/U}$ in lower/upper polariton only oscillate at a small amplitude around its mean value.

For the LP condensates, we parametrize $\psi_{L(R)} = \sqrt{n_{LP}(1 \pm z_{LP})/2}e^{i\theta_{LP,L(R)}}$ where n_{LP} is the total number of lower polaritons and $|z_{LP}| \leq 1$; Similar parametrization applies to

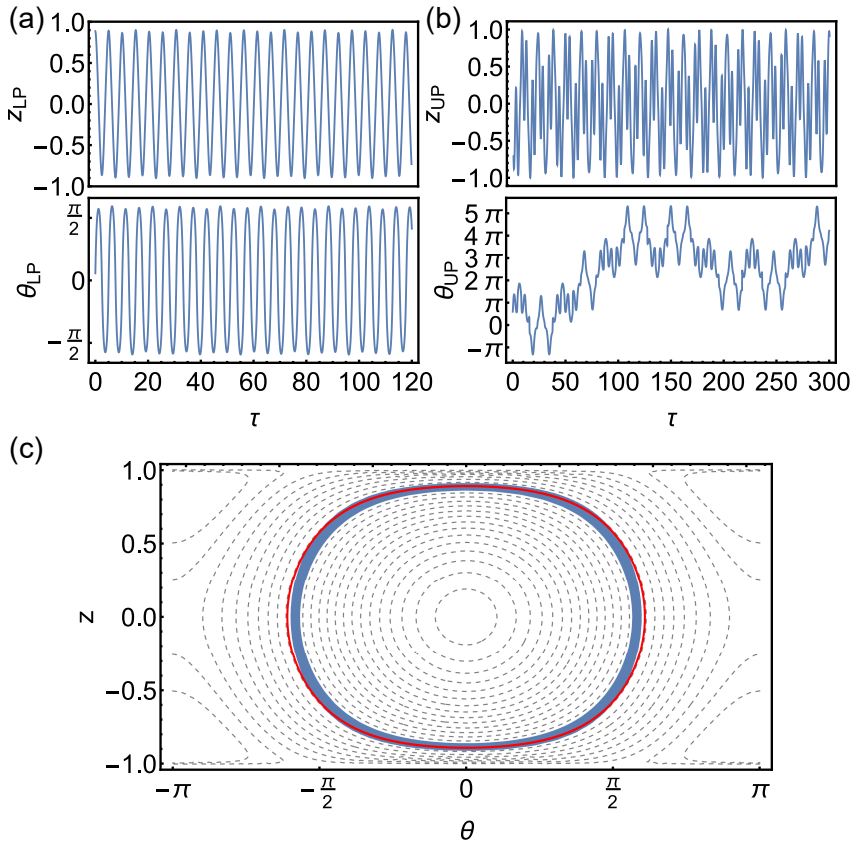

Figure 5.3: Dynamics of LP and UP condensates for low UP filling. We take $n_{LP} = 0.95$ and $n_{UP} = 0.05$. (a) and (b) Time evolution of LP and UP condensates, respectively. (c) Phase-space trajectory of LP condensates corresponding to (a). The red trace is a closed trajectory for the stable state of the two-component LP-only model (Color online).

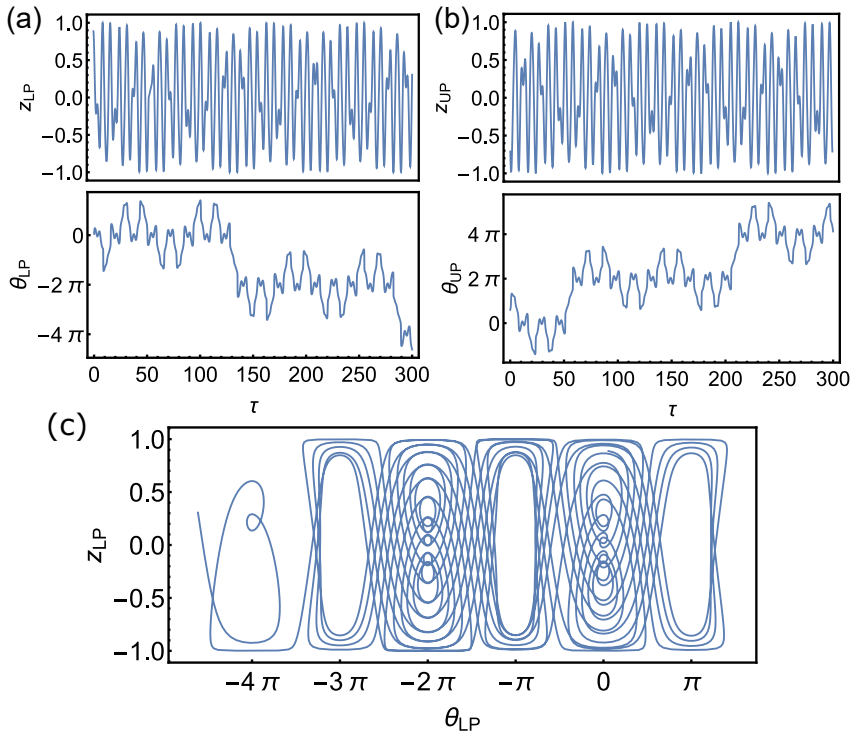

Figure 5.4: Dynamics of LP and UP condensates for equal UP and LP fillings $n_{LP} = n_{UP} = 0.5$. (a) and (b) Time evolution of LP and UP condensates, respectively. (c) Phase-space trajectory of LP condensates corresponding to (a).

the UP condensates. We transform Eq. (5.13) to

$$\begin{aligned}\dot{\theta}_\sigma &= \Lambda_\sigma(z_\sigma - z_{b,\sigma}) + \frac{z_\sigma}{\sqrt{1-z_\sigma^2}}\cos\theta_\sigma,\\ \dot{z}_\sigma &= -\sqrt{1-z_b^2}\sin\theta_\sigma,\end{aligned} \tag{5.14}$$

where $\sigma \in \{LP, UP\}$, $\theta_\sigma = \theta_{\sigma,L} - \theta_{\sigma,R}$, and the dynamical chemical potential bias $z_{b,\sigma} = z_{0,\sigma} + c_\sigma z_{\bar{\sigma}}$ consists of two parts: $z_{0,\sigma} = -\frac{\delta}{2\Lambda_\sigma}$ with $\Lambda_\sigma = gn_\sigma/4$ and $c_\sigma = n_{\bar{\sigma}}/n_\sigma$, the over-bar refers to the opposite EP component. The chemical potential in one branch is dynamically influenced by its counterpart.

When the UP branch is insufficiently populated $n_{LP} \gg n_{UP}$, as shown in Fig. 5.3, we find that the UP condensate exhibits small-amplitude but chaotic oscillations due to the periodic driving force generated by the LP condensate through interactions. However, the LP condensate still exhibits a low-frequency and large-amplitude periodic oscillation governed by the Josephson effect, with only a trace of the high-frequency chaotic

noises induced by the UP condensate. We have confirmed that the two-component GP equation (5.11) for LP condensates is valid in this limit.

In contrast, when the populations of the two EP condensates are comparable, the temporal oscillations in one component can act as a significant driving force in the other, which strongly depends on the initial population. In this limit, we always obtain chaotic behavior for both LP and UP condensates, and neither can be neglected because the amplitudes of the chaotic oscillations are comparable to the polariton total particle number, as shown in Fig. 5.4(a)(b). The LP branch trajectory in $\{\theta, z\}$ phase space no longer fluctuates around a closed contour(Fig. 5.3(c)) but rather slips out of the $(0, 2\pi)$ domain and shows a few temporary attractors(Fig. 5.4(c)).

5.5 Discussion of Physical Limits

As discussed in the previous chapter, a widely used theoretical model [66, 29]3.5 describes a polariton condensate coupled to a non-condensate reservoir below the "bottleneck", where polariton-phonon scattering is less efficient. The coupling to the condensate and its decay via photon leaking are represented by imaginary source and sink terms; the thermal effects in the host material are absorbed in the parameters of the model, which remain constant in typical experiments. Our EP junction model (5.9) assumes the existence of well-defined and conserved condensates since we propose to work in a steady state where the source and sink terms are balanced, and its validity depends on time scales. If the re-population and decay rates are slow compared to the Josephson frequency, the many-body system adiabatically adjusts to minimal energy while the gain and loss are balanced, which satisfies the particle-conserved GP equation, and all the dynamical behaviors predicted in our work should be observed. Otherwise, if the decay rate is much larger than the Josephson frequency, the condensates are unstable and the oscillations are damped [66, 79, 60]; if the re-population is much larger than the Josephson frequency, the oscillations are absent and a steady and phase-dependent flow of polaritons occurs across the junction.

In a non-equilibrium polariton gas, the re-population rate of the condensate depends on the temporary distribution in the non-condensate reservoir, and the chemical potential is not well defined, making it difficult to maintain a steady state or to drive the Josephson current dynamically. Thankfully, recent experiments have demonstrated that true thermal equilibrium can develop in LPs with a long lifetime $\sim 270\,\mathrm{ps}$ [82, 59], and directly controlling their chemical potential via the Stark effect is possible. The UPs are usually very lossy, possibly due to the strong match between the polariton Rabi splitting and longitudinal optical(LO) phonon($\sim$ 30meV) in the host material. Research shows that even with the LO phonon relaxation, it is possible to temporarily create an UP condensate by non-resonant pumping [61]. Nevertheless, as we have discussed in the four-component dynamics, it is possible to initialize an LP junction in a desired state by controlled phase evolution, and to dynamically drive the system within and between two types of trajectories; while the stable control in the LP branch will not be disturbed by temporary fluctuations in the UP branch.

5.A Four-Component Model

If not consider the decay process via optical phonons, the lower and upper polaritons are orthogonal normal modes with similar lifetimes due to cavity photon leakage; therefore, a complete model for the polariton junction should include condensates in both the lower and the upper polariton branches, and the tunneling effect is present in both branches based on the corresponding double-well potential.

We project the macroscopic wavefunction of the polariton condensate into the spatial modes defined by the trapping potentials in the polariton basis,

$$\Psi_\zeta(\mathbf{r},t) \approx \psi_{\zeta,L}(t)\phi_{\zeta,L}(\mathbf{r}) + \psi_{\zeta,R}(t)\phi_{\zeta,R}(\mathbf{r}), \quad \zeta \in \{\mathrm{LP},\mathrm{UP}\} \tag{5.15}$$

Note the single-well states are almost orthogonal except for slightly overlapping in the barrier, we can project the polariton field into the two spatial modes defined by the orthogonalized basis $\tilde{\phi}_{\zeta,\sigma}(\mathbf{r}) \approx \phi_{\zeta,\sigma}(\mathbf{r}), \sigma \in \{L,R\}$ where $\int d^2\mathbf{r}\ \tilde{\phi}_{\zeta,\sigma}(\mathbf{r})\tilde{\phi}_{\zeta,\sigma'}(\mathbf{r}) = \delta_{\sigma,\sigma'}$,

which leads to the definition,

$$P(\mathbf{r}) \approx \sum_{\sigma=L,R} \phi_{\mathrm{LP},\sigma}(\mathbf{r})\, P_\sigma, \quad Q(\mathbf{r}) \approx \sum_{\sigma=L,R} \phi_{\mathrm{UP},\sigma}(\mathbf{r})\, Q_\sigma. \tag{5.16}$$

Therefore we organize the four-component model into the matrix form as follows,

$$H = \begin{pmatrix} P_L^\dagger & P_R^\dagger & Q_L^\dagger & Q_R^\dagger \end{pmatrix} \begin{pmatrix} \varepsilon_{LP,L} & J_{LP} & I_{LL} & I_{LR} \\ J_{LP} & \varepsilon_{LP,R} & I_{RL} & I_{RR} \\ I_{LL} & I_{RL} & \varepsilon_{UP,L} & J_{UP} \\ I_{LR} & I_{RR} & J_{UP} & \varepsilon_{UP,R} \end{pmatrix} \begin{pmatrix} P_L \\ P_R \\ Q_L \\ Q_R \end{pmatrix} \tag{5.17}$$

where the matrix elements are found by integrating over the spatial modes,

$$\begin{aligned} \varepsilon_{\zeta,\sigma} &= \int d^2\mathbf{r}\ \tilde{\phi}_{\zeta,\sigma}(\mathbf{r}) h_\zeta(\mathbf{r})\ \tilde{\phi}_{\zeta,\sigma}(\mathbf{r}) \\ J_\zeta &= -\int d^2\mathbf{r}\ \tilde{\phi}_{\zeta,L}(\mathbf{r}) h_\zeta(\mathbf{r}) \tilde{\phi}_{\zeta,R}(\mathbf{r}) \\ I_{\sigma,\sigma'} &= \int d^2\mathbf{r}\ \tilde{\phi}_{\mathrm{LP},\sigma}(\mathbf{r}) U(\mathbf{r}) \tilde{\phi}_{\mathrm{UP},\sigma'}(\mathbf{r}) \end{aligned} \tag{5.18}$$

Near zero detuning $X_0 = C_0 = 1/2$, the lower and upper polaritons near the anticrossing have the same effective mass, and their trapping potentials only differ by a constant energy offset, therefore the upper and lower branches of condensates share the same left and right spatial modes, which allows us to define $J_{LP} = J_{UP} = J,\ I_{LL} = I_{RR} = I_1,\ I_{LR} = I_{RL} = I_2$.

The interaction among polaritons attributed to the exciton component also can be rewritten in the spatial modes,

$$\begin{aligned} H_{\mathrm{int}} = \frac{g_s}{l_z} \sum_\sigma \big[& c_{\sigma,0}\, \hat{P}_\sigma^\dagger \hat{P}_\sigma^\dagger \hat{P}_\sigma \hat{P}_\sigma + 2c_{\sigma,1} \left(\hat{P}_\sigma^\dagger \hat{P}_\sigma^\dagger \hat{P}_\sigma \hat{Q}_\sigma + \hat{P}_\sigma^\dagger \hat{Q}_\sigma^\dagger \hat{P}_\sigma \hat{P}_\sigma \right) \qquad (5.19) \\ & + c_{\sigma,2} \left(\hat{P}_\sigma^\dagger \hat{P}_\sigma^\dagger \hat{Q}_\sigma \hat{Q}_\sigma + \hat{Q}_\sigma^\dagger \hat{Q}_\sigma^\dagger \hat{P}_\sigma \hat{P}_\sigma + 4 \hat{P}_\sigma^\dagger \hat{Q}_\sigma^\dagger \hat{P}_\sigma \hat{Q}_\sigma \right) \\ & + 2c_{\sigma,3} \left(\hat{P}_\sigma^\dagger \hat{Q}_\sigma^\dagger \hat{Q}_\sigma \hat{Q}_\sigma + \hat{Q}_\sigma^\dagger \hat{Q}_\sigma^\dagger \hat{P}_\sigma \hat{Q}_\sigma \right) + c_{\sigma,4}\, \hat{Q}_\sigma^\dagger \hat{Q}_\sigma^\dagger \hat{Q}_\sigma \hat{Q}_\sigma \big], \qquad (5.20) \end{aligned}$$

where the coefficients $c_{\sigma,n} \equiv X_0^{4-n} C_0^n \int d^2\mathbf{r} \phi_{LP,\sigma}^{4-n}(\mathbf{r}) \phi_{LP,\sigma}^n(\mathbf{r})$ are defined for the normal ordering of the field operators.

We cast the trapped condensate into the coherent states of each spatial mode, which satisfies $\hat{P}_\sigma|\psi_\sigma\rangle = \psi_\sigma$ and $\hat{Q}_\sigma|\chi_\sigma\rangle = \chi_\sigma|\chi_\sigma\rangle$. The total Hamiltonian is then a function of the mean-field amplitudes $H[\Psi^*, \Psi]$, where $\Psi = (\psi_L, \psi_R, \chi_L, \chi_R)^T$.

We minimize the Hamiltonian with respect to each component of Ψ^*, finally arrived at the four-component Gross-Pitaevskii equations(5.9),

5.B Exciton Confinement and Stark Effect in 2D

The potential trap acting on excitons and the electrical control via the Stark effect can be described by a model based on the quasi-2D state of quantum well excitons.

The Schrödinger equation for an electron-hole pair in 2D space reads,

$$\Big(-\frac{\hbar^2}{2m_e}\nabla^2_{\mathbf{r_e}}\psi_e(\mathbf{r_e}) - \frac{\hbar^2}{2m_h}\nabla^2_{\mathbf{r_h}}\psi_h(\mathbf{r_h}) + V(\mathbf{r_e}, \mathbf{r_h}) + \frac{e^2}{\varepsilon_B|\mathbf{r_e} - \mathbf{r_h}|}\Big)\psi(\mathbf{r_e}, \mathbf{r_h}) = E\psi(\mathbf{r_e}, \mathbf{r_h}) \tag{5.21}$$

where $V(\mathbf{r_e}, \mathbf{r_h})$ describes the total potential energy induced by external fields, which may include the energy landscape variations in the semiconductor heterostructure, stress or phonon-induced shift of crystal field, and any directly applied electrical fields.

Recall the definition of coordinates

$$\mathbf{R} = \frac{m_e\mathbf{r_e} + m_h\mathbf{r_h}}{m_e + m_h}, \quad \mathbf{r} = \mathbf{r_e} - \mathbf{r_h}$$

we can rewrite Eq.(5.21) as,

$$\Big(-\frac{\hbar^2}{2M}\nabla^2_{\mathbf{R}} - \frac{\hbar^2}{2m}\nabla^2_{\mathbf{r}} + V(\mathbf{R}, \mathbf{r}) + \frac{e^2}{\varepsilon_B}\frac{1}{r}\Big)\psi(\mathbf{R}, \mathbf{r}) = E\psi(\mathbf{R}, \mathbf{r}) \tag{5.22}$$

Note the potential energy induced by external fields can be written as,

$$V_e(\mathbf{r_e}) + V_h(\mathbf{r_h}) = V_e\big(\mathbf{R} + \frac{m_h}{M}\mathbf{r}\big) + V_h\big(\mathbf{R} - \frac{m_e}{M}\mathbf{r}\big)$$

and the series expansion of the scalar potential near $\mathbf{R}$ with respect to small displacement

$\mathbf{r}$ gives

$$\begin{aligned} V_e(\mathbf{R}+\frac{m_h}{M}\mathbf{r}) &= V_e(\mathbf{R})+\frac{m_h}{M}\nabla_R V_e(\mathbf{R})\cdot\mathbf{r}+O(|r|^2) \\ V_h(\mathbf{R}-\frac{m_e}{M}\mathbf{r}) &= V_h(\mathbf{R})-\frac{m_e}{M}\nabla_R V_h(\mathbf{R})\cdot\mathbf{r}+O(|r|^2) \end{aligned} \tag{5.23}$$

The general wavefunction for an arbitrary exciton state would be the following superposition,

$$\Psi(\mathbf{R},\mathbf{r})=\sum_\nu \psi_\nu(\mathbf{R})\phi_\nu(\mathbf{r}) \tag{5.24}$$

where $\phi_\nu(\mathbf{r})$ is the ν-orbital wavefunction for a bound exciton state, and $\psi_\nu(\mathbf{R})$ is the center of mass envelope function associated with the orbital. However, given the largely different length scale between its center of mass $\mathbf{R}$ (device size $\sim 10^0\mu m$) and relative position $\mathbf{r}(\sim 10nm)$, we can safely cast it in the ansartz, $\Psi(\mathbf{R},\mathbf{r})=\psi(\mathbf{R})\phi(\mathbf{r})$, where $\phi(\mathbf{r})=\sum_\nu c_\nu\phi_\nu(\mathbf{r})$ is the perturbed orbital state.

This allows us to separate the Schrödinger equation and for the electron-hole relative position,

$$\Big(-\frac{\hbar^2}{2m}\nabla_{\mathbf{r}}^2+\frac{e^2}{\varepsilon_B}\frac{1}{r}+f(\mathbf{r})\Big)\phi(\mathbf{r})=E\phi(\mathbf{r}) \tag{5.25}$$

where

$$\Big(-\frac{\hbar^2}{2m}\nabla_{\mathbf{r}}^2+\frac{e^2}{\varepsilon_B}\frac{1}{r}\Big)\phi_\nu(\mathbf{r})=E_\nu\phi_\nu(\mathbf{r})$$

gives the unperturbed orbital states, and

$$f(\mathbf{r})=\frac{m_h}{M}\nabla_{\mathbf{R}}V_e(\mathbf{R})\cdot\mathbf{r}-\frac{m_e}{M}\nabla_{\mathbf{R}}V_h(\mathbf{R})\cdot\mathbf{r}$$

provides the potential for perturbation.

Consider a potential gradient that comes from a static electrical field $\mathbf{E}=-\nabla_{\mathbf{R}}V$. Since the electron and hole carry the opposite charge $\nabla_{\mathbf{R}}V_e=-e\nabla_{\mathbf{R}}V,\quad \nabla_{\mathbf{R}}V_h=e\nabla_{\mathbf{R}}V$, one can recover the form of perturbation potential in Stark Effect, $f(\mathbf{r})=e\mathbf{E}\cdot\mathbf{r}$.

In general, the interface in the heterostructure between two types of semiconductors would not strongly restrict the electrical field so the Coulomb interaction remains 3D, but the electrical fields generated between a pair of nano-fabricated electrodes can lie in the plane of the quantum well and polarize the quasi-2D state of exciton along the same

	$GaAs$	$CdTe$	$CsPbBr_3$
$E_B(m\text{eV})$	18	39	130
$\alpha(e^2\mu\text{m}^2\text{eV}^{-1})$	1.4×10^{-3}	2.2×10^{-4}	8.5×10^{-6}

Table 5.1: Binding energy and Polarizability of 2D excitons

direction. Therefore, the Stark effect can be calculated in the ideal 2D exciton state, while averaging over the envelope wavefunction perpendicular to the plane.

The perturbation correction to the 2D exciton ground-state energy can be written as $\mathcal{E} = \frac{1}{2}\alpha|\mathbf{E}|^2$ where the polarizability

$$\alpha = -e^2 \sum_{n>1,l=\pm1} \frac{|\langle\phi_{10}|\hat{\mathbf{x}}|\phi_{nl}\rangle|^2}{E_{10} - E_{nl}} \tag{5.26}$$

is calculated based on the transition.

Applying the analytical solution of the 2D hydrogen atom while using parameters found in the literature [52, 90, 91], we estimate the binding energy and polarizability for a few materials commonly used in polariton condensate study (Table 5.1). Taking into account the dielectric constant of the host semiconductor, we estimate an electric field of $\sim 1\,V/\mu$m is needed to create a dipole energy of ~ 0.1 meV in the quasi-2D exciton of GaAs.

Finally, for the exciton trapping area with an applied electrical field, we have the Schrödinger equation for the center of mass,

$$\left(-\frac{\hbar^2}{2M}\nabla^2_{\mathbf{R}} + V_e(\mathbf{R}) + V_h(\mathbf{R}) + \frac{1}{2}\alpha|\mathbf{E}(\mathbf{R})|^2\right)\psi(\mathbf{R}) = E\psi(\mathbf{R}) \tag{5.27}$$

In summary, the exciton total potential energy can be represented by the electron-hole joint potential $V_e(\mathbf{R}) + V_h(\mathbf{R})$ and locally tuned by the electrical field $E(\mathbf{R})$.

5.C Tunneling on a Double-Square-Well Potential

The non-resonantly pumped scheme of polariton condensate allows a flexible geometry for the junction where the width and height of the tunneling barrier are highly customizable.

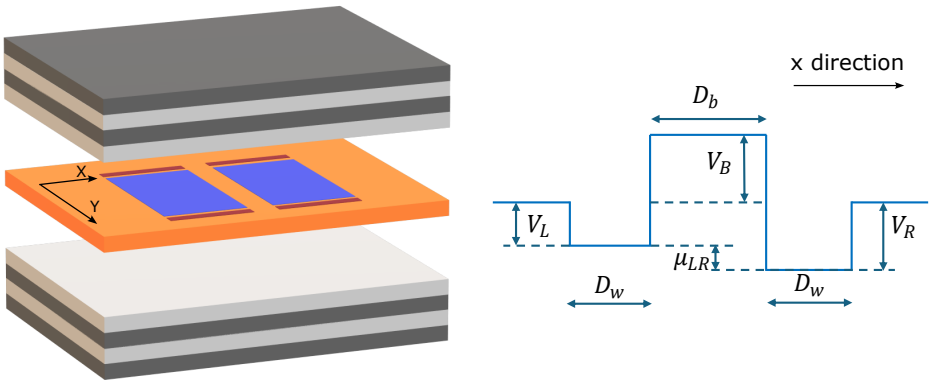

Figure 5.5: Device Sketch and Confinement Potential

As a result, simply estimating the tunneling energy by the symmetric and anti-symmetric summation of the single-well ground states would be inaccurate. Here, we develop a formal theory to calculate the tunneling energy and the resulting Josephson frequency based on the design parameters of a double square well. This model captures the dependence on barrier width and height and can be modified for other detailed geometries.

We start with the polariton Hamiltonian with the exciton confinement potential,

$$h(\mathbf{r}) = -\frac{\hbar^2\nabla^2}{2m} + \frac{1}{2}V_{\text{ex}}(\mathbf{r}) \tag{5.28}$$

The exciton confinement potential sees a variation along the x-direction, allowing it to be broken down into two single wells, which in general are asymmetric (see figure),

$$V_{\text{ex}}(x,y) = \begin{cases} V_L(x), & x < 0 \\ V_R(x), & x > 0 \end{cases} \tag{5.29}$$

where

$$V_L(x) = \begin{cases} 0, & x < -D_w - D_b/2 \\ -\mathcal{V}_L, & -D_w - D_b/2 < x < -D_b/2 \\ \mathcal{V}_B, & x > -D_b/2 \end{cases} \tag{5.30}$$

and

$$V_R(x) = \begin{cases} 0, & x > D_w + D_b \\ -\mathcal{V}_R, & D_b/2 < x < D_w + D_b/2 \\ \mathcal{V}_B, & x < D_b/2 \end{cases} \tag{5.31}$$

where D_w, D_b are the width of the well and the barrier, $\mathcal{V}_B$ is the height of the barrier, $\mathcal{V}_L, \mathcal{V}_R$ are the depth of the two wells.

The bound state solution in the well to the equation,

$$\frac{d^2}{dx^2}\psi(x) + k^2\psi(x) = 0, \quad k = \frac{\sqrt{2m(E+\mathcal{V}_\sigma)}}{\hbar}, \quad \sigma \in \{L, R\} \tag{5.32}$$

and the tunneling solution in the barrier to the equation

$$\frac{d^2}{d^2x}\psi(x) - \kappa^2\psi(x) = 0, \quad \kappa = \frac{\sqrt{2m(\mathcal{V}_B - E)}}{\hbar} \tag{5.33}$$

are well known to be characterized by the wave vectors k and κ. Define the corresponding length parameters.

$$\xi_{1,\sigma} = \frac{\hbar}{\sqrt{m\mathcal{V}_\sigma}}, \quad \xi_{2,\sigma} = \frac{\hbar}{\sqrt{m(\mathcal{V}_\sigma + \mathcal{V}_B)}}, \quad \sigma \in \{L, R\} \tag{5.34}$$

We are in the strong confinement limit if $\xi \ll D$, where $D \equiv \min\{D_w, D_b\}$ and $\xi = \max\{\xi_{1,L}, \xi_{1,R}, \xi_{2,L}, \xi_{2,R}\}$. This allows us to approximate the exact wavefunction in the leading order of ξ/D,

$$\psi_L(x) \approx \sqrt{\frac{2}{D_w}} \times \begin{cases} \sin(\delta_{1,L}) e^{(x+D_w+D_b/2)\xi_{1,L}}, & x < -D_w - D_b/2 \\ \sin\left[\frac{(\pi-\delta_{1,L}-\delta_{2,L})(x+D_w+D_b/2)}{D_w} + \delta_{1,L}\right], & -D_w - D_b/2 < x < -D_b/2 \\ \sin(\delta_{2,L}) e^{-(x+D_b/2)/\xi_{2,L}}, & x > -D_b/2 \end{cases} \tag{5.35}$$

and

$$\psi_R(x) \approx \sqrt{\frac{2}{D_w}} \times \begin{cases} \sin(\delta_{2,R}) e^{(x-D_b/2)/\xi_{2,R}}, & x < D_b/2 \\ \sin\left[\frac{(\pi-\delta_{1,R}-\delta_{2,R})(x-D_w-D_b/2)}{D_w} + \delta_{2,L}\right], & D_b/2 < x < D_w + D_b/2 \\ \sin(\delta_{1,R}) e^{-(x-D_w-D_b/2)/\xi_{1,R}}, & x > D_w + D_b/2 \end{cases} \tag{5.36}$$

The corresponding eigenenergies are,

$$E_L \approx -\frac{\mathcal{V}_L}{2} + E_0, \quad E_R \approx -\frac{\mathcal{V}_R}{2} + E_0 \tag{5.37}$$

where $E_0 = \hbar^2\pi^2/(2mD_w^2)$, $\delta_{1(2),\sigma} = \pi\xi_{1(2),\sigma}/D_w \ll 1$.

Note that the two single-well wavefunctions are not exactly orthogonal in the overlapping area $-D_b/2 < x < D_b/2$. It is usually acceptable when calculating the coupling energy between two closely placed single wells by the integral,

$$J = -\int \Big[\frac{\hbar^2}{2m}\Big(\frac{d}{dx}\psi_L(x)\frac{d}{dx}\psi_R(x)\Big) + \psi_L(x)V(x)\psi_R(x)\Big]dx \tag{5.38}$$

But it would cause ambiguity when estimating the tunneling effect on a sizable barrier, which should only be attributed to the kinetic energy and not be dependent on the choice of potential energy zero point.

Therefore, we apply the Gram-Schmidt orthogonalization process to the overlapping wavefunctions,

$$\tilde{\psi}_L(x) = \psi_L(x), \quad \tilde{\psi}_R(x) = \frac{\psi_R(x) - \psi_L(x)\big(\psi_R(x), \psi_L(x)\big)}{||\psi_R(x) - \psi_L(x)\big(\psi_R(x), \psi_L(x)\big)||^2} \tag{5.39}$$

where

$$\Big(\psi_L(x), \psi_R(x)\Big) = \int_{-D_b/2}^{D_b/2} \psi_R(x)\psi_L(x)dx \tag{5.40}$$

is the inner product in the overlapping area.

The orthogonal wavefunctions allow us to calculate the tunneling energy,

$$\begin{aligned} J =& -\int \frac{\hbar^2}{2m}\Big(\frac{d}{dx}\tilde{\psi}_L(x)\frac{d}{dx}\tilde{\psi}_R(x)\Big)dx \\ =&\Big[\sqrt{(\mathcal{V}+\mathcal{V}_\mathcal{B})^2-\mu_{LR}^2}-\mathcal{V}_B\Big]\frac{\pi^2\xi_{2,L}\xi_{2,R}}{D_w^2}\frac{e^{-D_b/\xi_{2,L}}-e^{-D_b/\xi_{2,R}}}{D_w/\xi_{2,R}-D_w/\xi 2,L} \\ \approx&\pi^2\mathcal{V}\frac{D_b\xi^2}{D_w^3}e^{-D_b/\xi}+\mathcal{O}(\mu_{LR}^2/\mathcal{V}^2) \end{aligned} \tag{5.41}$$

where we have defined,

$$\mu_{LR}=\frac{\mathcal{V}_L-\mathcal{V}_R}{4},\quad \mathcal{V}=\frac{\mathcal{V}_L+\mathcal{V}_R}{4},\quad \xi=\frac{\hbar}{\sqrt{m(2\mathcal{V}+\mathcal{V}_B)}} \tag{5.42}$$

From (5.41) we find the physical limit in which the proposed device can operate. First, when the potential bias introduced by the external field is much smaller than the preset potential well depth $\mu_{LR}\ll\mathcal{V}$, the tunneling energy effectively remains a constant because the correction is second-order in $|\mu_{LR}/\mathcal{V}|$,

Second, the tunneling energy is sensitive to the height of the potential barrier. In the limit of small variation $\mathcal{V}_B\ll\mathcal{V}$, we obtain the tunability,

$$\Big|\frac{J(\mathcal{V}_B)-J(0)}{J(0)}\Big|\sim\frac{D_b}{\xi}\frac{\mathcal{V}_B}{\mathcal{V}} \tag{5.43}$$

which is very effective due to the large prefactor D_b/ξ. With nanofabricated elements incorporated in the microcavity, the barrier can be easily controlled by a gate voltage.

5.D Gross-Pitaevskii Equations in a Rotating Frame

The four-component model is described by the coupled Gross-Pitaevskii equations. $\mathrm{i}d_t\Psi = H[\Psi,\Psi^*]\Psi$, where $\Psi=(\psi_L,\psi_R,\chi_L,\chi_R)^T$. After rescaling the energies and time,

$$\delta=\frac{\mu_{LR}}{J},\ \Delta=\frac{\mu_{UL}}{J},\ g=\frac{U}{J},\ \lambda_1=\frac{I_1}{J},\ \lambda_2=\frac{I_2}{J},\ \tau=\frac{2J}{\hbar}t \tag{5.44}$$

we obtain the Hamiltonian in matrix form,

$$H = \begin{pmatrix} H_{LP} & V \\ V^\dagger & H_{UP} \end{pmatrix} \tag{5.45}$$

where

$$H_{LP} = \begin{pmatrix} \frac{\delta-\Delta}{2} + \frac{g}{4}|\psi_L|^2 + \frac{g}{2}|\chi_L|^2 & -1 \\ -1 & -\frac{\delta+\Delta}{2} + \frac{g}{4}|\psi_R|^2 + \frac{g}{2}|\psi_R|^2 \end{pmatrix} \tag{5.46a}$$

$$H_{UP} = \begin{pmatrix} \frac{\delta+\Delta}{2} + \frac{g}{4}|\chi_L|^2 + \frac{g}{2}|\psi_L|^2 & -1 \\ -1 & -\frac{\delta-\Delta}{2} + \frac{g}{4}|\chi_R|^2 + \frac{g}{2}|psi_R|^2 \end{pmatrix} \tag{5.46b}$$

$$V = \begin{pmatrix} \frac{g}{4}\psi_L^*\chi_L + \frac{g}{2}n_L + \lambda_1 & \lambda_2 \\ \lambda_2 & \frac{g}{4}\psi_R^*\chi_R + \frac{g}{2}n_R + \lambda_1 \end{pmatrix} \tag{5.46c}$$

where $n_\sigma = |\psi_\sigma|^2 + |\chi_R|^2,\ \sigma \in \{L.R\}$ is the total number of LP and UP on each side.

We simulate the dynamics by numerically integrating the coupled GP equations. The highest intrinsic frequency comes from the Rabi splitting between the LP and UP branches. Following the numerical errors at this high frequency will mislead the simulation to lose track of the physics on the time scale of the tunneling effect. Therefore, we decomposed the Hamiltonian into two parts $H = H_\Delta + H'$ where $H_\Delta = \text{diag}\{-\Delta/2, -\Delta/2, \Delta/2, \Delta/2\}$ and perform the "rotating frame" transformation,

$$(\tilde{\psi}_L, \tilde{\psi}_R, \tilde{\chi}_L, \tilde{\chi}_R)^T = e^{iH_\Delta \tau}\Psi, \quad \begin{pmatrix} h_{LP} & v \\ v^\dagger & h_{UP} \end{pmatrix} = e^{iH_\Delta \tau} H' e^{-iH_\Delta \tau} \tag{5.47}$$

The coupled GP equation is eventually transformed into Eq. (5.12).

Chapter 6

Conclusion

In this dissertation, I have surveyed the general concept of the Josephson effect in the context of dilute exciton and exciton-polariton gases. A comparison is drawn between the fundamental principles of a Josephson junction based on homogeneous exciton condensates and one based on trap-defined polariton condensates. While the correlated tunneling of electron-hole pair is proposed as the Josephson coupling mechanism for the former, a model unifying the exciton and photon trapping methods is developed for the latter, where the effective trapping potential acting on the polaritons determines the Josephson coupling strength.

Based on the unified model, a polariton junction using an exciton potential trap and external electrical control is proposed. Exciton trapping and polaritons with long lifetimes allow a more flexible device design operating in the thermal equilibrium limit, where the condensate is robust and well-conserved. Thus, the junction can work as an active device at a reasonable frequency for real-time control. In Numerical simulations, I demonstrated the unique dynamics of the proposed polariton junction, including the switching between periodic trajectories, and the chaos induced either by external driving or by intrinsic interactions between the lower and upper polariton branches.

Original contributions in this dissertation are the model of electron-hole pair tunneling, the Stark effect calculated in semiconductor parameters, the unified junction model for exciton and photon trapping and its tunneling mechanism, and the simulation of its

dynamics based on the rotating frame formalism.

There are interesting open questions related to the proposed device. First, the polariton junction model described by equation (5.9) neglects the incoherent tunneling of uncondensed thermal polaritons at finite temperatures. This incoherent tunneling may give rise to a dissipative current in addition to the supercurrent of EP condensates, in analogy to the quasi-particle tunneling in superconducting Josephson junctions. This effect, along with the spatial inhomogeneity and diffusion discussed in Eq. (3.22)(3.23), should be crucial in the design of a practical device continuously operating in thermal equilibrium.

Second, the pseudo-spin of polaritons is not discussed in this work. Like hyperfine states to atomic condensates, the pseudo spin provides additional degrees of freedom to polariton condensates, which can lead to unique macroscopic phenomena. It has been predicted that for lower polariton condensates, the spin degrees of freedom allow a chaotic behavior in the Josephson oscillations [92]. Spin relaxation [77] could also couple the polariton condensates to dark exciton states [93]. This mechanism may introduce even richer dynamics and provide a potential technique for detecting dark excitons via their influence on the capacitance. Small variations in capacitance can be measured very precisely by their effect on the resonance frequency of co-fabricated circuit elements, which may provide information on the total condensate density, including the possibility of observing "dark" condensates that are not optically observable.

In conclusion, the proposed polariton junction is not only a simulator of the Josephson effect but also an active device with sufficient external control, By combining the powerful techniques in nanoelectronics and nanophotonics, it opens up new opportunities for fundamental physics research and future quantum technologies.

Bibliography

[1] M. H. Anderson, J. R. Ensher, M. R. Matthews, C. E. Wieman, and E. A. Cornell, "Observation of bose-einstein condensation in a dilute atomic vapor," *Science*, vol. 269, no. 5221, pp. 198–201, 1995.

[2] K. B. Davis, M. O. Mewes, M. R. Andrews, N. J. van Druten, D. S. Durfee, D. M. Kurn, and W. Ketterle, "Bose-einstein condensation in a gas of sodium atoms," *Phys. Rev. Lett.*, vol. 75, pp. 3969–3973, Nov 1995.

[3] B. Keimer, S. A. Kivelson, M. R. Norman, S. Uchida, and J. Zaanen, "From quantum matter to high-temperature superconductivity in copper oxides," *Nature*, vol. 518, pp. 179–186, Feb 2015.

[4] Q. Cao, F. Grote, M. Huβmann, and S. Eigler, "Emerging field of few-layered intercalated 2d materials," *Nanoscale Adv.*, vol. 3, p. 963–982, Feb 2021.

[5] M. A. Nielsen and I. L. Chuang, *Quantum Computation and Quantum Information*. Cambridge University Press, 2nd ed., 2010.

[6] F. Arute *et al.*, "Quantum supremacy using a programmable superconducting processor," *Nature*, vol. 574, p. 505–510, Sept 2019.

[7] H. J. Kimble, "The quantum internet," *Nature*, vol. 453, p. 1023–1030, Jun 2008.

[8] C. L. Degen, F. Reinhard, and P. Cappellaro, "Quantum sensing," *Rev. Mod. Phys.*, vol. 89, p. 035002, Jul 2017.

[9] C. Gross and I. Bloch, "Quantum simulations with ultracold atoms in optical lattices," *Science*, vol. 357, no. 6355, pp. 995–1001, 2017.

[10] M. Tinkham, *Introduction to Superconductivity (2nd Edition)*. Dover Publications, 1996.

[11] A. Smerzi, S. Fantoni, S. Giovanazzi, and S. R. Shenoy, "Quantum coherent atomic tunneling between two trapped bose-einstein condensates," *Phys. Rev. Lett.*, vol. 79, pp. 4950–4953, Dec 1997.

[12] S. Raghavan, A. Smerzi, S. Fantoni, and S. R. Shenoy, "Coherent oscillations between two weakly coupled bose-einstein condensates: Josephson effects, π oscillations, and macroscopic quantum self-trapping," *Phys. Rev. A*, vol. 59, pp. 620–633, Jan 1999.

[13] M. Albiez, R. Gati, J. Fölling, S. Hunsmann, M. Cristiani, and M. K. Oberthaler, "Direct observation of tunneling and nonlinear self-trapping in a single bosonic josephson junction," *Phys. Rev. Lett.*, vol. 95, p. 010402, Jun 2005.

[14] V. P. Singh, J. Polo, L. Mathey, and L. Amico, "Shapiro steps in driven atomic josephson junctions," *Phys. Rev. Lett.*, vol. 133, p. 093401, Aug 2024.

[15] C. Ryu and M. G. Boshier, "Integrated coherent matter wave circuits," *New Journal of Physics*, vol. 17, p. 092002, sep 2015.

[16] H. Rubinsztein-Dunlop *et al.*, "Roadmap on structured light," *Journal of Optics*, vol. 19, p. 013001, nov 2016.

[17] D. Barredo, V. Lienhard, S. de Léséleuc, *et al.*, "Synthetic three-dimensional atomic structures assembled atom by atom," *Nature*, vol. 561, pp. 79–82, Sept 2018.

[18] S. A. Moskalenko and D. W. Snoke, *Bose-Einstein Condensation of Excitons and Biexcitons: And Coherent Nonlinear Optics with Excitons*. Cambridge: Cambridge University Press, 2000.

[19] H. Haug and S. W. Koch, *Quantum Theory of the Optical and Electronic Properties of Semiconductors*. World Scientific Publishing Company, 5th ed., 2020.

[20] Alexey Kavokin author, *Microcavities / Alexey V. Kavokin, Jeremy J. Baumberg, Guillaume Malpuech, Fabrice P. Laussy.* No. 21 in Series on semiconductor science and technology, Oxford, United Kingdom: Oxford University Press, second edition.. ed., 2017.

[21] C. W. Lai, N. Y. Kim, S. Utsunomiya, G. Roumpos, H. Deng, M. D. Fraser, T. Byrnes, P. Recher, N. Kumada, T. Fujisawa, and Y. Yamamoto, "Coherent zero-state and π-state in an exciton–polariton condensate array," *Nature*, vol. 450, pp. 529–532, nov 2007.

[22] E. A. Cerda-Méndez, D. N. Krizhanovskii, M. Wouters, R. Bradley, K. Biermann, K. Guda, R. Hey, P. V. Santos, D. Sarkar, and M. S. Skolnick, "Polariton condensation in dynamic acoustic lattices," *Phys. Rev. Lett.*, vol. 105, p. 116402, Sep 2010.

[23] T. Jacqmin, I. Carusotto, I. Sagnes, M. Abbarchi, D. D. Solnyshkov, G. Malpuech, E. Galopin, A. Lemaître, J. Bloch, and A. Amo, "Direct observation of dirac cones and a flatband in a honeycomb lattice for polaritons," *Phys. Rev. Lett.*, vol. 112, p. 116402, Mar 2014.

[24] C. E. Whittaker, E. Cancellieri, P. M. Walker, D. R. Gulevich, H. Schomerus, D. Vaitiekus, B. Royall, D. M. Whittaker, E. Clarke, I. V. Iorsh, I. A. Shelykh, M. S. Skolnick, and D. N. Krizhanovskii, "Exciton polaritons in a two-dimensional lieb lattice with spin-orbit coupling," *Phys. Rev. Lett.*, vol. 120, p. 097401, Mar 2018.

[25] S. Klembt, T. H. Harder, O. A. Egorov, K. Winkler, R. Ge, M. A. Bandres, M. Emmerling, L. Worschech, T. C. H. Liew, M. Segev, C. Schneider, and S. Höfling, "Exciton-polariton topological insulator," *Nature*, vol. 562, no. 7728, pp. 552–556, 2018.

[26] R. Su, S. Ghosh, J. Wang, S. Liu, C. Diederichs, T. C. H. Liew, and Q. Xiong, "Observation of exciton polariton condensation in a perovskite lattice at room temperature," *Nature Physics*, vol. 16, no. 3, pp. 301–306, 2020.

[27] J. Kasprzak, M. Richard, S. Kundermann, A. Baas, P. Jeambrun, J. M. J. Keeling, F. M. Marchetti, M. H. Szymańska, R. André, J. L. Staehli, V. Savona, P. B. Littlewood, B. Deveaud, and L. S. Dang, "Bose–Einstein condensation of exciton polaritons," *Nature*, vol. 443, pp. 409–414, Sept. 2006.

[28] H. Deng, H. Haug, and Y. Yamamoto, "Exciton-polariton bose-einstein condensation," *Rev. Mod. Phys.*, vol. 82, pp. 1489–1537, May 2010.

[29] I. Carusotto and C. Ciuti, "Quantum fluids of light," *Rev. Mod. Phys.*, vol. 85, pp. 299–366, Feb 2013.

[30] F. London, H. London, and F. A. Lindemann, "The electromagnetic equations of the supraconductor," *Proceedings of the Royal Society of London. Series A - Mathematical and Physical Sciences*, vol. 149, no. 866, pp. 71–88, 1935.

[31] J. Bardeen, "Theory of the meissner effect in superconductors," *Phys. Rev.*, vol. 97, pp. 1724–1725, Mar 1955.

[32] L. N. Cooper, "Bound electron pairs in a degenerate fermi gas," *Phys. Rev.*, vol. 104, pp. 1189–1190, Nov 1956.

[33] J. Bardeen, L. N. Cooper, and J. R. Schrieffer, "Theory of superconductivity," *Phys. Rev.*, vol. 108, pp. 1175–1204, Dec 1957.

[34] B. D. Josephson, "Possible new effects in superconductive tunnelling," *Physics Letters*, vol. 1, no. 7, pp. 251–253, 1962.

[35] P. W. Anderson and J. M. Rowell, "Probable observation of the josephson superconducting tunneling effect," *Phys. Rev. Lett.*, vol. 10, pp. 230–232, Mar 1963.

[36] L. P. Gor'Kov, "MICROSCOPIC DERIVATION OF THE GINZBURG-LANDAU EQUATIONS IN THE THEORY OF SUPERCONDUCTIVITY," *JETP*, vol. 36, Dec. 1959.

[37] J. Frenkel, "On the Transformation of light into Heat in Solids. I," *Physical Review*, vol. 37, pp. 17–44, Jan. 1931.

[38] Y. Frenkel, "On the Adsorption of Light and the Trapping of Electrons and positive Holes in Crystalline Dielectrics.," *Physikalische Zeitschrift der Sowjetunion*, vol. 9, p. 158, 1936.

[39] G. H. Wannier, "The Structure of Electronic Excitation Levels in Insulating Crystals," *Physical Review*, vol. 52, pp. 191–197, Aug. 1937.

[40] N. F. Mott, "Conduction in polar crystals. II. The conduction band and ultra-violet absorption of alkali-halide crystals," *Transactions of the Faraday Society*, vol. 34, pp. 500–506, Jan. 1938.

[41] S. Pekar, "The Theory of Electromagnetic Waves in a Crystal in which Excitons Are Produced," *Journal of Experimental and Theoretical Physics(oringinal text in Russian)*, vol. 6, no. 4, p. 785, 1958.

[42] J. J. Hopfield, "Theory of the Contribution of Excitons to the Complex Dielectric Constant of Crystals," *Physical Review*, vol. 112, pp. 1555–1567, Dec. 1958.

[43] V. Agranovich, "Dispersion of Electromagnetic Waves in Crystals," *Journal of Experimental and Theoretical Physics(oringinal text in Russian)*, vol. 10, no. 2, p. 307, 1960.

[44] L. C. Andreani, "Exciton-Polaritons in Bulk Semiconductors and in Confined Electron and Photon Systems," in *Strong Light-Matter Coupling*, pp. 37–82, WORLD SCIENTIFIC, Jan. 2013.

[45] C. Weisbuch, M. Nishioka, A. Ishikawa, and Y. Arakawa, "Observation of the coupled exciton-photon mode splitting in a semiconductor quantum microcavity," *Physical Review Letters*, vol. 69, pp. 3314–3317, Dec. 1992.

[46] J. M. Kosterlitz and D. J. Thouless, "Ordering, metastability and phase transitions in two-dimensional systems," *Journal of Physics C: Solid State Physics*, vol. 6, p. 1181, Apr. 1973.

[47] R. Balili, V. Hartwell, D. Snoke, L. Pfeiffer, and K. West, "Bose-einstein condensation of microcavity polaritons in a trap," *Science*, vol. 316, no. 5827, pp. 1007–1010, 2007.

[48] O. Svelto, *Principles of Lasers*. Netherlands: Springer Nature, 5th ed. ed., 2010.

[49] R. I. Kaitouni, O. El Daïf, A. Baas, M. Richard, T. Paraiso, P. Lugan, T. Guillet, F. Morier-Genoud, J. D. Ganière, J. L. Staehli, V. Savona, and B. Deveaud, "Engineering the spatial confinement of exciton polaritons in semiconductors," *Phys. Rev. B*, vol. 74, p. 155311, Oct 2006.

[50] S. Pau, G. Björk, J. Jacobson, H. Cao, and Y. Yamamoto, "Microcavity exciton-polariton splitting in the linear regime," *Phys. Rev. B*, vol. 51, pp. 14437–14447, May 1995.

[51] D. M. Whittaker, "What determines inhomogeneous linewidths in semiconductor microcavities?," *Phys. Rev. Lett.*, vol. 80, pp. 4791–4794, May 1998.

[52] S. L. Chuang, *Physics of Photonic Devices*. Wiley, 2nd ed., 2009.

[53] J. M. Luttinger and W. Kohn, "Motion of Electrons and Holes in Perturbed Periodic Fields," *Physical Review*, vol. 97, pp. 869–883, Feb. 1955.

[54] A. Wachter, *Relativistic quantum mechanics / Armin Wachter.* Theoretical and mathematical physics (Springer (Firm)) ; 720, New York: Springer, 1st ed.. ed., 2011.

[55] X. L. Yang, S. H. Guo, F. T. Chan, K. W. Wong, and W. Y. Ching, "Analytic solution of a two-dimensional hydrogen atom. i. nonrelativistic theory," *Phys. Rev. A*, vol. 43, pp. 1186–1196, Feb 1991.

[56] M. Abramowitz, *Handbook of mathematical functions, with formulas, graphs, and mathematical tables, edited by Milton Abramowitz and Irene A. Stegun.* New York: Dover Publications, 1965.

[57] C. N. Yang, "Concept of off-diagonal long-range order and the quantum phases of liquid he and of superconductors," *Rev. Mod. Phys.*, vol. 34, pp. 694–704, Oct 1962.

[58] N. D. Mermin and H. Wagner, "Absence of ferromagnetism or antiferromagnetism in one- or two-dimensional isotropic heisenberg models," *Phys. Rev. Lett.*, vol. 17, pp. 1133–1136, Nov 1966.

[59] H. Alnatah, Q. Yao, J. Beaumariage, S. Mukherjee, M. C. Tam, Z. Wasilewski, K. West, K. Baldwin, L. N. Pfeiffer, and D. W. Snoke, "Coherence measurements of polaritons in thermal equilibrium reveal a power law for two-dimensional condensates," *Science Advances*, vol. 10, no. 18, p. eadk6960, 2024.

[60] M. Abbarchi, A. Amo, V. G. Sala, D. D. Solnyshkov, H. Flayac, L. Ferrier, I. Sagnes, E. Galopin, A. Lemaître, G. Malpuech, and J. Bloch, "Macroscopic quantum self-trapping and Josephson oscillations of exciton polaritons," *Nature Physics*, vol. 9, pp. 275–279, May 2013.

[61] X. Chen, H. Alnatah, D. Mao, M. Xu, Y. Fan, Q. Wan, J. Beaumariage, W. Xie, H. Xu, Z.-Y. Shi, D. Snoke, Z. Sun, and J. Wu, "Bose condensation of upper-branch exciton-polaritons in a transferable microcavity," *Nano Letters*, vol. 23, no. 20, pp. 9538–9546, 2023. PMID: 37818838.

[62] C. Piermarocchi, F. Tassone, V. Savona, A. Quattropani, and P. Schwendimann, "Nonequilibrium dynamics of free quantum-well excitons in time-resolved photoluminescence," *Physical Review B*, vol. 53, pp. 15834–15841, June 1996.

[63] T. D. Doan, H. T. Cao, D. B. Tran Thoai, and H. Haug, "Condensation kinetics of microcavity polaritons with scattering by phonons and polaritons," *Phys. Rev. B*, vol. 72, p. 085301, Aug 2005.

[64] L. P. Pitaevskii and S. Stringari, *Bose-Einstein condensation and superfluidity.* International series of monographs on physics (Oxford, England); 164, Oxford Science Publications, first edition.. ed., 2016.

[65] Y. Sun, Y. Yoon, M. Steger, G. Liu, L. N. Pfeiffer, K. West, D. W. Snoke, and K. A. Nelson, "Direct measurement of polariton–polariton interaction strength," *Nature Physics*, vol. 13, pp. 870–875, Sept. 2017.

[66] M. Wouters and I. Carusotto, "Excitations in a nonequilibrium bose-einstein condensate of exciton polaritons," *Phys. Rev. Lett.*, vol. 99, p. 140402, Oct 2007.

[67] H. Alnatah, Q. Yao, J. Beaumariage, S. Mukherjee, M. C. Tam, Z. Wasilewski, K. West, K. Baldwin, L. N. Pfeiffer, and D. W. Snoke, "Coherence measurements of polaritons in thermal equilibrium reveal a new power law for two-dimensional condensates," 2023.

[68] H. Deng, G. S. Solomon, R. Hey, K. H. Ploog, and Y. Yamamoto, "Spatial coherence of a polariton condensate," *Phys. Rev. Lett.*, vol. 99, p. 126403, Sep 2007.

[69] J. W. Goodman, *Introduction to Fourier optics / Joseph W. Goodman.* Englewood, Colo.: Roberts & Co., 3rd ed.. ed., 2005.

[70] J. Ziman, *Electrons and Phonons: The Theory of Transport Phenomena in Solids*. Oxford University Press, 02 2001.

[71] H. Deng, H. Haug, and Y. Yamamoto, "Exciton-polariton Bose-Einstein condensation," *Reviews of Modern Physics*, vol. 82, pp. 1489–1537, May 2010.

[72] C. Ciuti, V. Savona, C. Piermarocchi, A. Quattropani, and P. Schwendimann, "Role of the exchange of carriers in elastic exciton-exciton scattering in quantum wells," *Phys. Rev. B*, vol. 58, pp. 7926–7933, Sep 1998.

[73] F. Tassone and Y. Yamamoto, "Exciton-exciton scattering dynamics in a semiconductor microcavity and stimulated scattering into polaritons," *Phys. Rev. B*, vol. 59, pp. 10830–10842, Apr 1999.

[74] T. Takagahara, "Electronic and nuclear spin in the optical spectra of semiconductor quantum dots," in *Quantum Coherence Correlation and Decoherence in Semiconductor Nanostructures*, United Kingdom: Elsevier Science & Technology, 2003.

[75] R. P. Feynman, *The Feynman lectures on physics [by] Richard P. Feynman, Robert B. Leighton [and] Matthew Sands.* Reading, Mass.: Addison-Wesley Pub. Co, 1963.

[76] S. Giovanazzi, A. Smerzi, and S. Fantoni, "Josephson effects in dilute bose-einstein condensates," *Phys. Rev. Lett.*, vol. 84, pp. 4521–4524, May 2000.

[77] M. Z. Maialle, E. A. de Andrada e Silva, and L. J. Sham, "Exciton spin dynamics in quantum wells," *Phys. Rev. B*, vol. 47, pp. 15776–15788, Jun 1993.

[78] C. Schneider, K. Winkler, M. D. Fraser, M. Kamp, Y. Yamamoto, E. A. Ostrovskaya, and S. Höfling, "Exciton-polariton trapping and potential landscape engineering," *Reports on Progress in Physics*, vol. 80, p. 016503, nov 2016.

[79] K. G. Lagoudakis, B. Pietka, M. Wouters, R. André, and B. Deveaud-Plédran, "Coherent oscillations in an exciton-polariton josephson junction," *Phys. Rev. Lett.*, vol. 105, p. 120403, Sep 2010.

[80] R. B. Balili, D. W. Snoke, L. Pfeiffer, and K. West, "Actively tuned and spatially trapped polaritons," *Applied Physics Letters*, vol. 88, p. 031110, 01 2006.

[81] M. D. Fraser, H. H. Tan, and C. Jagadish, "Selective confinement of macroscopic long-lifetime exciton and trion populations," *Phys. Rev. B*, vol. 84, p. 245318, Dec 2011.

[82] Y. Sun, P. Wen, Y. Yoon, G. Liu, M. Steger, L. N. Pfeiffer, K. West, D. W. Snoke, and K. A. Nelson, "Bose-einstein condensation of long-lifetime polaritons in thermal equilibrium," *Phys. Rev. Lett.*, vol. 118, p. 016602, Jan 2017.

[83] X. Zhai, X. Ma, Y. Gao, C. Xing, M. Gao, H. Dai, X. Wang, A. Pan, S. Schumacher, and T. Gao, "Electrically controlling vortices in a neutral exciton-polariton condensate at room temperature," *Phys. Rev. Lett.*, vol. 131, p. 136901, Sep 2023.

[84] D. Liran, I. Rosenberg, K. West, L. Pfeiffer, and R. Rapaport, "Fully guided electrically controlled exciton polaritons," *ACS Photonics*, vol. 5, no. 11, pp. 4249–4252, 2018.

[85] D. Liran, R. Rapaport, J. Hu, N. Lydick, H. Deng, and L. Pfeiffer, "Electrically controlled photonic circuits of field-induced dipolaritons with huge nonlinearities," *Phys. Rev. X*, vol. 14, p. 031022, Aug 2024.

[86] H.-T. Lim, E. Togan, M. Kroner, J. Miguel-Sanchez, and A. Imamoğlu, "Electrically tunable artificial gauge potential for polaritons," *Nature Communications*, vol. 8, p. 14540, Feb. 2017.

[87] F. L. Lederman and J. D. Dow, "Theory of electroabsorption by anisotropic and layered semiconductors. i. two-dimensional excitons in a uniform electric field," *Phys. Rev. B*, vol. 13, pp. 1633–1642, Feb 1976.

[88] K. R. Hansen, C. E. McClure, J. S. Colton, and L. Whittaker-Brooks, "Franz-keldysh and stark effects in two-dimensional metal halide perovskites," *PRX Energy*, vol. 1, p. 013001, Apr 2022.

[89] S. Mukherjee, D. M. Myers, R. G. Lena, B. Ozden, J. Beaumariage, Z. Sun, M. Steger, L. N. Pfeiffer, K. West, A. J. Daley, and D. W. Snoke, "Observation of nonequilibrium motion and equilibration in polariton rings," *Phys. Rev. B*, vol. 100, p. 245304, Dec 2019.

[90] Bibin John and S. Varadharajaperumal, "Comprehensive Review on CdTe Crystals: Growth, Properties, and Photovoltaic Application," *Physics of Metals and Metallography*, vol. 124, pp. 1795–1812, Dec. 2023.

[91] D. R. Yakovlev, S. A. Crooker, M. A. Semina, J. Rautert, J. Mund, D. N. Dirin, M. V. Kovalenko, and M. Bayer, "Exciton–polaritons in cspbbr3 crystals revealed by optical reflectivity in high magnetic fields and two-photon spectroscopy," *physica status solidi (RRL) – Rapid Research Letters*, vol. 18, no. 3, p. 2300407, 2024.

[92] D. D. Solnyshkov, R. Johne, I. A. Shelykh, and G. Malpuech, "Chaotic josephson oscillations of exciton-polaritons and their applications," *Phys. Rev. B*, vol. 80, p. 235303, Dec 2009.

[93] M. Combescot, O. Betbeder-Matibet, and R. Combescot, "Bose-einstein condensation in semiconductors: The key role of dark excitons," *Phys. Rev. Lett.*, vol. 99, p. 176403, Oct 2007.